Two-Focus Fluorescence Correlation Spectroscopy

I n a u g u r a l - D i s s e r t a t i o n

zur

Erlangung des Doktorgrades

der Mathematisch-Naturwissenschaftlichen Fakultät

der Universität zu Köln

vorgelegt von

Thomas Dertinger

aus Heidelberg, Deutschland

5. Februar 2007

Berichterstatter: Priv. Doz. Dr. Jörg Enderlein

Prof. Dr. Klaus Meerholz

Prof. Dr. Markus Sauer

Tag der letzten mündlichen Prüfung: 19.04.2007

Content

1. Abstract

Fluorescence Correlation Spectroscopy (FCS) has been invented more than 30 years ago and experienced a renaissance after stable and affordable laser sources and low-noise single-photon detectors have become available. Its ability to measure diffusion coefficients at nanomolar concentrations of analyte made it a widely used tool in biophysics. However, in recent years it has been shown by many authors that aberrational (e.g. astigmatism) and photophysical effects (e.g. optical saturation) may influence the result of an FCS experiment dramatically, so that a precise and reliable estimation of the diffusion coefficient is no longer possible.

In this thesis, we report on the development, implementation, and application of a new and robust modification of FCS that we termed two-focus FCS (2fFCS) and which fulfils two requirements: (i) It introduces an external ruler into the measurement by generating two overlapping laser foci of precisely known and fixed distance. (ii) These two foci and corresponding detection regions are generated in such a way that the corresponding molecule detection functions (MDFs) are sufficiently well described by a simple two-parameter model yielding accurate diffusion coefficients when applied to 2fFCS data analysis.

Both these properties enable us to measure absolute values of the diffusion coefficient with an accuracy of a few percent. Moreover, it will turn out that the new technique is robust against refractive index mismatch, coverslide thickness deviations, and optical saturation effects, which so often trouble conventional FCS measurements. This thesis deals mainly with the introduction of the new measurement scheme, 2fFCS, but also presents several applications with far-reaching importance.

2. Zusammenfassung

Fluoreszenz-Korrelations-Spektroskopie (FCS) wurde vor mehr als 30 Jahren entwickelt und erfuhr durch die Entwicklung von stabilen und einfach handhabbaren Laserquellen sowie hocheffizienter Einzel-Photonen-Detektoren eine Renaissance. Die Fähigkeit, Diffusionskoeffizienten auch bei nanomolarer Probenkonzentration messen zu können, trug maßgeblich zur Verbreitung der FCS auf dem Gebiet der Biophysik bei. Die vergangenen Jahre haben jedoch gezeigt, dass sowohl optische Abberationen (z.B. Astigmatismus, Brechungsindex Abweichung) als auch photophysikalische Effekte (wie z.B. optische Sättigung) das Ergebnis eines FCS-Experimentes maßgeblich beeinflussen können, so dass eine zuverlässige und genaue Bestimmung des Diffusionskoeffizienten nicht mehr möglich ist.

In der vorliegenden Arbeit berichten wir über die Entwicklung, Implementation und Anwendung einer neuartigen und robusten Modifikation herkömmlicher FCS, die wir 2-Fokus-FCS (2fFCS) nennen und die zwei Voraussetzungen erfüllt: (i) es wird ein externer Maßstab in die Messung eingeführt, indem zwei lateral versetzte aber überlappende Laserfoki der gleiche Wellenlänge in einem wohldefinierten Abstand generiert werden. (ii) Diese Foki und deren korrspondierende Molekül-Detektions-Funktionen (MDF) können durch ein einfaches zwei-Parameter Modell ausreichend gut beschrieben werden.

Diese beiden Eigenschaften ermöglichen uns, Diffusionskoeffizienten mit höchster Genauigkeit zu messen. Desweiteren zeigt sich, dass das neue Messprinzip robust ist gegenüber Brechungsindex-Abweichungen, optischer Sättigung oder Deckglassdicken-Schwankungen. Diese Arbeit befasst sich hauptsächlich mit der Einführung des neuen Messprinzips der 2fFCS, jedoch werden auch etliche Anwendungen von weitreichender Bedeutung vorgestellt.

3. Introduction

Diffusion due to Brownian motion is a fundamental molecular process. It plays a paramount role in the functioning of cells where it is responsible for non-directed transport of molecules. At long distances diffusion is a relative inefficient and slow transport process but at short distances, as encountered for example in the cellular environment, it becomes very efficient and fast. Even processes such as signaling through the synaptic gap of two neighboring nerve cells are driven by diffusion. An important feature of the cellular environment, different from the macroscopic world around us, is the low Reynolds number at the cellular length scale (Purcell, 1977). The Reynolds number quantifies the ratio of inertial to viscous forces in a hydrodynamic system. A low Reynolds number thus signifies a viscosity dominated system. As a consequence of the low Reynolds number in cells, inertial movements are completely negligible and swimming at a speed faster than diffusion becomes a highly energy-consuming task. When calculating typical diffusion times of molecules (e.g. secondary messengers) across a cell, it turns out that they are sufficiently short to maintain cellular functions and therefore diffusion at the cellular level is the predominating transport process.

The fundamental parameter describing diffusion of a molecule in a solution is the diffusion coefficient. The ability to precisely measure the diffusion coefficient has a large range of potential monitoring applications, e.g. conformational changes in proteins upon ion binding or unfolding since it is directly related to the hydrodynamic radius of the molecules (Einstein, 1905b). Any change in that radius will alter the associated diffusion coefficient of the molecule. Such changes occur to most bio-molecules, in particular the proteins RNA and DNA, when they interact with other molecules (e.g. binding of ions or other bio-molecules), when they perform biologically functions (e.g. enzymatic activity), or when they react to changes in environmental parameters such as pH, temperature or ionic composition (e.g. protein unfolding). However, many biologically relevant conformational changes are connected with rather small changes in hydrodynamic radius in the order of Ångstrøms (see for example (Weljie *et al.*, 2003)). To monitor these small changes, it is necessary to measure the diffusion coefficient with an error smaller than a few percent. Standard methods for diffusion coefficient measurements achieving this accuracy are dynamic light scattering (Berne & Pecora, 2000), pulsed-field gradient NMR

(Callaghan, 1991), size-exclusion electrophoresis (Harvey, 2000). However, all these methods operate at rather high sample concentrations, far away from the limit of infinite dilution. For obtaining the correct infinite-dilution limit and thus a correct estimate of the hydrodynamic radius, one has often to measure at different concentrations and to extrapolate the concentration/diffusion coefficient curve towards zero concentration (see for example (Liu *et al.*, 2005)). Another problem is that proteins are often prone to aggregation (Kiefhaber *et al.*, 1991) at the concentrations needed for obtaining sufficient data quality. Moreover, these methods can rarely be applied *in-vivo*.

Fluorescence correlation spectroscopy (FCS) is able to measure at nanomolar concentrations and it can be applied *in-vivo*. It was invented more than 30 years ago (Magde *et al.*, 1972). In its original form it was designed for measuring diffusion, concentration, and chemical/biochemical interactions/reactions of fluorescent or fluorescently labeled molecules at nanomolar concentrations in solution. The core idea of the method is to analyze fluctuations of the fluorescence signal resulting from the entering and leaving of individual fluorescing molecules into or out of a certain detection volume. The conventional optical setup for performing FCS measurements is the confocal epi-fluorescence microscope as depicted in Fig. 1.

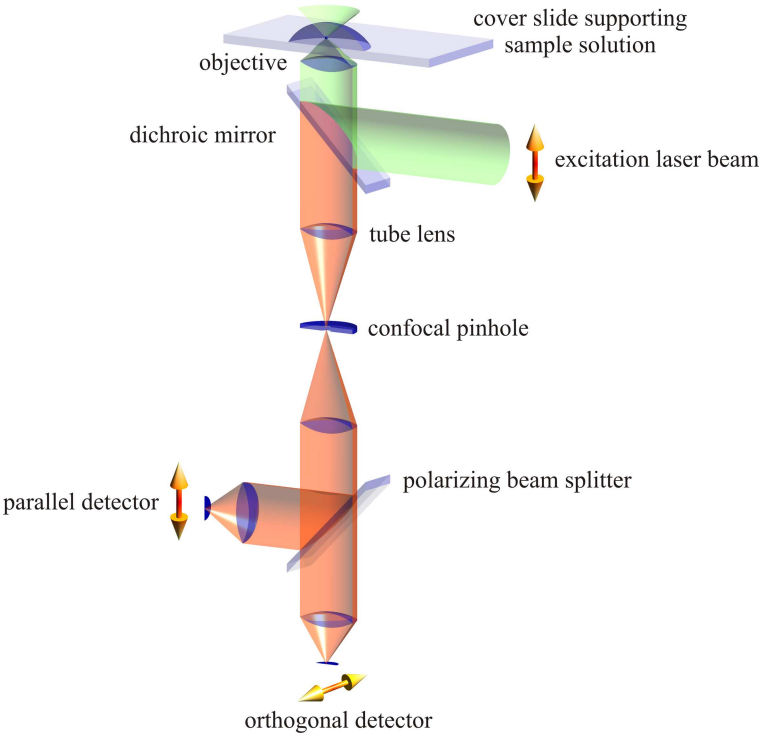

Fig. 1: Schematic of a conventional confocal microscope.

The confocal microscope is basically a measurement system for exciting and measuring the fluorescence of molecules in solution (let us postpone all the technical details for the moment). The system is characterized by an effective volume of detection. This volume is basically given by the laser focus which has been generated by the microscopes objective and the microscopes detection properties; it is a region in solution where efficient fluorescence excitation and detection takes place. If the concentration of

fluorescent molecules in solution is sufficiently small so that only one of very few molecules are within the detection volume at any moment in time, the resulting measured fluorescence signal is strongly fluctuating in response to the entering and leaving of individual fluorescing molecules into or out of this volume (see Fig. 2).

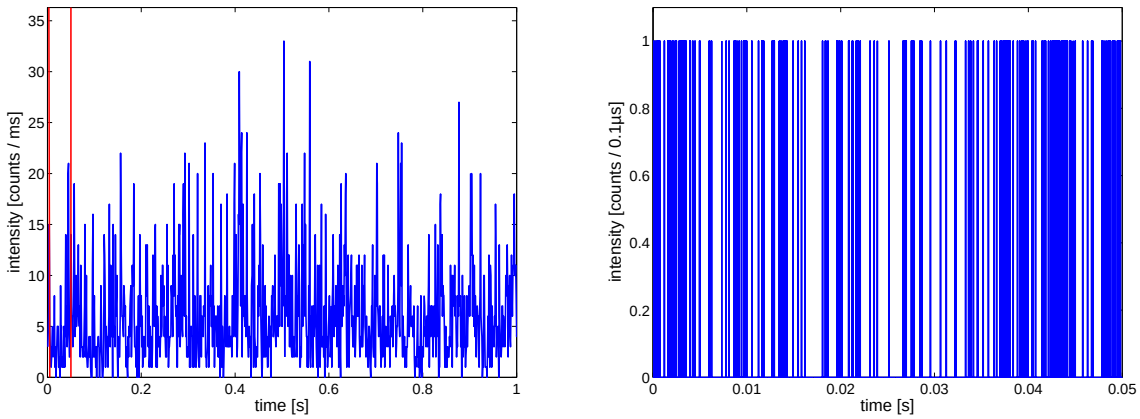

Fig. 2: Part of a typical intensity time trace recorded with a confocal microscope. Left: Intensity trace with a time binning of 1 ms. The intensity fluctuations due to entering and exiting fluorescent molecules of the detection volume are clearly visible. The red lines indicate the part which has been cut out and taken for the right figure. Right: Cut out of the same time trace with a time binning of 100 ns. With such a low time binning only single photons are detected. Thus, the detected intensity is either zero (no photon) or one (one photon) and is coded in the frequency of the detected signal rather than in its the amplitude.

In FCS, the detected fluorescence intensity is correlated with a time-shifted replica of itself for different values of time shift (lag time).

$$g(\tau) = \langle I(t+\tau) I(t) \rangle$$

$I(t)$ is the fluorescence intensity at time *t* and $I(t+\tau)$ is the intensity at time $t+\tau$, and the triangular brackets denote averaging over all time values *t*. The physical meaning of the autocorrelation is that it is directly proportional to the probability to detect a photon at time τ if there was a photon detection event at time zero. This probability is composed of two different terms: One term contains all contributions from uncorrelated signal, i.e. the two photons detected at time zero and at time τ are originating from uncorrelated background (backscattered laser light) or from different fluorescing molecules and therefore do not have any physical correlation (provided there is no interaction of the different fluorescing molecules). These events will contribute to a constant offset of $g(\tau)$ that is completely

independent on τ (the joint probability to detect two physically uncorrelated photons is completely independent of the time span between their detection). The other term contains correlated signal, i.e. the two photons are originating from one and the same molecule and are then physically correlated.

Let us start with some qualitative considerations concerning the lag-time dependence of $g(\tau)$. Suppose a molecule is close to the centre of the detection volume. Then there will be a high probability to detect a large number of consecutive fluorescence photons from this molecule, i.e. the fluorescence signal will be highly correlated in time. When the molecule (due to diffusion) starts to exit the detection volume, this correlation will continually decrease, i.e. the probability to see further fluorescence photons will decrease in time, until the molecule has completely diffused away and the correlation is completely lost. A typical autocorrelation curve is shown in Fig. 3.

Of course, the temporal decay of the correlation, i.e. the temporal decay of $g(\tau)$ with increasing lag time τ, will be proportional to the diffusion speed of the molecule; the larger the diffusion coefficient, the faster the fluorescence correlation decays.

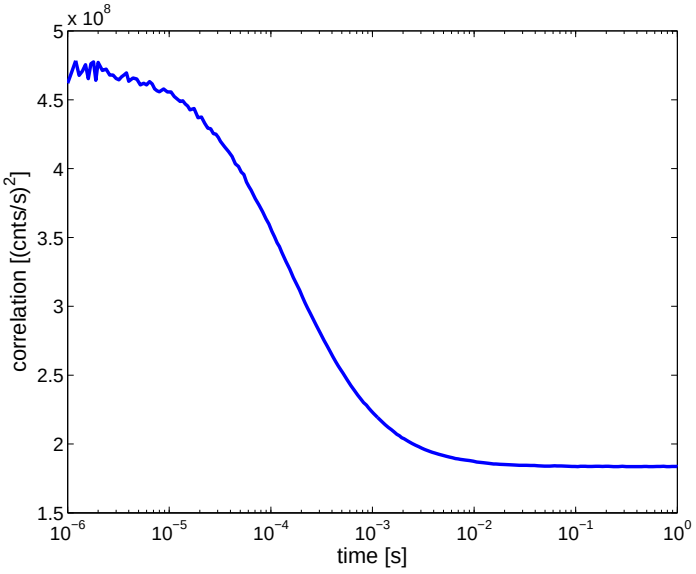

Fig. 3: A typical autocorrelation curve measured with a conventional FCS setup. As can be seen there is a prominent temporal decay caused by the mean time a dye molecule stays within the detection volume.

Thus, FCS measurements can provide information about diffusion of fluorescing molecules. Any process that alters the diffusion coefficient or the fluorescence of the molecule can therefore be measured by FCS. For example, consider the binding of two proteins in solution. By labeling one of the binding partners with a fluorescence label, and monitoring with FCS the changing value of the diffusion coefficient of the labeled molecules upon binding with their binding partner, one can directly measure binding affinities and kinetics. However, there is much more that can be measured with FCS: fast photophysical processes, fast

intramolecular structural dynamics or stoichiometry of molecular complexes, although these processes are not monitored via the diffusion coefficient but rather from µs dynamics of the detected fluorescence.

It took nearly two decades until the development of new lasers with high beam quality and temporal stability, low-noise single-photon detectors and high-quality microscope objectives with nearly perfect imaging quality at high numerical aperture, led the technique to a renaissance in single molecule spectroscopy. Achieving values of the detection volume within the range of a few μm^3 made the technique applicable for samples at reasonably high concentrations and short measurement times.

The advantage of FCS is its relative simplicity. Its drawback is that it works only within a very limited concentration range. If the concentration of fluorescing molecules becomes too large (typically > 10^{-8} M), then the contribution from correlated photons from individual molecules, scaling with the number N of molecules within the detection volume, becomes very small compared with the contribution from uncorrelated photons from different molecules, scaling with N^2. If the concentration is too low (typically < 10^{-13} M), then the probability to find a molecule within the detection region becomes extremely low. In both cases, the measurement time for obtaining a high-quality autocorrelation function gets prohibitively large, although a remedy to that problem is to rapidly scan the laser focus through the solution (Petersen, 1986; Petersen *et al.*, 1986).

There are numerous excellent reviews and overviews of FCS, see Ref. (Schwille, 2001; Hess *et al.*, 2002; Widengren & Mets, 2002) and there is even a complete book devoted to it (Rigler & Elson, 2001). The present chapter gives a very general introduction into the philosophy of FCS, trying to be self-contained, developing the fundamental principles of FCS, but also describing recent methodological advances that are not well covered by previous reviews.

To quantitatively evaluate an FCS measurement, one has to exactly know the shape of the detection volume which is described by the so-called molecule detection function (MDF) giving the probability to detect a fluorescence photon from a molecule at a given position in sample space (Enderlein *et al.*, 2004; Gregor *et al.*, 2005). The molecule detection function sensibly depends on manifold parameters of the optical setup, such as the peculiarities of laser focusing or fluorescence light collection, which are difficult or impossible to control exactly, making an exact, quantitative evaluation of FCS measurements rather difficult (Hess & Webb, 2002; Nagy *et al.*, 2005a; Perroud *et al.*, 2005). For example, even the smallest changes of refractive index of the sample solution

can dramatically change the molecule detection function and thus the outcome of an FCS measurement (Enderlein *et al.*, 2005). This becomes particularly problematic when measuring in biological cells or studying proteins under chemical denaturing conditions.

But not only refractive index mismatches influence the molecule detection function. It also depends on laser-beam distortions, such as beam astigmatism, or on sample properties, such as the thickness of the coverslide used (Gregor & Enderlein, 2005; Enderlein *et al.*, 2005). One of the most impairing observations was the dependence of the molecule detection function (and thus of the FCS results) on excitation intensity due to optical saturation of fluorescence, even at very low total excitation power of only few μW (Berland & Shen, 2003; Nishimura & Kinjo, 2004; Nagy *et al.*, 2005b). This makes even comparative measurements problematic because the photophysics, and thus optical saturation properties, of even the same dye may change when it is chemically bound to a target molecule. Additionally so called 'dead-times' of the signal-processing electronics may lead to distorted correlation curves as well (Nishimura & Kinjo, 2005). All these potential error sources are linked to a fundamental problem of standard FCS - the absence of an intrinsic length scale in the measurement. The fluorescence correlation decay depends on diffusion speed *and* the spatial extend and shape of the molecule detection function, but the former is to be measured and the latter is not well known. Fig. 4 depicts the effect of the molecule detection function under different conditions on measured autocorrelation functions (ACFs).

Their have been several attempts to develop robust FCS measurement schemes by introducing an *external ruler* into the measurement, which is absent in conventional FCS. Among these attempts were: FCS in front of dielectric mirrors (Rigneault & Lenne, 2003), standing wave FCS (Davis S.K. & Bardeen C.J, 2002), or spatial correlation FCS between two detection volumes generated by detecting fluorescence through two laterally shifted pinholes (Jaffiol *et al.*, 2006). The external ruler was provided either by the known modulation length of a standing light wave, or the estimated distance between the detection volumes. However, all the proposed methods suffer from the problem that for a precise quantification of the diffusion coefficient, one still needs precise knowledge of the overall shape of the molecule detection function, evoking the same problems as in conventional FCS. In fact, it is possible to describe the molecule detection function and the resulting autocorrelation function perfectly for any kind of aberration with the help of wave optical calculations (Enderlein *et al.*, 2005), but due to the multitude of parameters describing the molecule detection function, this approach can not be used successfully for fitting recorded

autocorrelation functions. Thus, a suitable fit-model for measured autocorrelation curves should contain as few as possible fit parameters.

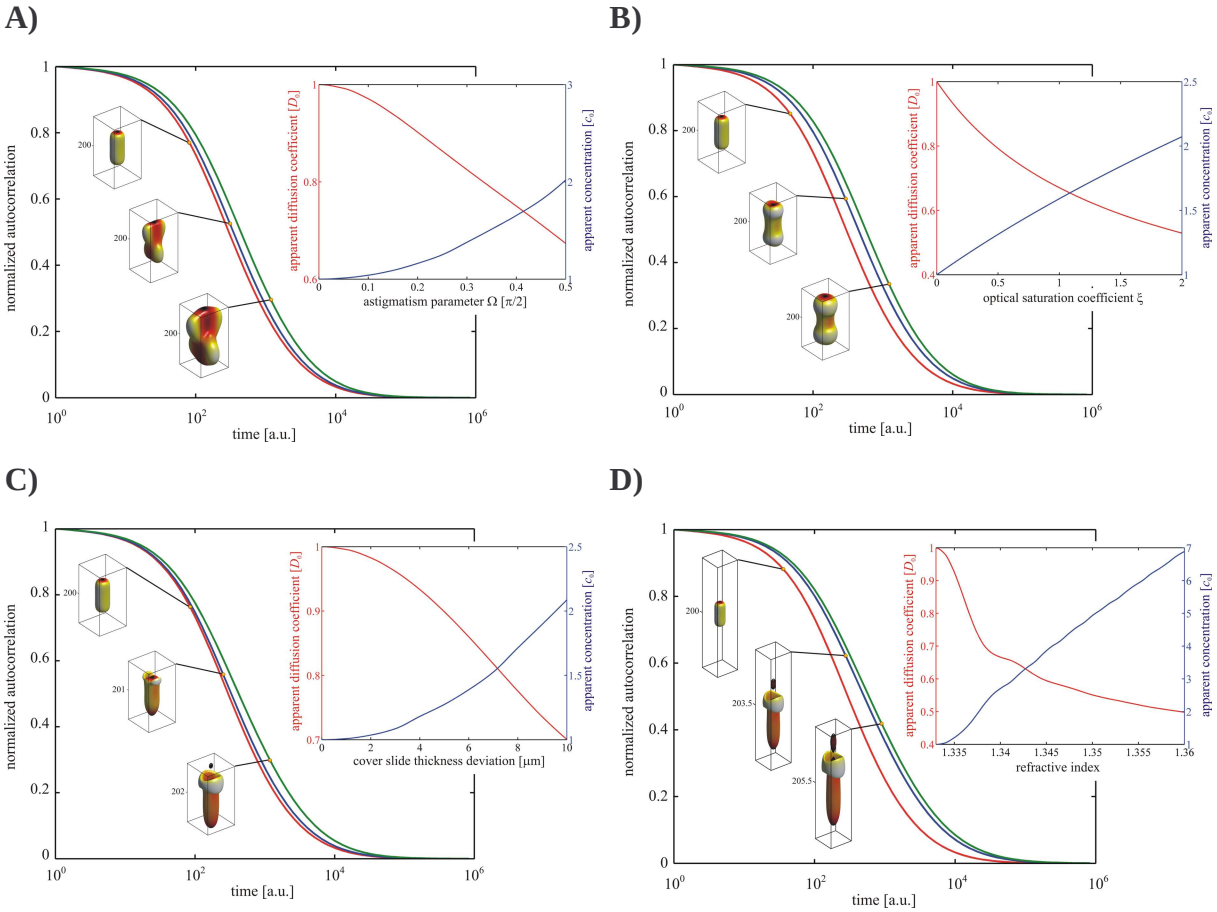

Fig. 4: Wave-optical calculations concerning the effect of the molecule detection function on measured autocorrelation functions for different measurement conditions. The large windows show the measured autocorrelation functions and the corresponding molecule detection function (within small boxes) The red curve is the ideal autocorrelation function, as it would appear if no aberrations are present. Blue and green curves are calculated for an increasing influence of the aberration. The insets show the extracted, apparent diffusion coefficients and concentrations. A) Laser beam astigmatism. B) Optical saturation. C) Coverslide thickness deviation. D). Refractive index mismatch. The setup parameters (such as position of the focus above the coverslide, excitation wavelength, etc.) were chosen to be the likely parameters of a commercial available FCS system, even though they are not necessary the ideal set of parameters. Figures are taken from (Enderlein *et al.*, 2005).

In this thesis we report on the development, implementation and application of a new and robust modification of FCS that we termed two-focus FCS (2fFCS) that fulfils two requirements:

1. It introduces an external ruler into the measurement by generating two overlapping laser foci of precisely known and fixed distance.
2. These two foci and corresponding detection regions are generated in such a way that the corresponding molecule detection functions are sufficiently well described by a simple two-parameter model yielding accurate diffusion coefficients when applied to two-focus FCS data analysis.

Both these properties enable us to measure absolute values of the diffusion coefficient with very high accuracy (relative error of ca. 2 %). Moreover, it will turn out that the new technique is robust against refractive index mismatch, coverslide thickness deviations, and optical saturation effects, which so often impair conventional FCS measurements. This thesis deals mainly with the introduction of the two-focus measurement scheme but also presents several applications reaching into the field of biophysics.

Thus, the result section of this work will start with proofing the robustness and precision of the new method. The newly developed molecule detection function model is checked against measurements, and it is shown that diffusion measurements give exact quantitative values and are no longer dependent on all the above mentioned artifacts.

Applications will be shown in section 7. There, we will demonstrate that even smallest changes in the hydrodynamic radius originating from conformational changes of proteins, namely calmodulin and recoverin, can be monitored.

The two-focus FCS measurement scheme will also be applied to measurements of diffusion in membranes (planar diffusion). We present results of lipid diffusion in supported lipid bilayers and lipid diffusion in giant unilamellar vesicles. In supported lipid bilayers, we observed surface adsorption/desorption of the diffusing molecules and thus had to develop an extended model for data evaluation (section 6).

A preliminary protein unfolding experiment is presented in section 7.3, pointing towards future applications.

4. Basic features of two-focus FCS

Here, the basic features of two-focus FCS (2fFCS) will be introduced. At first, the working principle and the setup will be presented and subsequently essential measurements will be shown in order to proof the validity of the proposed 2fFCS measurement scheme and also to characterize it.

4.1. Working principle and setup

As stated in the introduction, the two-focus FCS measurement scheme is based on two distinct features; one is the accurate description of the molecule detection function (MDF) with a simple two-parameter model, and the other is the use of two identical but laterally shifted and overlapping laser foci (laser A and B) of the same wavelength. For each of the laser foci separately, the measured autocorrelation curves (ACF) are identical because both foci (or more precisely their MDFs) are identical.

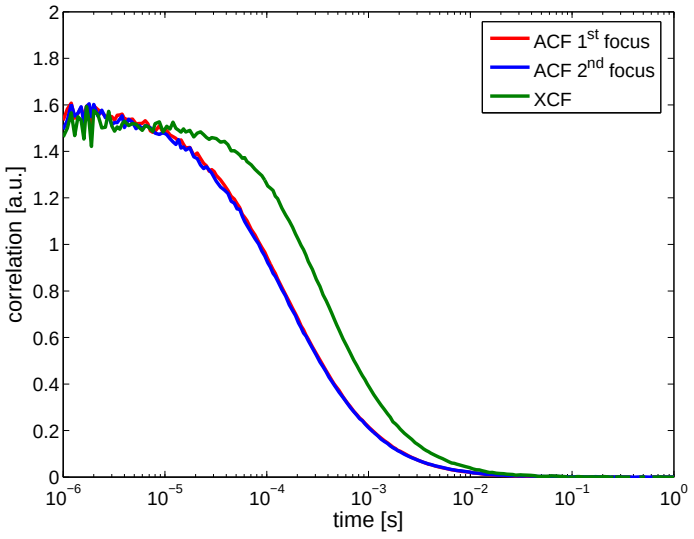

Fig. 5: Typical 2fFCS measurement result. The (normalized) autocorrelation curves for both lasers are identical (red and blue line), whereas the cross-correlation (green line) is shifted to longer lag times. To better visualize the shift in lag time, the amplitude of the cross-correlation curve is multiplied by a factor of 2.

However, in addition to the autocorrelation curves, one can also correlate the signal recorded from laser focus A with the signal from laser focus B and vice versa. This kind of correlation is called cross-correlation. The resulting cross-correlation function (XCF) is directly proportional to the probability to detect a photon caused by laser B at time τ if there was a photon detection event from laser A at time zero

(or *vice versa*). As long as there is no flow or any other active transport in the sample, the cross-correlation curves ($A \rightarrow B$ and $B \rightarrow A$) are identical and can be summed up. Thus, a typical 2fFCS-measurement consists of three correlation curves (two autocorrelation- and one cross-correlation curve) as shown in Fig. 5.

The shape of an autocorrelation curve is completely determined by the shape and size of the underlying MDF, whereas the shape of the cross-correlation curve is also dependent on the overlap of both foci. The equations describing these features can be found in the Appendix. Here we will focus on the qualitative aspects of the three correlation curves.

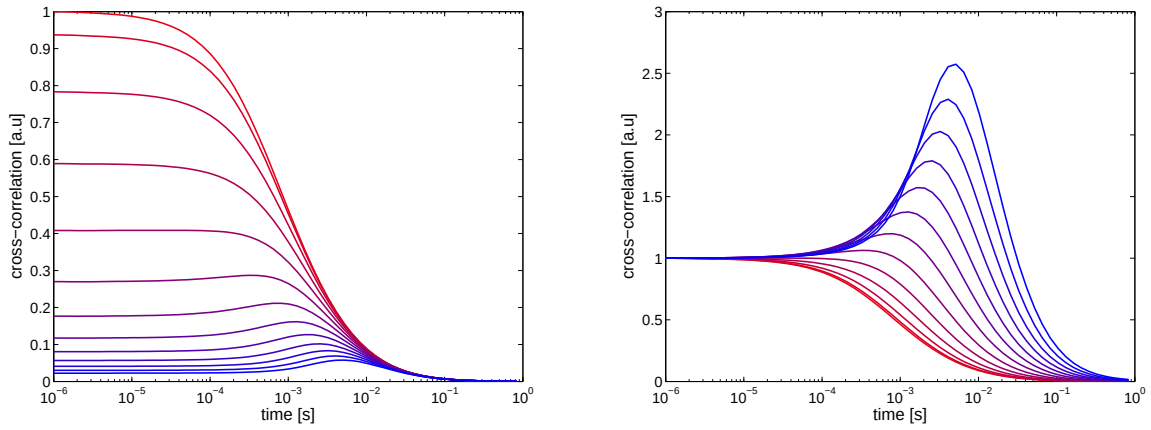

Fig. 6: Wave-optically calculated correlation curves for a typical 2fFCS setup for different degrees of foci overlap. The degree of overlap was realized by changing the distance between the foci. The figures on the left and right are representing the same cross-correlations, however in the right figure all curves are normalized to an initial amplitude of one. In case of vanishing distance between the foci, the XCF is identical to the ACF (red line), whereas stepwise (100 nm) incrementing the distance (red to blue lines) leads to a drop of amplitude (see left figure) and shifts the decay to longer lag times (see right figure). In the case of only a small overlap, the XCF experiences an increase before dropping to zero. This can be understood when taking into account, that for large distances the molecule basically diffuses out of one focus before entering the second.

It is evident that the more the two foci overlap, the more the resulting cross-correlation curve will resemble the autocorrelation curves because the time necessary for diffusing from one focus to the other approaches zero as the distance between them approaches zero. On the other hand, if the foci are put farther apart, the inter-diffusion time will increase, whereas the probability that a molecule is seen in laser focus A and subsequently in laser focus B decreases as the overlap decreases. As a consequence, the cross-correlation amplitude will drop as the overlap decreases, whereas its decay will shift to longer lag times. Also, the measurement time will increase because it will take longer time to record

less probable events. For illustration, Fig. 6 shows results from wave-optical calculations concerning the shape of the cross-correlation function for different degrees of focus overlap.

If the distance between the foci is known, a global fitting of both auto- and cross-correlation curves will yield an absolute value of the diffusion coefficient because the time delay of the cross-correlation relative to the autocorrelation scales with the square of the distance between foci divided by the diffusion coefficient. Moreover, the relation between cross-correlation to autocorrelation amplitude will be a direct measure of focus overlap. This poses a very restrictive and thus stabilizing fit-criterion. However, before applying a quantitative fit, it is still necessary to have an appropriate description of the MDF. This description will be given and verified in the following section 4.2.

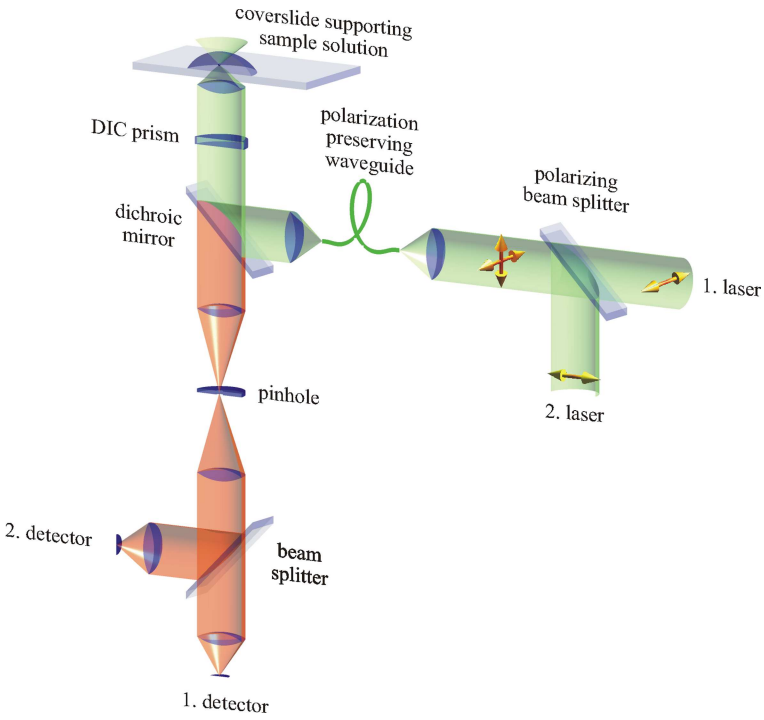

Fig. 7: Schematic of the 2fFCS setup. Excitation is done by two interleaved pulsed lasers of the same wavelength. The polarization of each laser is linear but orthogonal to each other. Light is then combined by a polarizing beam splitter and coupled into a polarization-maintaining, single-mode optical fiber. After exiting the fiber, the laser light is collimated by an appropriate lens and reflected by a dichroic beam splitter through a DIC prism. The DIC prism separates the laser light into two beams according to the polarization of the incoming laser pulses. The microscope objective focuses the two beams into two laterally shifted foci. Fluorescence is collected by the same objective. The tube lens focuses the detected fluorescence from both excitation foci on a single pinhole. Subsequently, the fluorescence light is split by a 50/50 beam splitter and detected by two single-photon avalanche diodes.

Concerning the technical realization of a 2fFCS setup, there are two key problems to be solved: (i) A sub-micron distance between the laser foci has to be established which is not to vary during an experiment. Furthermore, for sake of simplicity, it would be favorable if the distance would be fixed at a known value, otherwise one would have to readjust (or at least to re-measure) this distance every time before a 2fFCS-measurement is started. (ii)

One has to consider that in confocal microscopy there is no information on the spatial origin of the detected photons. When working with overlapping laser foci, this circumstance raises the question how detected photons can be assigned to one or the other laser focus. In the following, the setup of the 2fFCS measurement scheme will be presented and thus it will be explained how the above mentioned problems have been solved.

The 2fFCS setup is based on a conventional, confocal epi-fluorescence microscope as described in detail by Böhmer *et al.* (Böhmer *et al.*, 2001) and schematically shown in Fig. 7. However, instead of using a single excitation laser, the light of two identical, linearly polarized, pulsed diode lasers at 640 nm wavelength (LDH-P-635, PicoQuant, Berlin, Germany) is combined by a polarizing beam splitter (Narrow Band Polarizing Beamsplitter Cube 633, Ealing Catalogue, St. Asaph, UK).

The laser pulses have 50 ps pulse duration, and both lasers are pulsed *alternately* with an overall repetition rate of 40 MHz (pulsed interleaved excitation or PIE (Müller *et al.*, 2005)). Alternate pulsing is accomplished by dedicated laser driver electronics (PDL 808 “Sepia”, PicoQuant, Berlin, Germany). Both beams are then coupled into a polarization-maintaining single-mode fiber. At the output, the light is again collimated. Thus, the combined light consists of a train of laser pulses with alternating orthogonal polarization. The beam is then reflected by a dichroic mirror (Q 660 LP, Chroma Technology, Rockingham, VT, USA) towards the microscope’s water-immersion objective (UPLAPO 60× W, 1.2 N.A., Olympus Europa, Hamburg, Germany). Before entering the objective, the light beam is passed through a Nomarski prism (U-DICTHC, Olympus Europa, Hamburg, Germany) that is normally exploited for differential interference contrast (DIC) microscopy. The principal axes of the Nomarski prism are aligned with the orthogonal polarizations of the laser pulses, so that the prism deflects the laser pulses into two different directions according to their corresponding polarization. After focusing the light through the objective, two overlapping excitation foci are generated, with a small lateral shift between them. The distance between the beams is uniquely defined by the chosen DIC prism and is, in our system, equal to 403 nm, as measured by z-scan FCS (see section 4.3).

Fluorescence is collected by the same objective (epi-fluorescence setup), passed through the DIC prism and the dichroic mirror, and focused into a single circular aperture (diameter 200 μm) which is positioned symmetrically with respect to both focus positions and chosen to be large enough to let the light from both foci pass easily. Magnification of

imaging onto the confocal aperture was 58×, using a tube lens of 175 mm focal length. After the pinhole, the light is collimated, split by a non-polarizing beam splitter cube (Linos Photonics GmbH & Co. KG, Göttingen, Germany) and focused onto two single-photon avalanche diodes (SPCM-AQR-14, Perkin Elmer, Wellesley, MA, USA). Photon correlation was only calculated between photons of different SPADs in order to prevent any deterioration of the ACF due to SPAD afterpulsing, see e.g. (Enderlein & Gregor, 2005). A dedicated single-photon counting electronics (TimeHarp 200, PicoQuant, Berlin, Germany) is used to record the detected photons. The electronics operates in time-tagged, time-resolved (TTTR) mode (Böhmer *et al.*, 2001), recording for every detected photon its macroscopic arrival time with 100 ns temporal resolution, and its arrival time with respect to the last laser pulse with picosecond temporal resolution (time-correlated, single-photon counting or TCSPC (O'Connor & Phillips, 1984)).

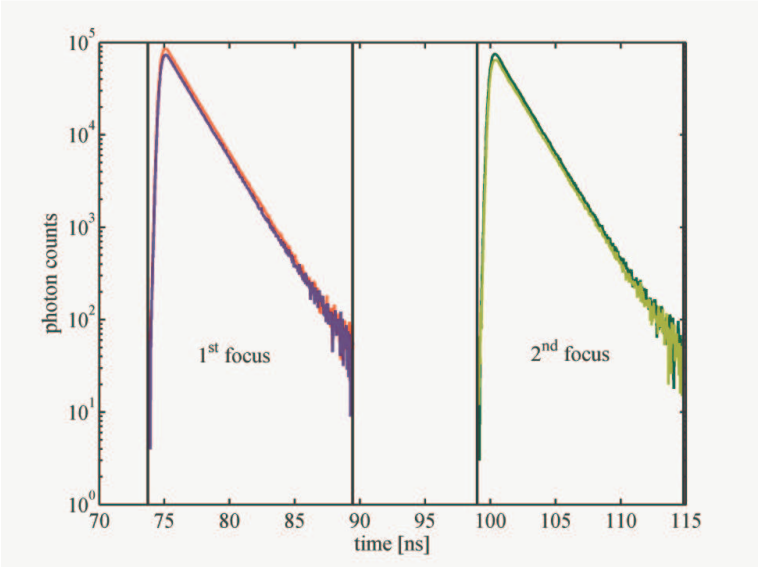

Fig. 8: TCSPC histograms measured on an aqueous solution of Atto655. The photon counts in left time window (73 ns ≤ *t* ≤ 89 ns) are generated by the first laser, i.e. first focus, the photon counts in the second time window (99 ns ≤ *t* ≤ 115 ns) are generated by the second laser, i.e. second focus. In both time windows (limited by gray lines in the figure), there are two curves corresponding to the two SPAD detectors, respectively.

The TCSPC times of each recorded photon are used to decide which laser has excited which fluorescence photon, i.e. in which laser focus/detection volume the light was generated. A typical TCSPC histogram measured on an aqueous solution of Atto655 is shown in Fig. 8. The figure shows two time-shifted fluorescence decay curves (fluorescence lifetime of ca. 2 ns) that correspond to the two alternately pulsing lasers. Temporal distance between laser pulses was 25 ns so that the total probability of detecting a photon from a previous pulse after the next one is $e^{-12.5} \approx 4 \cdot 10^{-6}$, and the chance of associating a detected photon with the wrong laser focus is negligibly small. For fluorescent dyes with significantly longer lifetime, one has to use a sufficiently

lower repetition rate for preventing bleed-through between the two time windows. Knowing which photon was generated in which detection volume, autocorrelations for each detection volume, as well as cross-correlation functions between the two detection volumes are calculated by custom-written software on a PC using *Matlab* (Wahl *et al.*, 2003). When scanning beads, the resulting point spread function can be extracted following the same principle.

When working with water immersion objectives, a crucial experimental parameter is the correct adjustment of the objective's correction collar to the actual thickness of the used coverslide. Even small deviations between adjusted and actual thickness can have profound effects on the resulting MDF (Enderlein *et al.*, 2005). We used the method proposed in (Schwertner *et al.*, 2005) for setting the objective's adjustment collar correctly.

4.2. Measuring and fitting the molecule detection function

Having introduced the working principle and the 2fFCS-setup, we now turn to the first prerequisite feature of 2fFCS – the two-parameter MDF-model.

For a quantitative evaluation of recorded fluorescence correlation curves it is crucial to have a realistic description of the underlying MDF. Unfortunately, there is no direct way to measure the MDF. Instead, we will equivalently evaluate the point spread function (PSF) of confocal imaging microscopy by scanning a fluorescent point source along all three dimensions. The equivalence between PSF and MDF in an FCS experiment however applies only if the fluorescing molecules exhibit sufficiently fast rotational diffusion leading to a decoupling between their orientation during light absorption and fluorescence emission (Enderlein *et al.*, 2005). This requirement is most likely matched in all presented measurements, because a single dye has sufficiently fast rotational diffusion times (< ns). If bound to a protein or lipid it is most likely that due to the dyes linker there is also no coupling between absorption and emission dipole of the dye molecule.

In conventional FCS, the MDF is often described by a three-dimensional Gaussian (3DG) distribution. This has the advantage that the resulting correlation function can be written in a closed analytical form. Although the 3DG distribution is a common assumption when evaluating correlation curves (Rigler *et al.*, 1993; Kettling *et al.*, 1998; Chen *et al.*, 1999; Schwille *et al.*, 2000; Chattopadhyay *et al.*, 2005; Nagy *et al.*, 2005a), it is definitely not an accurate description of the actual MDF. Here, we introduce an

alternative description of the MDF that also depends (like the 3DG distribution) on only two parameters but is much better suited for evaluating recorded correlation curves.
A matching expression for the MDF is given by.

$$U(\boldsymbol{r}) = \frac{\kappa(z)}{w^2(z)} exp\left[-\frac{2}{w^2(z)}\left(x^2+y^2\right)\right] \tag{4.1}$$

where $\{x, y, z\}$ are Cartesian coordinates with z along the optical axis, $U(\boldsymbol{r})$ denotes the MDF and $w(z)$ and $\kappa(z)$ are given by:

$$w(z) = w_0\left[1+\left(\frac{\lambda_{ex} z}{\pi w_0^2 n}\right)^2\right]^{1/2} \tag{4.2}$$

and

$$\kappa(z) = 2\int_0^a \frac{\rho}{R^2(z)} exp\left(-\frac{2\rho^2}{R^2(z)}\right) d\rho = 1 - exp\left(-\frac{2a^2}{R^2(z)}\right) \tag{4.3}$$

The function $R(z)$ is defined by an expression similar to Eq. (4.2):

$$R(z) = R_0\left[1+\left(\frac{\lambda_{em} z}{\pi R_0^2 n}\right)^2\right]^{1/2} \tag{4.4}$$

In the above equations, λ_{ex} is the excitation wavelength, and λ_{em} the center emission wavelength, n is the refractive index of the immersion medium (water), a is the radius of the confocal aperture divided by magnification, and w_0 and R_0 are two (generally unknown) model parameters. Eq. (4.2) is nothing other than the scalar approximation for the radius of a diverging laser beam with beam waist radius w_0 (see for example (Enderlein & Pampaloni, 2004)), and Eq. (4.3) is inspired by earlier work of Qian and Elson (Qian & Elson, 1991) and Rigler *et al.* (Rigler *et al.*, 1993) concerning the point spread function of confocal imaging. It should be noted that, although Eq. (4.1) looks like the sometimes-used Gauss-Lorentz profile, it is *not* such a profile due to the presence of

the non-trivial amplitude function $\kappa(z)$ given in Eq. (4.3). Thus, in each plane perpendicular to the optical axis, the MDF is approximated by a 2D-Gaussian distribution having width $w(z)$ and amplitude $\kappa(z)/w^2(z)$.

The above equations are becoming slightly more complex when the laser focus is not described by a circular but an elliptic Gaussian distribution (which is always the case when focusing a linearly polarized beam). Assuming that the principal axes of the laser beams are parallel to the *x*- and *y*-axes, and denoting now the smallest beam waist radii along the principal axes with $w_{0,x}$ and $w_{0,y}$, one now has two functions $w_x(z)$ and $w_y(z)$ describing the laser profile, and $w^2(z)$ has to be replaced by $\left[w_x^2(z)+w_y^2(z)\right]/2$. To keep things simple and not to increase the number of independent parameters, we will assume that the *effective* radius $w_{eff}(z)=\sqrt{\left[w_x^2(z)+w_y^2(z)\right]/2}$ is still sufficiently well described by the right hand side of Eq. (4.2) with a single parameter w_0.

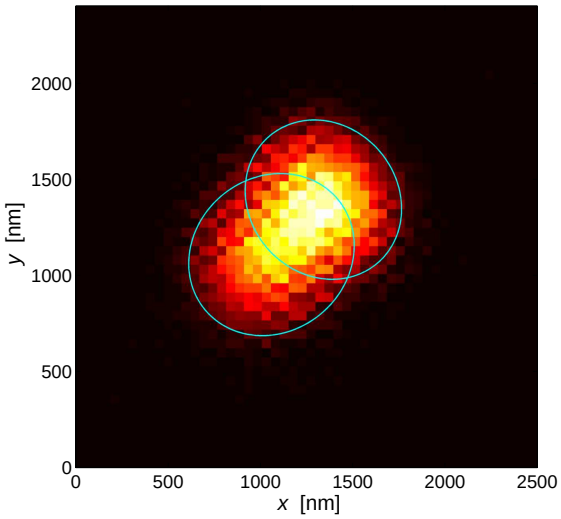

Fig. 9: Fluorescence intensity scan of a fluorescent bead. Scan plane was the plane of laser beam waist. Solid line shows the 1/e^2-contour of the Gaussian distributions fitted to both laser foci separately. Notice the ellipticity of the laser foci, which is the result of focusing linearly polarized lasers with an objective of high numerical aperture. The 1/e^2-half axes of the foci are 425 nm and 455 nm for the first focus (top right) and 425 nm and 465 nm for the second focus (bottom left). Because both lasers are polarized orthogonally to each other, elongation of both foci is also orthogonal to each other. Laser polarizations as well as principal axes of the Nomarski prism are parallel to the image diagonals.

The MDF-model in Eq. (4.1) was checked by direct measurement. Immobilized fluorescent beads were scanned at different vertical positions of the objective, choosing a distance of 0.5 µm between adjacent scan planes. Each scan consisted of 200 x 200 pixels^2 of 50 x 50 nm^2 size. Total excitation power was below 1 µW. Using PIE (or ALEX, see

section 4.1), separate fluorescence images for each laser were reconstructed simultaneously for each scan. A typical scan result is displayed in Fig. 9, showing the measured fluorescence intensity distributions in the plane of the beam waist of the focused lasers.

The recorded fluorescence intensity distribution in each plane was fitted by a two-dimensional Gaussian distribution, thus obtaining values of the functions $w_{x,y}(z)$ and $\kappa(z)$ at the various *z*-positions of the objective. The result for the *effective* radius $w_{eff}(z)$ for both detection regions is shown in Fig. 10, together with a fit using Eq. (4.2).

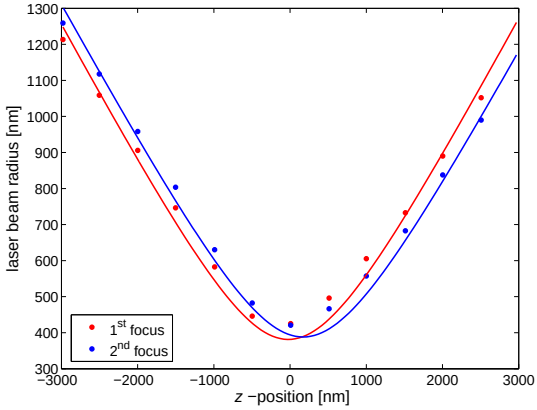

Fig. 10: Dependence of the effective beam radius $w_{eff}(z)$ of the two MDFs on vertical scan position. Solid lines are fits of Eq. (4.2) to the measured values (circles). Note that the three-dimensional Gaussian model would expect a constant beam waist over the whole z-position range.

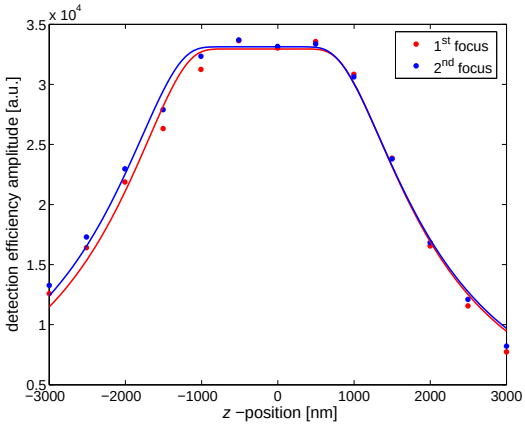

Fig. 11: Dependence of the amplitude factor $\kappa(z)$ of the two MDFs on vertical scan position. Solid lines are fits of Eqs. (4.3) and (4.4) to the measured values (circles).

Fig. 11 shows the determined values of $\kappa(z)$ together with a fit using Eqs. (4.3) and (4.4). As can be seen from both Fig. 10 and Fig. 11, the empirical two-parameter model of the MDF fits the measured MDF amazingly well. It has to be emphasized that this is far from trivial: Eq. (4.2) fixes the relation between minimum width w_0 of the MDF and its divergence. This assumption is inspired by the scalar approximation of the intensity profile of a focused laser beam. However, there is no *a priori* reason why Eq. (4.2) should be an excellent description of the *z*-dependence of the Gaussian width of the MDF, taking into account that (i) laser focusing is done with a high-N.A. objective when one could expect increasing deviation from a scalar beam approximation due to strong non-paraxiality of focusing in connection with the vector character of the electromagnetic field, and that (ii)

the MDF is not only defined by the laser intensity distribution, but also by the confocal detection.

Considering a fit with a 3DG model, it turns out, that the amplitude of the MDF can be fitted equally well (not shown). However, when looking at Fig. 10 it is evident, that the beam waist radius w_0 is dependent on *z*-position, whereas the 3DG model postulates a constant beam waist radius w_0 all along the optical axis. Thus, the 3DG model fails to fit the MDF sufficiently well.

As stated in the beginning of this section, a good description of the MDF is crucial to evaluate the measured correlation curves quantitatively. The new model fulfils this requirement and will be used to fit measured 2fFCS curves. Out of these fits it is then possible to draw reliable values of the concentration of the dye, the effective volume of the MDF and of course the diffusion coefficient. This will be shown in section 5. In the next section the second essential parameter of the 2fFCS measurement scheme will be determined - the distance between the foci.

4.3. Determining the distance of the foci

Having a valid MDF model, this section deals with the determination of the exact distance between the two foci of the 2fFCS setup. Since the diffusion coefficient scales proportional to the square of the adopted focus distance (see Appendix), the knowledge of the exact distance between the two foci is crucial in order to achieve precise, absolute values for diffusion coefficients. For example, for keeping the error of the estimated diffusion coefficient smaller than 4 %, this value has to be known with an error smaller than 2 %.

We repeated MDF scans several times with different beads and determined the lateral shift between the two detection volumes as the distance between the centers of the fitted Gaussian distributions in the plane of the beam waist. We found the value of δ to be equal to 400 ± 40 nm. The large variation of this value has several origins. One of them occurred to be the inaccuracy of the stepping of the used piezo-table which showed non-systematic step-size variations of up to 10 %, as was checked by direct imaging of the piezo-table movement using a transparent grid structure with known grid periodicity. Another origin was the limited signal-to-noise ratio and resulting inaccuracy of the Gaussian distribution fits. In order to determine the distance δ between the foci more precisely we adopted another method.

When considering FCS measurements in planar systems, there exists another method that yields absolute values of diffusion coefficients without *a priori* knowledge of the exact MDF of the confocal system, namely the *z*-scan technique developed by Martin Hof and his group (Benda *et al.*, 2003; Humpolickova *et al.*, 2006). It is based on the validity of Eq. (4.2), i.e. on a stringent correlation between divergence and waist of the MDF. We have verified the accuracy of this assumption by direct wave-optical calculation (Enderlein & Dertinger, 2007) as well as by scanning the MDF as was shown in the preceding section (see Fig. 10). In what follows, we give a brief introduction into the *z*-scan technique; a more detailed derivation is given in Appendix.

Since two-dimensional, planar diffusion proceeds orthogonally to the optical axis (z-direction) of the microscope, the corresponding two-dimensional MDF can be derived by taking a slice of the three-dimensional MDF in Eq. (4.1) at the appropriate *z*-position. Thus, the two-dimensional MDF is given by

$$U(\boldsymbol{r}) = U(x,y \mid z_0) = \frac{\kappa(z_0)}{w^2(z_0)} exp\left[-\frac{2}{w^2(z_0)}\left(x^2+y^2\right)\right] \tag{4.5}$$

Note that in the above equation z_0 is fixed and for each plane $U(\boldsymbol{r})$ is described by a two-dimensional Gaussian distribution with a focus radius given by (see also Eq. (4.2)):

$$w(z_0) = w_0\left[1+\left(\frac{\lambda_{ex} z_0}{\pi w_0^2 n}\right)^2\right]^{1/2} \tag{4.6}$$

When applying the *z*-scan technique, one measures ACFs of diffusing molecules within a planar lipid membrane for different vertical positions z_0 of the membrane with respect to the focal plane and estimates the diffusion time $\tau_D(z_0)$ by fitting the ACF. The diffusion time τ_D is defined as the time the ACF has dropped to 50 % of its initial value and in the case of two-dimensional planar diffusion is given by:

$$\tau_D(z_0) = \frac{w(z_0)^2}{4D} = \frac{w_0^2}{4D}\left[1+\left(\frac{\lambda_{ex} z_0}{\pi w_0^2 n}\right)^2\right] \tag{4.7}$$

wherein *D* denotes the diffusion coefficient.

Thus, as can be seen from Eq. (4.7), plotting $\tau_D(z_0)$ as a function of the vertical position of the laser focus z_0 (i.e. the objectives position) will lead to a parabolic graph. This graph is fitted with the diffusion coefficient *D* and the focus beam waist w_0 as fit parameters and yields absolute values for both independently. This measurement scheme is called *z*-scan FCS or *z*-scan technique.

Of course, 2fFCS can also yield the absolute value for the diffusion coefficient in planar systems. As shown in Appendix, the (normalized) correlation functions of 2fFCS for two-dimensional planar diffusion are given by:

$$g_{norm}(t \mid z_0, \delta) = \frac{1}{\pi c} \frac{1}{4Dt + w(z_0)^2} \exp\left[-\frac{\delta^2}{4Dt + w(z_0)^2} \right] \tag{4.8}$$

Since a 2fFCS measurement yields two (identical) ACFs and one XCF (see section 4.1), dividing the measured XCF by the ACF (setting $\delta = 0$ in the above equation) leads to:

$$\frac{XCF_{norm}}{ACF_{norm}} = \exp\left[-\frac{\delta^2}{4Dt + w(z_0)^2} \right] = \exp\left[-\frac{\overbrace{\delta^2/4D}^{p_1}}{\underbrace{w(z_0)^2/4D}_{p_2} + t} \right] \tag{4.9}$$

It is evident that from the fitting parameter p_1 either the diffusion coefficient or the distance between the two foci can be extracted already from a single measurement. From p_2 the focus radius $w(z_0)$ can be derived. Thus, we have estimated the distance between the two foci in the following way:

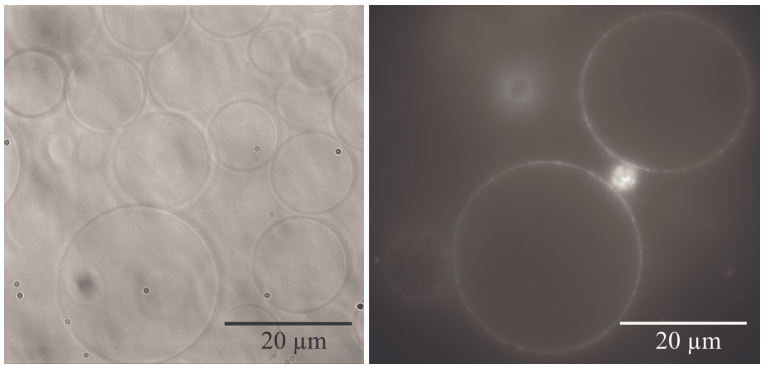

Fig. 12: Wide field microscopy images of typical GUVs made of DOPC labeled with DOPE-Atto655. Left: Light microscope image of GUVs. Right: Fluorescence image of fluorescently labeled GUVs.

We performed 2fFCS measurements on lipid diffusion within the lipid bilayer of a giant unilamellar vesicle (GUV, see Fig. 12) at different *z*-positions. Then, we applied the *z*-scan data evaluation for the whole set of measured ACFs and estimated $\tau_D(z)$ respectively $w(z)$ and therefore extracted the diffusion coefficient *D* as described in Eq. (4.7). Simultaneously, for each vertical position z_0, Eq. (4.9) was used to globally fit the auto and cross-correlation functions and to yield a diffusion coefficient. Demanding that the estimated diffusion coefficients *D* from both methods are identical yielded the correct value of δ of the 2fFCS setup.

A typical 2fFCS measurement including the corresponding fits is shown in Fig. 13. The 2fFCS *z*-scan was performed on the same GUV twice; by first moving the focus up and afterwards down, thus verifying that there was no mechanical vertical drift of the measurement system during the experiment. Both *z*-scans yielded the identical value of 403 nm for δ, a value in excellent agreement with the manufacturer's specifications for the used Nomarski (or

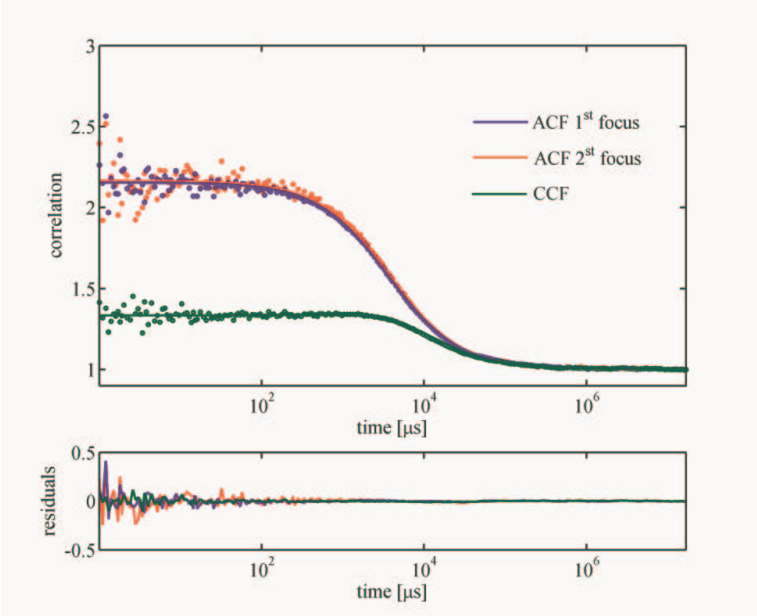

Fig. 13: 2fFCS measurement of lipid diffusion in a GUV. Lipids were sparsely labeled with Atto655. Total cw-excitation power (both lasers together) was 2 µW, measurement time was 10 min. Circles are experimental values, solid lines are global fits using Eq. (4.8).

DIC) prism. We adopted the value of $\delta = 403$ nm for the whole subsequent 2fFCS data analysis. This parameter is the basic characteristic of the 2fFCS setup; fixing the length scale of the diffusion measurement. For a given excitation wavelength, it is completely determined by the optical properties of the used Nomarski prism and does not depend on optical parameters such as coverslide thickness, sample refractive index, laser beam diameter etc.

Since the Nomarski prism generates two *parallel* light beams in the sample, which are identical to the laser foci generated without the prism, but shifted perpendicularly to the optical axis (Munro & Török, 2005), any aberrations caused by stratified media oriented perpendicular to optical axis may deform the focused light intensity-distribution but does not change the distance between the axes of propagation of both foci (Török *et al.*, 1995; Török & Varga, 1997). A similar optical argument applies also for the detection, see again (Munro & Török, 2005) and (Haeberlé *et al.*, 2003; Enderlein & Böhmer, 2003).

In practice, the best way to determine precise value of the interfocal distance is to perform a 2fFCS measurement on a reference sample with precisely known diffusion, which is much simpler than performing a full *z*-scan on a GUV. Since we could not find a reliable reference value for a diffusion coefficient of a suitable red fluorescent dye, we used the *z*-scan approach in order to evaluate the distance between the two foci precisely. It should be noted that we performed the measurements on GUVs instead of using supported lipid bilayers for preventing any potential artifacts stemming from the interaction between lipids and the support.

5. Diffusion of Atto655 and Cy5 under various conditions

After having determined the distance between the foci (4.3) and having checked the quality of the new MDF model (4.2), this section will show that the 2fFCS measurement scheme is independent of typical artifacts of conventional FCS, i.e. that the measured diffusion coefficient is neither dependent on refractive index mismatch between the immersion water and the sample solvent, nor on optical saturation. Concerning optical saturation effects in conventional FCS, it was stated (Enderlein *et al.*, 2005):

"Optical saturation occurs when the excitation intensity becomes so large that the molecule spends more and more time in a non-excitable state, so that increasing the excitation intensity does not lead to a proportional increase in emitted fluorescence intensity […]. The most common sources of optical saturation are: (i) excited-state saturation, that is, the molecule is still in the excited state when the next excitation photon arrives; (ii) triplet-state saturation, that is, the molecule undergoes intersystem crossing from the excited to the triplet state so that it can no longer become excited until it returns back to the ground state; (iii) other photoinduced transitions into a non-fluorescing state, such as the photoinduced cis–trans isomerization in cyanine dyes, or the optically induced dark states in quantum dots."

The exact relationship between fluorescence emission intensity and excitation intensity can be very complex (Enderlein, 2005) and is even dependent on the excitation mode (pulsed or continuous wave) (Gregor *et al.*, 2005). In contrast to other optical artifacts of FCS, optical saturation makes even comparative measurements of diffusion coefficients problematic because the fluorescence properties of many fluorescing dyes used for labeling of proteins, DNA, or RNA, are changing upon binding to the molecules (most often due to changes in intersystem crossing rate). Even worse, as was shown both experimentally (Gregor *et al.*, 2005) and theoretically (Enderlein *et al.*, 2005), the change of apparent diffusion coefficient with increasing excitation intensity is largest in the limit of infinitely small intensity, making even an extrapolation of measured values toward zero excitation-intensity difficult and imprecise.

It should be noted that any kind of aberration inflates the MDF (see for example Fig. 4 in the Introduction). Thus, depending on the degree of aberration, the overlap of the two

shifted foci will change as well as the relative amplitudes between the ACF and the XCF (see section 4.1). Also the resulting fit-values for the beam waist parameter w_0 of the new MDF-model (section 4.2, Eq. (4.1), (4.2)) and its amplitude-determining parameter R_0 from Eq. (4.4), will reflect aberrations of the MDFs. But since the distance between the foci remains constant, the diffusion coefficient should not be affected.

We determined the diffusion coefficient of the red fluorescent dye Atto655 (in its carboxylic acid (COOH) form) under refractive-index mismatch as well as under optical saturation. Atto655-(COOH) was chosen because it has the particular property that it does not show any discernable triplet-state dynamics when solved in water. This makes it an ideal dye for checking FCS-based diffusion measurements. The missing triplet dynamics eases the impact of optical saturation on the resulting ACFs because only excited state saturation can take place but no switching into a long-living non-fluorescent triplet state. Thus, the impact of optical saturation on 2fFCS was additionally checked by measuring diffusion of the red fluorescent cyanine dye Cy5-(COOH) which shows strong photoinduced cis-trans isomerization. Since the cis-state is non-fluorescent and has a relaxation time in the order of microseconds (Widengren & Schwille, 2000), optical saturation is much stronger for Cy5 than for Atto655.

In the following we will introduce the equations needed for this section (for a detailed derivation refer to Appendix). We will turn our attention to the explicit expression of the 2fFCS correlation function, since this function will be used to fit the achieved correlation curves.

Starting from the very general description of the correlation function

$$g(\tau) = \langle I(t+\tau) I(t) \rangle \tag{5.1}$$

which describes the probability to detect a photon at time $\tau + t$ when there was a photon detected at time *t,* it is possible to further specify this description for a conventional confocal microscope to

$$g(t) = \varepsilon^2 c \int_V \int_V U(\mathbf{r}_1) G(\mathbf{r}_1 - \mathbf{r}_2, t) U(\mathbf{r}_2) d\mathbf{r}_1 d\mathbf{r}_2 + \left[\varepsilon c \int_V U(\mathbf{r}) d\mathbf{r} + I_{bg} \right]^2 \tag{5.2}$$

wherein ε represents the overall excitation power and detection efficiency (including the fluorophores properties, such as quantum yield and extinction coefficient). c is the concentration of fluorescent molecules in *molecules / sample volume V*; $U(\boldsymbol{r})$ denotes the probability density to detect a photon from a molecule located at $\boldsymbol{r}$, that is the MDF; I_{bg} is the background intensity which accounts for uncorrelated detection events, such as dark counts from the detectors etc. and $G(\boldsymbol{r_1}\text{-}\boldsymbol{r_2},t)$ the Green's function describing the probability density that a molecule moves from $\boldsymbol{r_1}$ to $\boldsymbol{r_2}$ within time *t*.

For free diffusing in *d* dimensions, the Green function is given by

$$G(\boldsymbol{r}_1-\boldsymbol{r}_2,t)=\frac{1}{(4\pi Dt)^{d/2}}exp\left[-\frac{(\boldsymbol{r}_1-\boldsymbol{r}_2)^2}{4Dt}\right] \tag{5.3}$$

where D is the Diffusion coefficient. As can be seen from Eq. (5.2), the first term of the correlation function is time dependent, whereas the second term is a constant offset. For most applications, the time dependent part is most important because it contains all information of the temporal behavior of the fluorescent molecule. For this reason, one often displays the normalized correlation function, which is divided by the offset and decaying to zero for long lag times as:

$$g_{norm}(t)=\frac{g(t)}{g(\infty)}-1 \tag{5.4}$$

To extend this formalism to the cross-correlation of an 2fFCS measurement, the distance δ has to be introduced into Eq. (5.2). This is surprisingly easy since a laterally shifted MDF can be described by the simple coordinate transformation (without losing generality, we shift one MDF along the x-axis) $\boldsymbol{r_1}\rightarrow\boldsymbol{r_1}+\delta\boldsymbol{x}$. Also, if excitation power is different in both foci, ε in Eq. (5.2) has to be replaced by two values ε_1 and ε_2, respectively. Then, Eq. (5.2) can be written as:

$$g(t,\delta)=\varepsilon_1\varepsilon_2 c\int_V\int_V U(\boldsymbol{r}_1)G(\boldsymbol{r}_1-\boldsymbol{r}_2-\delta\boldsymbol{x},t)U(\boldsymbol{r}_2)\,d\boldsymbol{r}_1 d\boldsymbol{r}_2+g_\infty \tag{5.5}$$

where g_∞ is given by:

$$g_\infty = \left[\varepsilon_1 c \int_V U(\boldsymbol{r_1})\, d\boldsymbol{r_1} + I_{bg} \right] \left[\varepsilon_2 c \int_V U(\boldsymbol{r_2})\, d\boldsymbol{r_2} + I_{bg} \right] \tag{5.6}$$

Inserting the MDF model from 4.2, Eq. (4.1) does not lead to a closed analytical form of the auto/cross-correlation in the case of three-dimensional diffusion (in contrast to two-dimensional diffusion). Evaluation of the resulting expression has to be done numerically, which is fast and poses no hindrance to practical applications using state-of-the-art PCs. The explicit expression of Eq. (5.5), which is used for numerical integration, is given in the Appendix (Eq. (10.34)). Here we will give the correlation function as it appears after inserting the MDF model and the Green function for three-dimensional diffusion:

$$g(t) = g_\infty + \frac{\varepsilon_1 \varepsilon_2 c}{4} \sqrt{\frac{\pi}{Dt}} \int_{-\infty}^{\infty} \int_{-\infty}^{\infty} \frac{\kappa(z_1)\,\kappa(z_2)}{8Dt + w^2(z_1) + w^2(z_2)} \exp\left[-\frac{(z_2 - z_1)^2}{4Dt} \frac{2\delta^2}{8Dt + w^2(z_1) + w^2(z_2)} \right] dz_2 dz_1 \tag{5.7}$$

Least square data fitting is performed by applying Eq. (5.7) to the measured ACF ($\delta = 0\,nm$, $\varepsilon_1\varepsilon_2$ replaced by either ε_1^2 or ε_2^2) and XCF ($\delta = 403\,nm$) *simultaneously* in a global fit. As fit parameters one has $\varepsilon_1\sqrt{c}$, $\varepsilon_2\sqrt{c}$, D, w_0 and R_0, as well as three offset values g_∞ (one for each curve). As already stated in section 4.1, a crucial criterion of fit quality is not only to simultaneously reproduce the temporal shape of both ACFs and the XCF, but also to reproduce their three amplitudes $g_{t\to 0} - g_\infty$ using only the two parameters $\varepsilon_1\sqrt{c}$ and $\varepsilon_2\sqrt{c}$. Typical fitting time on a standard PC takes ca. 1 min using a custom written *Matlab* routine.

5.1. Refractive Index Mismatch

We measured correlation curves of Atto655 in aqueous solutions of guanidine hydrochloride (GdHCl) at different GdHCl concentrations. Both the refractive index and the viscosity of GdHCl solutions are strongly changing with increasing GdHCl

concentration (Kawahara & Tanford, 1966). Each measurement lasted for 10 minutes and for each GdHCl concentration, measurements were repeated ten times to determine a standard deviation for the estimated diffusion coefficient. A typical measurement result in an aqueous solution of Atto655 is shown in Fig. 14, together with a global fit of all three curves using Eq. (5.7). As can be seen, the obtained fit quality is excellent.

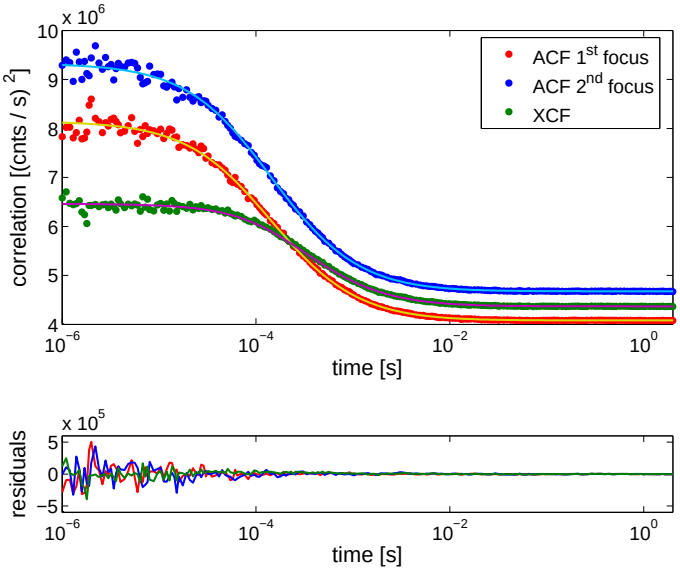

Fig. 14: 2fFCS measurement on a nanomolar aqueous solution of Atto655. Cw-excitation power (both lasers together) was 40 µW, measurement time was 10 min. The shape of both ACFs is virtually identical. Circles are experimental values, solid lines are global fits using Eq. (5.7). The different in offset value of both ACFs is due to slightly different excitation power for each focus.

The determined values of the diffusion coefficient for all measured solutions of GdHCl are shown in Fig. 15 as a function of the inverse value of viscosity. For checking the validity of the 2fFCS results, diffusion of Atto655 was measured in deuterated methanol using pulsed-field gradient NMR. The corresponding value is also shown in Fig. 15. Assuming that the diffusion coefficient is strictly proportional to the inverse of the viscosity (as the Stokes Einstein equation postulates, see Appendix), independent of the chemical nature of the solvent (GdHCl in water, deuterated methanol), a linear least square fit was applied to all GdHCl values of the diffusion coefficient and is also displayed in Fig. 15. The results demonstrate (i) that there is excellent agreement between the diffusion coefficient as determined by pulsed field gradient NMR and the absolute values obtained with 2fFCS; (ii) that the 2fFCS measurements at different GdHCl concentrations excellently reproduce the expected linear dependence of diffusion coefficient on the inverse value of viscosity, thus demonstrating that 2fFCS works well even for large mismatch between sample refractive index and the refractive index of the objective's immersion medium (pure water).

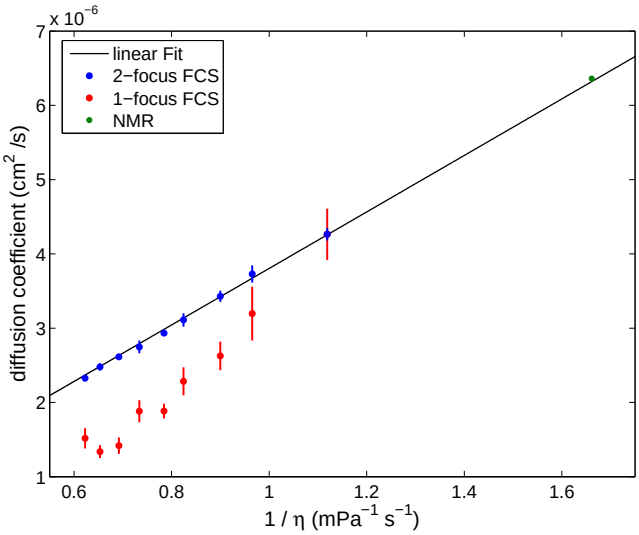

Fig. 15: Dependence of the diffusion coefficient of Atto655-(COOH) in aqueous GdHCl solutions and d4-methanol at 25 °C as a function of the inverse of solvent viscosity. Solid line is linear least square fit to all data. Standard deviations are shown as error bars and are each derived from ten repeated measurements for 2fFCS. The error bar of the NMR value indicates standard deviation of 0.5 %. The absolute value may vary by 4%. For comparison, the results of single-focus FCS using a standard model that assumes a three-dimensional Gaussian MDF are also shown. Because single-focus FCS can only measure relative values of diffusion coefficient, we took the value for pure water as the reference value.

In absolute numbers, the diffusion coefficient of Atto655-(COOH) in water at 25 °C, as determined with 2fFCS, is equal to (4.26 ± 0.08) 10^{-6} cm^2/s. The NMR value extrapolated to the viscosity of water is (4.29 ± 0.13) 10^{-6} cm^2/s. The increasing refractive index mismatch with increasing GdHCl concentration leads to increasingly larger fit values of w_0 and R_0 as shown in Fig. 16. This reflects the increasingly larger detection volume due to increasingly larger refractive index mismatch-induced optical aberrations. However, the used two-parameter model for the MDF is obviously flexible enough to approximate the shape of the distorted detection volumes well enough so that one still obtains correct values for the diffusion coefficient. This is an important feature of 2fFCS, making it an ideal tool for monitoring e.g. hydrodynamic radii of proteins during chemical unfolding in GdHCl solutions (Chattopadhyay *et al.*, 2005).

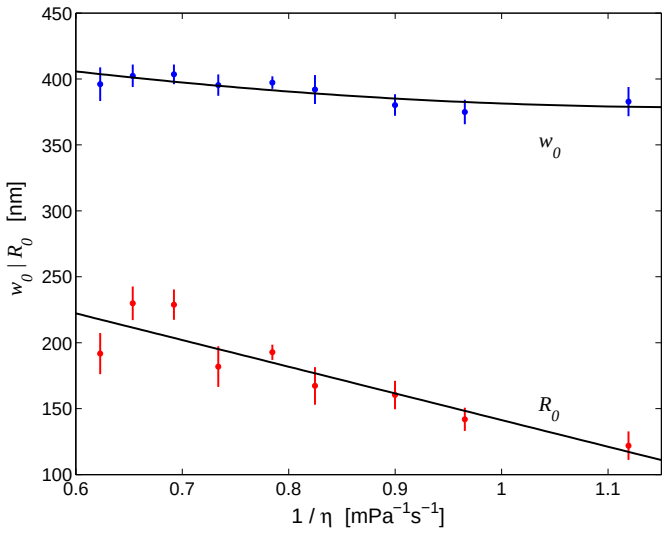

Fig. 16: Dependence of the fitted values of w_0 and R_0 on inverse viscosity (for better comparison with Fig. 15). Shown are experimental values (circles) and second order polynomial fits (solid lines). Both values increase with increasing viscosity and thus refractive index of the solution, reflecting a MDF changed by aberrations that are induced by refractive-index mismatch.

It should be mentioned that the insensitivity of 2fFCS with respect to refractive index mismatch also implies its insensitivity with respect to coverslide thickness deviations because these deviations introduce quite similar spherical aberrations as the refractive index mismatch. A rough comparison between aberrations induced by coverslide thickness deviation and refractive index mismatch can be done by equating the differences in the corresponding optical paths. For a solvent refractive index mismatch, the optical path difference is given by the difference of the solvent refractive index to the immersion medium's refractive index times the position of the focus above the coverslide, $\left(n_{solvent} - n_{immersion}\right) \cdot d_{focus}$. For a coverslide thickness deviation, the equivalent value can be calculated by taking the refractive index mismatch of glass to the immersion medium times the deviation in thickness from the design value, $\left(n_{glass} - n_{immersion}\right) \cdot d_{glass}$.

$$\left(n_{solvent} - n_{immersion}\right) \cdot 20\mu m \overset{!}{=} \left(n_{glass} - n_{immersion}\right) \cdot d_{glass}$$

$$\left(1.441 - 1.333\right) \cdot \quad 20\mu m \overset{!}{=} \left(1.51 - 1.333\right) \cdot \quad d_{glass}$$

$$\Leftrightarrow d_{glass} = 12\,\mu m$$

Thus, the highest value of refractive index mismatch that was measured with GdHCl ($n_{solvent} = 1.441$) corresponds to a coverslide thickness deviation of 12 µm.

5.2. Optical Saturation

To check whether 2fFCS is sensitive to changes in excitation intensity, we performed measurements on aqueous solutions of Atto655 at different excitation powers between 2.5 and 70 µW per laser. The resulting dependence of the determined diffusion coefficient on excitation intensity is shown in Fig. 17. As can be seen, there is virtually no dependence of the determined diffusion coefficient on excitation intensity up to ca. 40 µW for each laser. We interpret the subsequent rise in apparent diffusion coefficient as the increasing impact of photobleaching. It can be observed that the diffusion coefficient measured with 2fFCS remains constant over a large range of excitation intensities; in stark contrast to conventional FCS, where a prominent decrease of the apparent diffusion coefficient (i.e. increase in observed diffusion times) for increasing excitation intensities is observed (as long as this is not counterweighted by increasing photobleaching at large intensities). Fig. 18 presents the change in fitted values of w_0 and R_0 with increasing excitation intensity.

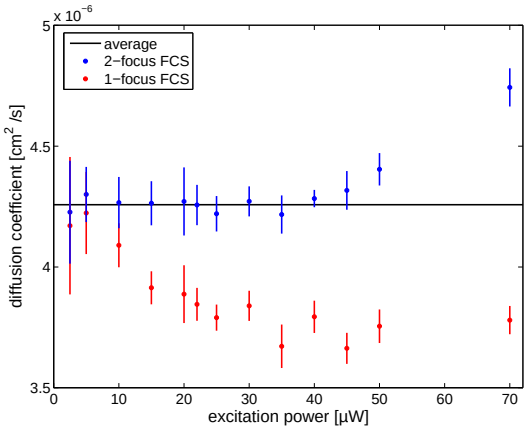

Fig. 17: Measured diffusion coefficient of Atto655-(COOH) in aqueous solution at 25 °C as a function of excitation power (cw-power of each laser). Solid line is the value of the diffusion coefficient for pure water as derived from the measurements shown in Fig. 15. Again, the results of single-focus FCS are also shown. As reference value we extrapolated the single-focus FCS results towards zero intensity.

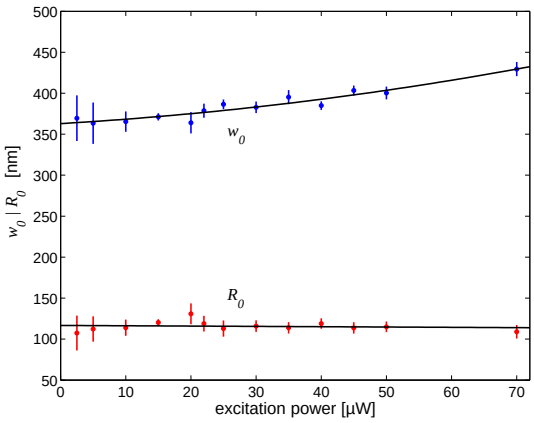

Fig. 18: Atto655: Dependence of the fitted values of w_0 and R_0 on excitation power. Shown are experimental values (circles) and second / first order polynomial fits (solid lines) for w_0 and R_0 respectively. Here, the value of w_0 changes most with increasing aberrations induced by optical saturation, whereas R_0 remains relatively unchanged.

Similar to the case of refractive index mismatch (see previous section), the value of w_0 increases with increasing excitation intensity whereas the value of R_0 changes only slightly. This shows again that the two-parameter model of the MDF is flexible enough to accommodate aberrations, but that the aberrations introduced by refractive index mismatch and by optical saturation are clearly different.

We checked also the intensity dependence of 2fFCS using the red fluorescent dye Cy5-(COOH). Three additional exponential decay parameters (one for each curve, see Appendix) were introduced in order to fit the fast blinking contributions to the correlation curves. A typical measurement result is shown in Fig. 19. As can be seen from Fig. 20 no dependence of diffusion coefficient on excitation power is observed in 2fFCS, even for the strong light-driven blinking dynamics of Cy5, whereas single-focus FCS is very sensitive to optical saturation. It remains to be checked whether 2fFCS will prove to be insensitive to optical saturation when using dyes showing significantly different saturation photophsysics than excited state saturation (Atto655) or light-induced conformational changes (Cy5).

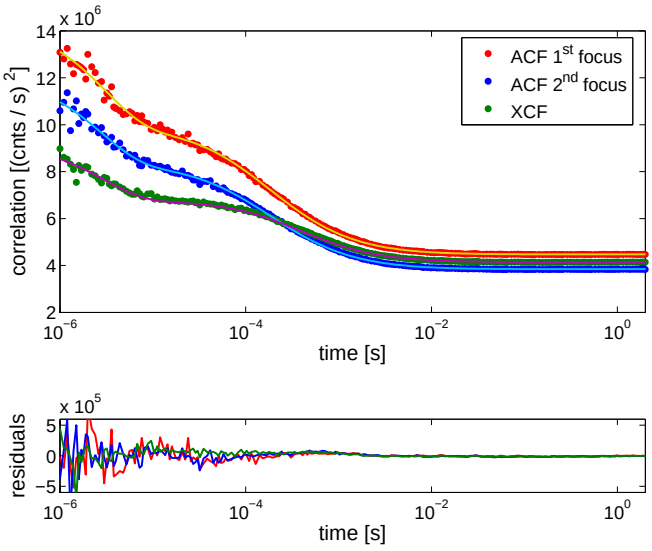

Fig. 19: 2fFCS measurement on a nanomolar aqueous solution of Cy5. Cw-excitation power (both lasers together) was 20 µW, measurement time was 60 min. The shape of both ACFs is virtually identical. Circles are experimental values; solid lines are global fits using Eq. (5.7) additionally using one exponential decay parameter for each correlation curve to describe the fast µs-dynamics. The introduced, additional fit parameters, which are thought to fit the intersystem crossing contribution of the correlation-curves, yielded a mean value of 6 µs.

Finally, it should be noted that our method (and, as far as we know, no other FCS method) is not capable of compensating or dealing correctly with photobleaching. Photobleaching is an irreversible photo-destruction of fluorescent molecules in solution, leading to a *time-dependent* inhomogeneous concentration profile and thus invalidating the fundamental assumption of all FCS analysis, namely the stationarity of the measurement (measurement should be invariant with respect to time shift). Thus, one has always to check that the used excitation intensity is below the threshold where any photobleaching effects are detected.

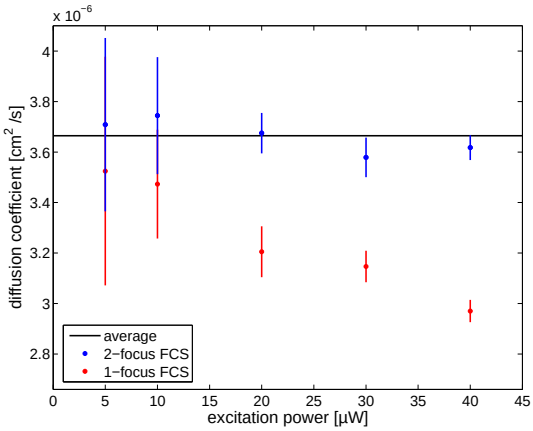

Fig. 20: Dependence of the measured diffusion coefficient of Cy5 in aqueous solution at 25 °C as a function of excitation power (cw-power of each laser). Solid line is the average value of all measurements. Again, results of single-focus FCS are also shown. As reference value we extrapolated the single-focus FCS results towards zero intensity, assuming this value to be equal to the value as measured by 2fFCS (solid horizontal line).

6. Planar diffusion

A topic of particular interest is the diffusion of membrane proteins in biological cell membranes. As a model system for cell membranes supported phospholipid-bilayers (SPBs) are well established (Richter *et al.*, 2006). SPBs are easily prepared and their properties can be well controlled (Sackmann, 1996). An alternative to SPB are Giant Unilamelar Vesicles (GUVs) (Angelova & Dimitrov, 1986; Kahya *et al.*, 2001). GUVs consist of a unilamellar lipid bilayer that forms under favorite circumstances a vesicle of several to hundred microns diameter, depending on experimental parameters such as lipid type, buffer composition etc. Working with GUVs has the advantage that there are no potential artifacts induced by a supporting surface as in SPBs (Przybylo *et al.*, 2006; Dertinger *et al.*, 2006). In the following section, we will mainly focus on SPB measurements but will conclude this section with a short comparison of lipid diffusion in SPBs and in GUVs.

In two-dimensional diffusion measurements, the diffusion time and thus the estimated diffusion coefficient as measured by single-focus FCS sensitively depends on the diameter of the MDF within the membrane's plane. It is therefore necessary to have exact knowledge about the position of the laser focus relative to the membrane. Due to the large beam divergence of a focused laser beam, and the difficulty to exactly locate the membrane's position relative to the laser's beam waist, it is usually difficult to obtain exact knowledge on focus diameter within the plane of the membrane. The resulting uncertainty when estimating the diffusion coefficient by applying conventional single-focus FCS can be as large as 20 % (Korlach *et al.*, 1999; Benes *et al.*, 2002). In other words, the limiting factor is again the difficulty to exactly know the size of the MDF.

From section 4.1, it should be evident that 2fFCS is insensitive to the exact position of the laser beam waist relative to the membrane because the determining parameter for calculating the diffusion coefficient is the distance between the foci and not the size of the MDF itself. Ideally, the distance between the two foci is not changing along the optical axis and therefore the estimated diffusion coefficient should remain constant in different planes of measurement. However, it can be observed that the distance is virtually decreasing when moving away from the plane of the laser's beam waist. This is due to an asymmetric cut-off of the MDFs because of the slight off-center position of the two laser

foci with respect to the pinhole. Nevertheless, within a range of ~2 µm, the distance can be considered to be nearly constant.

In contrast to the z-scan technique (see also section 4.3 and Appendix) developed in Martin Hof's group in Prague (Benda *et al.*, 2003), 2fFCS should be able to resolve the correct diffusion coefficient by a single measurement instead of having to perform a whole *z*-scan through the membrane. Thus, in this section we will compare the diffusion coefficients of labeled lipids in SPBs obtained with the *z*-scan method and with 2fFCS respectively. We will show how adsorption of molecules to the coverslide affects the shape of the resulting correlation curves and that for both methods the newly developed theory for surface-sticking molecules will lead to identical results. Finally, when comparing the measured diffusion coefficients of lipids in GUVs, we will find perfect agreement between 2fFCS and *z*-scan FCS as presented in (Przybylo *et al.*, 2006).

6.1. Diffusion in supported phospholipid-bilayers

In this subsection *z*-scan-FCS and 2fFCS are compared, and the effect of surface sticking molecules will be treated. Both methods find equal values for diffusion coefficients after full treatment with the extended diffusion theory that takes into account adsorption and desorption processes. The theoretical framework for adsorption and desorption processes in two-dimensional diffusion is presented in Appendix.

In brief, starting from the correlation function for two laterally shifted foci (see also section 5)

$$g(t,\delta) = \varepsilon_1 \varepsilon_2 c \int_A \int_A U(\boldsymbol{r}_1) G(\boldsymbol{r}_1 - \boldsymbol{r}_2 - \delta \boldsymbol{x}, t) U(\boldsymbol{r}_2) d\boldsymbol{r}_1 d\boldsymbol{r}_2 + g_\infty \tag{6.1}$$

the problem is to find an expression which describes the adsorption and desorption process of a two-dimensionally diffusing molecule. Since the Green function $G(\boldsymbol{r}_1 - \boldsymbol{r}_2 - \delta \boldsymbol{x}, t)$ in Eq. (6.1) contains all information on the kinetic behavior of the molecule, the problem can be reduced to find the appropriate Green function. It turns out that the result can not be given in a closed analytical form. Thus, correlation curves have to be calculated

numerically. For further details and for the explicit expression for the correlation function which is used for fitting the measured correlation curves the reader is referred to Appendix.

To apply the *z*-scan technique fluorescence was measured on Atto655-labeled SPBs at different vertical positions of the objective, thus obtaining autocorrelation and cross-correlation curves for different relative positions of the diverging laser beams with respect to the layer (*z*-scan). Each measurement lasted for ca. 15 min. As a first step, the autocorrelation curves were evaluated by applying a *z*-scan analysis as described in (Benda *et al.*, 2003) and also briefly introduced in section 4.3, assuming that the laser beam diameter as a function of vertical position is well described by the scalar field approximation of a Gaussian laser beam.

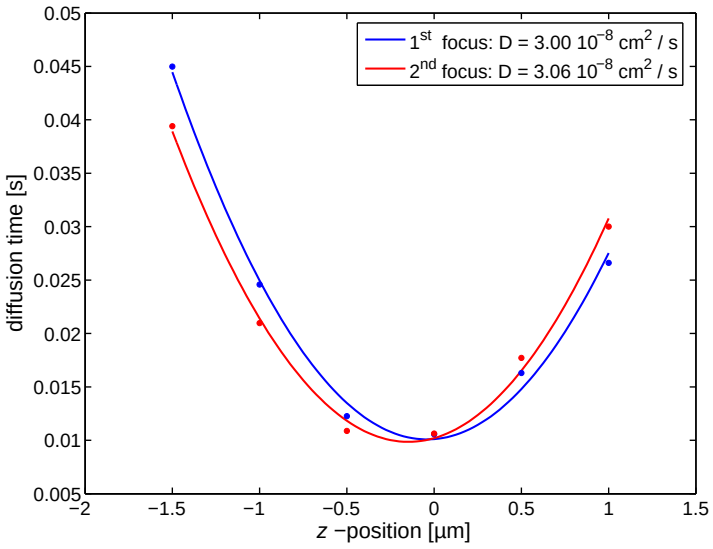

Fig. 21: Dependence of diffusion time on vertical z-position for the first (blue) and the second (red) laser focus. Solid lines represent least-squares fits of the data using the scalar approximation of a Gaussian laser beam.

Thus, each autocorrelation curve was first fitted with the standard model for free two-dimensional planar diffusion (i.e. Eq. (4.8) with $\delta = 0$) using the diffusion time $\tau_D(z) = w^2(z)/4D$ as fit parameter. The obtained values of diffusion time as a function of vertical position *z* were fitted by the function

$$\tau_D(z) = \frac{w_0^2}{4D}\left[1+\left(\frac{\lambda_{ex} z}{\pi w_0^2 n}\right)^2\right] \tag{6.2}$$

(see also Eq. (4.7)), using beam waist w_0 and diffusion coefficient *D* as fit parameters. For each focus, the fit of the diffusion time as function of the vertical position is presented in

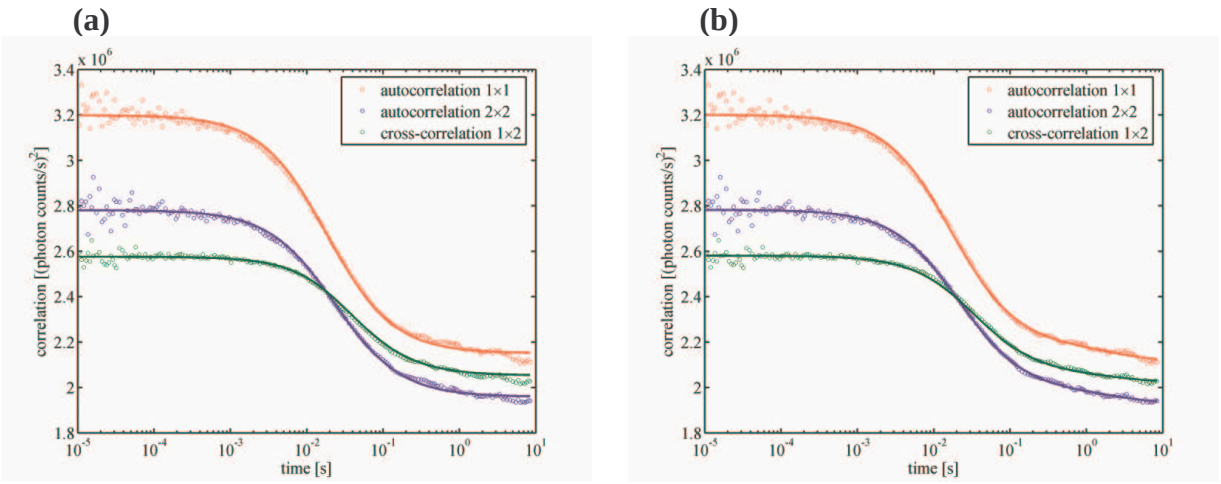

Fig. 21. The obtained values of the diffusion coefficient were $3.00 \cdot 10^{-8}\,\mathrm{cm}^2/\mathrm{s}$ and $3.06 \cdot 10^{-8}\,\mathrm{cm}^2/\mathrm{s}$, respectively. However, when inspecting the individual fits of the auto-

Fig. 22: (a) Simultaneous least-squares fit of the two auto- and one cross-correlation curves for one *z*-position using the free-diffusion model. (b) Same as (a) but using the kinetic reaction diffusion model including adsorption and desorption kinetics (see Eq. (10.49) in the Appendix).

and cross-correlation curves, as shown for one *z*-position in Fig. 22a, the poor fit quality indicates that the measured correlations are not well described by a free 2D diffusion model. We attribute that to unspecific adsorption and desorption of labeled lipid molecules to the supporting glass substrate, which was also observed by direct imaging of the samples with single molecule sensitivity.

Thus, we repeated the analysis of the correlation curves employing the extended model derived in the Appendix Eq. (10.49), now using w_0, D and the adsorption and desorption rate constants k_+ and k_- as fit parameters. Fit result for the same measurement as shown in Fig. 22a is presented in Fig. 22b, showing a clear improvement of fit quality.

The resulting values of diffusion coefficient as well as adsorption and desorption rate constants are presented in Fig. 23 and Fig. 24 respectively. Still, there is considerable variation in all obtained values with varying *z*-position, besides systematically increased values of the diffusion coefficient when compared with the values obtained from the free-diffusion model. A possible explanation of this strong variation is the slowness of the observed adsorption/desorption kinetics: On average, a molecule adsorbs to the surface ca. every hundred milliseconds, and the desorption kinetics is even slower by more than an order of magnitude. Thus, during the measurement time (15 min) of one curve, only a statistically small number of adsorption and desorption events takes place, and therefore,

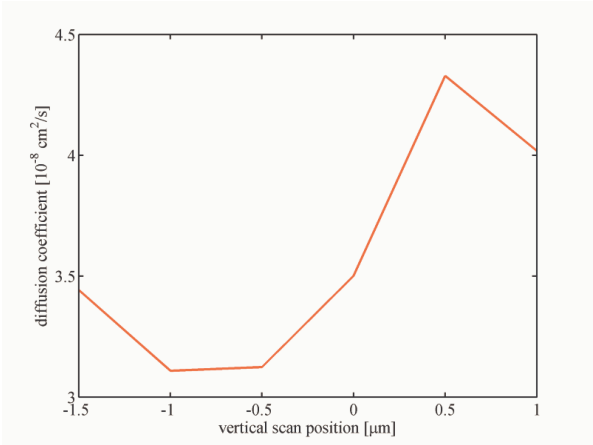

Fig. 23: Dependence of diffusion coefficient on vertical scan position as obtained from fitting the 2fFCS measurements using the full model of Eq. (10.49) given in the Appendix.

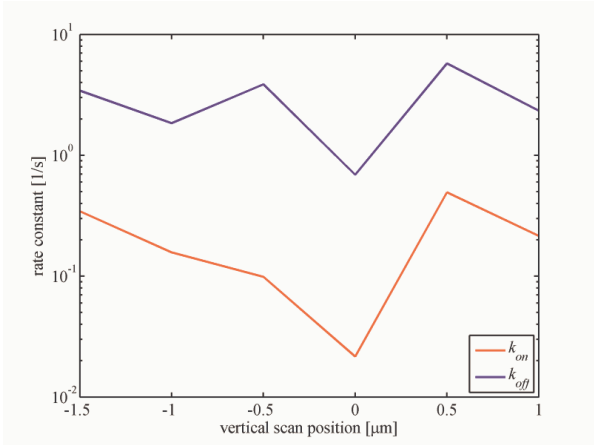

Fig. 24: Dependence of adsorption and desorption rate constants on vertical scan position as obtained from fitting the 2fFCS measurements using the the full model of Eq. (10.49) given in the Appendix.

curves measured at different times vary considerably and give strongly varying fit results. Another peculiarity is that the obtained desorption rates are so small that the assumed desorption process is probably rather photobleaching than real desorption with subsequent diffusion out of focus. Extending the measurement time is not a practicable option: To obtain a reasonable statistical accuracy, measurement times of several hours would be needed, assuring that no change in the sample takes place. To alleviate the situation to some extent, we performed a global fit of all *z*-scan-sets of curves, with one set of parameters w_0, D, k_+ and k_- for each *z*-scan, and assuming that laser beam radius depends

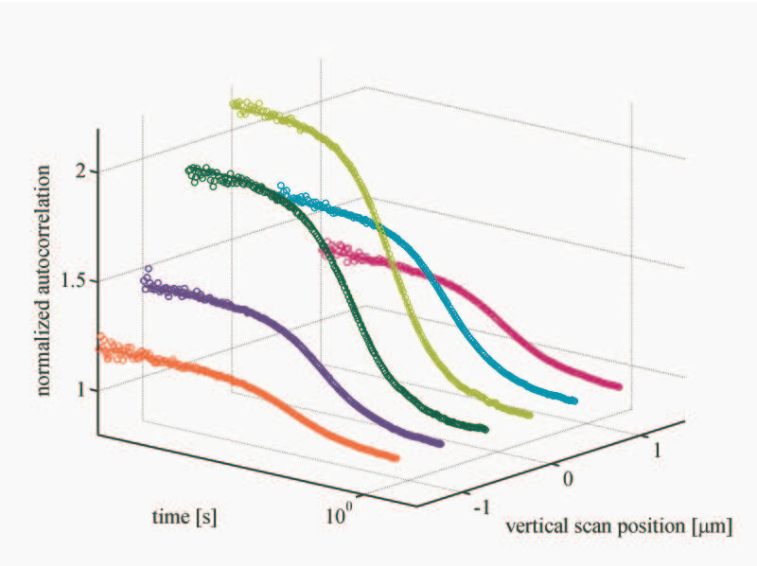

Fig. 25: Global fit (solid lines) of the measured autocorrelation curves (circles) for the first focus using Eq. (10.49)in the Appendix with δ = 0 and one set of parameters assuming that the dependence of laser beam radius on vertical scan position is given by the scalar approximation of a Gaussian laser beam.

on vertical scan position as described by the scalar approximation of a Gaussian laser beam (similar to the assumption underlying *z*-scan analysis). A typical fit result is shown in Fig. 25 for the autocorrelation curves of the first focus. All fit results are listed in Table 1. Employing a global fit approach yields consistent results for both the two separate autocorrelation sets as well as the cross-correlation set of curves. The obtained diffusion coefficient is ca. 10 % larger than the value obtained from the *z*-scan analysis with neglected adsorption/desorption kinetics. Remarkably, as shown by the values listed in Table 1 only 3 % of all molecules are bound to the surface on average at each time. However, this small fraction has a profound influence on the fit performance and the extracted diffusion coefficients, due to the extended time span these molecules remain within the detection region.

Table 1: *z*-scan-FCS and 2fFCS measurements evaluated with the kinetic reaction diffusion theory

	$k_{on}\,[s]$	$k_{off}\,[s]$	$K_{eq} = k_{on}/k_{off}$	$D\left[10^{-8}\,cm^2/s\right]$
Focus 1	0.071	2.3	0.031	3.28
Focus 2	0.090	3.4	0.026	3.22
2fFCS	0.086	2.7	0.031	3.30

6.2. Diffusion in the membrane of giant unilamellar vesicles

One advantage of 2fFCS over the *z*-scan FCS technique is that, in principle, one needs only one single measurement to estimate the diffusion coefficient, whereas the *z*-scan technique requires a full scan through the membrane. Thus, 2fFCS is comparably faster than *z*-scan FCS, an important property when applying FCS to e.g. cell membranes.

We performed 2fFCS measurements on GUVs prepared in different buffers (glucose, sucrose, pure water and glucose / sucrose inside the GUV and calcium buffer outside of the GUV) in order to check how different buffer solutions influence the diffusion coefficient. It turned out that glucose and sucrose solutions slow down the diffusion within the membrane, whereas salt-containing buffers on the outside of the GUV seem to compensate this effect. A more striking feature of diffusion in GUVs is the approximately twice bigger diffusion coefficient ($(8.0 \pm 0.4)\cdot 10^{-8}\,cm^2/s$, in water) as compared to diffusion in SPBs

($3.3 \cdot 10^{-8} cm^2 s^{-1}$, in water, see preceding section and Dertinger *et al.* (Dertinger *et al.*, 2006)). In glucose a diffusion coefficient of $(7.5 \pm 0.4) \cdot 10^{-8} cm^2 s^{-1}$ on GUVs was found.

These results are in perfect agreement with *z*-scan results of Przybylo *et al.* who find a diffusion coefficient in GUVs of $(7.6 \pm 1.1) \cdot 10^{-8} cm^2 s^{-1}$ (measured in glucose) and $(3.0 \pm 0.7) \cdot 10^{-8} cm^2 s^{-1}$ in SPBs (also prepared in glucose) (Przybylo *et al.*, 2006). The authors attribute the discrepancy of diffusion coefficients measured in GUVs and SPBs to a strong coupling between the bilayer leaflets of SPBs as suggested in (Merkel *et al.*, 1989; Zhang & Granick, 2005) and which is absent in GUVs.

7. Proteins

In this chapter, applications of 2fFCS in the field of biophysics will be presented. We will observe minute changes of the hydrodynamic radius of two calcium-binding proteins (calmodulin and recoverin) upon calcium binding and also we will use the hydrodynamic radius to monitor thermal unfolding of a small protein, named tryptophan cage.

7.1. Conformational changes of calmodulin

Calmodulin (CaM) is an extensively characterized protein and therefore an ideal system to check the performance of 2fFCS for studying conformational changes in proteins. In this section we present 2fFCS results of monitoring the conformational change of CaM upon calcium binding.

CaM belongs to the family of calcium-binding proteins and is a key component of the calcium second messenger system. This small, acidic protein (~16.7 kD) is ubiquitous in all eukaryotic cells and can bind up to four calcium ions at four different binding sites (I – IV), so called EF-hands. To date the calcium loaded form is known to regulate the functions of about 100 diverse target enzymes and structural proteins (O'Neil & DeGrado, 1990; Crivici & Ikura, 1995).

Crystallographic (Babu *et al.*, 1988; Taylor *et al.*, 1991; Chattopadhyaya *et al.*, 1992) and NMR studies (Ikura *et al.*, 1991; Barbato *et al.*, 1992) of calcium-saturated (Ca_4^{2+}-) CaM have shown that it has two distinct half-molecule domains (N-terminal and C-terminal) with nearly identical backbone structures; each has a contiguous pair of interacting calcium-binding sites. In earlier crystallographic studies, a long “central helix” was evident between sites II and III, giving CaM a dumb-bell shape (Babu *et al.*, 1988). However, crystallization conditions have been shown to promote helix formation (Török *et al.*, 1992), and NMR studies indicated that residues 78-81 are generally disordered in solution (Ikura *et al.*, 1991; Barbato *et al.*, 1992). Recently, a different crystal structure has been published, where native Ca_4^{2+}-CaM is in a compact ellipsoidal conformation and shows a sharp bend in the linker helix and a more contracted N-terminal domain (Fallon & Quiocho, 2003).

When comparing the high resolution structural studies of the calcium free (apo-) CaM (Kuboniwa *et al.*, 1995; Zhang *et al.*, 1995) and Ca_4^{2+}-CaM, it can be seen that the binding of calcium causes almost no change in the amount of secondary structure, but leads to a significant rearrangement of the helices surrounding the calcium-binding sites. It has been shown that the binding sites III and IV in the C-terminal domain have higher calcium-affinities than binding sites I and II from the N-terminal domain. Calcium binding in each domain is taking place cooperatively (Linse *et al.*, 1991).

For partially calcium-loaded native (Ca_2^{2+}-) CaM, there are no high resolution structural studies available. Yet several publications have found strong evidence that the transition between apo-CaM and Ca_4^{2+}-CaM is a two step process (Grabarek, 2005). It has been shown that half-saturated Ca_2^{2+}-CaM adopts an intermediate structure, which can not be assigned to an average of both - the apo and the Ca_4^{2+}-CaM conformation (Shea *et al.*, 1996). With thrombin footprinting (a proteolytic technique) Shea *et al.* demonstrated that Arg37/Ser38 is not accessible to cleavage in the calcium-free and calcium-saturated conformations, whereas at intermediate calcium concentrations cleavage of the bond Arg37/Ser38 is taking place. Since all evidence for a global structural change of is based on data coming from single structural elements of CaM, conclusions drawn out of these observations are difficult.

In the following we will measure the Stokes radius as a function of the free calcium-concentration. The results will give direct evidence to the existence of an intermediate Ca_2^{2+}-CaM conformation and prove that 2fFCS is able to monitor smallest changes in hydrodynamic properties of bio-molecules.

7.1.1. Hydrodynamic characterization of globular proteins

The fundamental equation which characterizes the hydrodynamic properties of a particle is the Stokes-Einstein equation:

$$D = \frac{k_B T}{6\pi\eta r_0} \tag{7.1}$$

where D is the diffusion coefficient of a sphere with radius r_0 at temperature T in a solvent of viscosity η; k_B denotes the Boltzmann constant. When applying this formula to globular proteins, one has to consider that the protein carries a hydration layer, and that its shape may deviate from a simple sphere. Thus, instead of using the *geometric* radius r_0 of a sphere one replaces r_0 in Eq. (7.1) with an *effective* radius, namely the Stokes radius r_S or hydrodynamic radius. The Stokes radius accounts for the above mentioned geometric deviations from a simple sphere as well as for the hydration. Since most particles carry a layer of hydration, the Stokes-Einstein equation is often directly formulated with the Stokes radius:

$$D = \frac{k_B T}{6\pi\eta r_S} \tag{7.2}$$

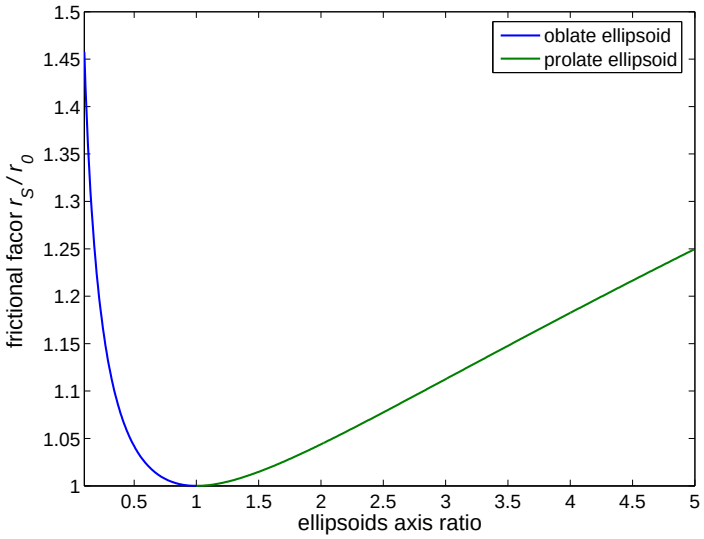

Fig. 26: Frictional factor as a function of major axis relation of a diffusing ellipsoid calculated from Bloomfield (Bloomfield, 2000) after Perrin's formula.

The ratio between the Stokes radius and a simple sphere with radius r_0 leads to the frictional factor r_S/r_0. Thus, deviations from unity of the frictional factor indicate the effects of hydration and a non spherical particle shape. Since most globular proteins are well described by an ellipsoidal geometry, it is a common approach to use Perrin's formula (Bloomfield, 2000) to estimate frictional factors for globular proteins, even though the effect of hydration is then completely neglected. The axial ratios to describe the ellipsoidal geometry are taken from the protein's crystal structures. Fig. 26 shows the dependence of the frictional factor on ellipsoidal geometry according to Perrin's formula.

We measured the diffusion coefficient of CaM at different calcium concentrations at 25 °C. CaM was labeled nonspecifically with NHS-functionalized red fluorescent dye

Atto655. Each measurement lasted for 10 min, and for each calcium concentration, measurements were repeated several times on different days to determine a standard deviation for the diffusion coefficient.

A typical measurement result of CaM in a calcium buffer is shown in Fig. 27, together with a global fit of all three curves using Eq. (5.7) and one additional decay parameter for each curve in order to fit the µs dynamics at short lag times (see Appendix Eq. (10.52)). As can be seen, the obtained fit quality is excellent. For the whole set of measurements the corresponding Stokes radii were derived from the estimated diffusion coefficients using Eq. (7.2) and are shown in Fig. 28 as a function of the free calcium concentration. The obtained curve was fitted with the following formula derived from a standard Hill equation

$$r_S(c) = \frac{a}{\left(1+\frac{p_1}{c}\right)^2} - \frac{b}{\left(1+\frac{p_2}{c}\right)^2} + offset \tag{7.3}$$

where p_1 and p_2 are the major fit parameters, and a, b and $offset$ are auxiliary fit parameters for matching amplitude and offset values of the measured curve. The calcium concentration is denoted with c.

At very low calcium concentrations (16 nM) CaM is in the apo-conformation, whereas

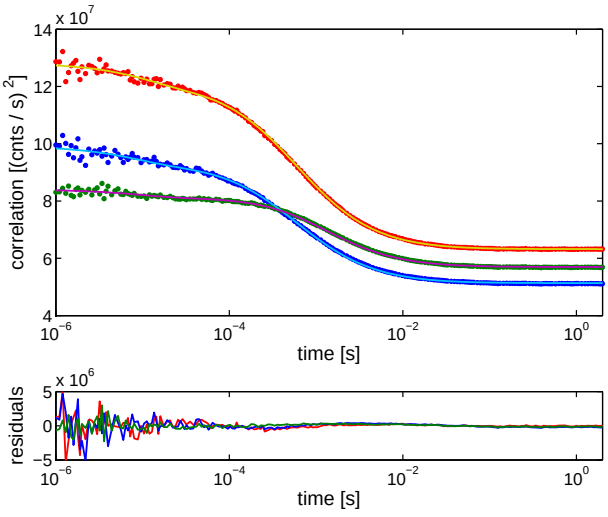

Fig. 27: 2fFCS measurement of CaM in an 1.8 µM free calcium containing buffer. Measurement time was 12 min. Circles are experimental values. Solid lines are the global fits for all three curves together. The offset between both autocorrelation curves is due to slightly different excitation powers of the lasers. For fitting, three exponential decay parameters (one for each curve) were used to describe the blinking dynamics occurring at short lag-times.

at high calcium concentrations (0.5 - 2mM), CaM is calcium saturated and adopts the Ca_4^{2+}-conformation.

7.1.2. Intermediate calmodulin conformation

Between the apo- and the Ca_4^{2+}-conformation a rise in Stokes radius of up to 23.7 Å at 3µM free calcium can be observed (see Fig. 28). We attribute this rise in Stokes radius to a conformational change of CaM upon calcium binding and an associated rearrangement of the hydration layer. Above 3µM, the Stokes radius is decreasing down to 22.8 Å. Since the calcium binding constants range from 0.2µM to 40 µM under comparable conditions (Linse *et al.*, 1991), it is likely that we monitor an intermediate conformation of CaM where only some of the EF-hands are occupied by calcium ions, but not all. Comparing the observed biphasic behavior with published results, it is most likely that this change in conformation can be attributed to the formation of Ca_2^{2+}-CaM. NMR studies find that major changes in chemical shifts are taking place only when CaM has bound 0, 2 or 4 calcium ions, whereas the binding of the first and the third ion does not induce large changes in protein structure (Seamon, 1980). Also, the results from proteolytic studies support the existence of an intermediate CaM conformation (Shea *et al.*, 1996). The authors observe biphasic behavior of susceptibility of the bond Arg 37 / Ser 38 of CaM: Between 0 and 3µM free calcium they could observe an increase in susceptibility, whereas above 3 µM they find a decrease of susceptibility. The authors address this behavior to a discrete conformation which cannot be explained by a simple superposition of the apo- and Ca_4^{2+}-CaM conformation.

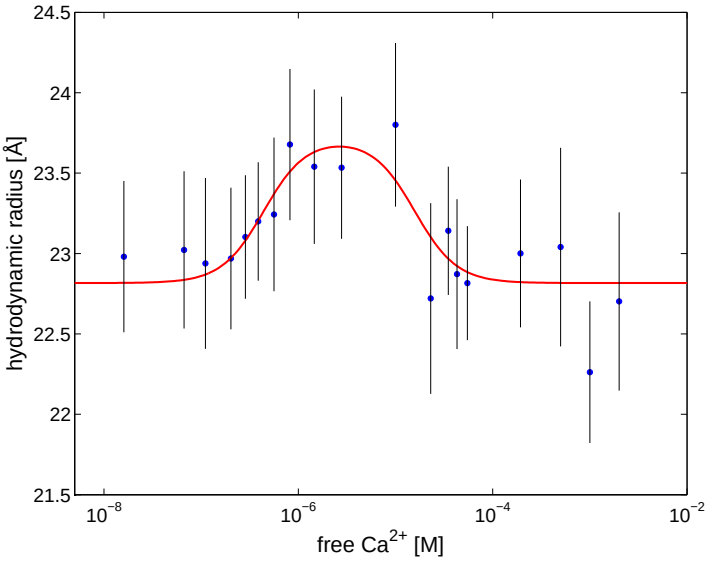

Fig. 28: The Stokes radius of CaM labeled with Atto655 as a function of free calcium. The red line is a fit corresponding to Eq. (7.3). Standard deviations are shown as vertical error bars are calculated from all measurements done on a single calcium concentration ($n \geq 10$). Temperature was 25 °C.

7.1.3. Apo- and calcium-saturated calmodulin

Comparing our obtained results for the Stokes radii of apo- and Ca_4^{2+}-CaM with previously measured values using pulsed-field gradient NMR (PFG-NMR), dynamic light scattering (DLS) or gel permeation chromatography (GPC), the results found with 2fFCS tend to be systematically smaller (~5 - 9 %, see Table 2) Lucas and Larive pointed out that protein-concentration dependent viscosity changes might slow down the apparent diffusion coefficient by up to 5 % in NMR experiments, and additionally crowding effects can affect the obtained results as well (Lucas & Larive, 2004; Wang, 1954). This potential error source originates from the fact that measurements of PFG-NMR, DLS and also GPC are performed far away from the infinite dilution limit.

When comparing the measured Stokes radii of CaM with other globular proteins of similar molecular weight or similar hydrodynamic properties, it turns out that CaM has an extraordinary large Stokes radius (see Table 3). Further investigation shows that this large Stokes radius is caused by an unusual high frictional factor $r_S/r_0 = 1.25$ (see Table 3) this is quite surprising because high-resolution structures of CaM do not show a stretched geometry which would support a frictional factor of 1.25. The axial ratio of the prolate ellipsoid corresponding to a frictional factor of 1.25 is 4 – 5 (see Fig. 26)!

Table 2: Stokes radius of CaM, measured with different techniques

Technique	*apo-CaM*	Ca_4^{2+} **-CaM**
	Stokes radius [Å]	
2fFCS	22.8 ± 0.5	22.8 ± 0.6
PFG-NMR[a)]	24.8 ± 0.8	24.5 ± 0.4
GPC[b)]	24.9 ± 0.1	24.0 ± 0.1
DLS[c)]	25 ± 1	30 ± 1

[a)] (Weljie *et al.*, 2003)
[b)] (Sorensen & Shea, 1996)
[c)] (Papish *et al.*, 2002)

There are only very few globular proteins which show a bigger frictional factor, i.e. bovine serum albumin, which in turn at least somehow reflects the resulting frictional factor in its shape dimensions of 140 Å / 40 Å (Squire & Himmel, 1979). In this context, a smaller Stokes radius for CaM might be more consistent with findings on other comparable globular proteins listed in Table 3. It is important to note that hydration can vary

considerably between different proteins. It starts from values of 0.12 gram water per gram protein and can reach up to one gram of water per gram protein (Squire & Himmel, 1979). These huge variations make precise predictions on frictional factors difficult, since the frictional factor is depending not only on the protein's shape but also on its layer of hydration.

Table 3: Hydrodynamic properties of CaM and globular proteins comparable to CaM:

	Molecular weight [kDa]	*Frictional factor* r_S/r_0	*Stokes Radius* [Å]
Ca_4^{2+}-CaM[b)]	16.7	**1.24**	24.0
Apo-CaM[b)]	16.7	**1.25**	24.9
Myoglobin[a)]	17	1.17	18.9
Trypsin[a)]	23	1.19	23.0
Subtlysin (novo)[a)]	27	1.18	23.6
Bovine serum albumin[a)]	66	1.31	35.1

[a)] (Squire & Himmel, 1979), the Stokes radii are calculated out of the diffusion coefficients (measured at 20 °C), assuming the viscosity of water at 20 °C.
[b)] (Sorensen & Shea, 1996)

7.1.4. Influence of the attached dye

The impact of the attached dye molecule on the overall shape of labeled CaM can be neglected. To estimate the influence of the attached dye on the diffusion coefficient, one may use the fact that, in good approximation, the hydrodynamic volume of a globular protein is proportional to its molecular mass. The reciprocal cubic root of the hydrodynamic volume is in turn proportional to the diffusion coefficient:

$$D \propto r_s^{-1} \propto V_s^{-1/3} \propto MW^{-1/3} \tag{7.4}$$

The molecular mass of CaM is 16.7 kDa and the molecular mass of Atto655-NHS is 0.7 kDa. Thus, the relative change of the diffusion coefficient as estimated by Eq. (7.4) is around 1 %:

$$\frac{D^*}{D} = \left(\frac{16.7}{16.7 + 0.7} \right)^{-\frac{1}{3}} = 1.01 \tag{7.5}$$

Of course, it cannot be completely ruled out that the attached dye influences the calcium-binding behavior of CaM. However, the good agreement of our findings with the cited results of other authors using label-free methods are a good indication that the labeling has no significant effect on Ca-binding and induced conformational changes.

7.1.5. Conclusion

Using 2fFCS, we have measured the Stokes radius of CaM as a function of calcium concentration. A biphasic behavior of the Stokes radius was observed. This change in Stokes radius was attributed to an intermediate CaM conformation at half calcium-saturation. When comparing our findings with previously obtained results by other groups, it is most likely that the observed intermediate CaM-conformation is due to CaM with two calcium ions bound. Additionally, we demonstrated that 2fFCS is sensitive enough to monitor even small changes in Stokes radius of bio-molecules down to one Ångstrøm. This accuracy is comparable to that achievable with pulsed-field-gradient-NMR, however necessitating only nanomolar concentrations of analyte and a fraction of measurement time.

7.2. Conformational changes of recoverin

Recoverin is a 23 kD calcium-binding protein which regulates visual phototransduction in retinal rods and cones (Senin *et al.*, 2002a; Makino *et al.*, 2004). It has two functional calcium-binding sites (EF-hands), and calcium binding takes place sequentially. Upon calcium binding, recoverin changes its conformation and exposes a myristoyl group at its N-terminus. This so-called calcium-myristoyl switch operates like a molecular trigger that translocates recoverin to the membrane (Zozulya & Stryer, 1992; Dizhoor *et al.*, 1993). The myristoyl group induces co-operativity in the calcium binding mechanism (Ames *et al.*, 1995). When the myristoyl group is buried within a hydrophobic pocket, the protein is released from the membrane. For a detailed review of the role of recoverin within the visual process see (Fain *et al.*, 2001) and (Pugh *et al.*, 1999).

As far as we know the hydrodynamic radius of recoverin has never been published. The goal of this section is to estimate the hydrodynamic radius of recoverin, and to use this radius for monitoring conformational changes of recoverin upon calcium binding. For this purpose we recorded the hydrodynamic radius of fluorescently labeled recoverin as a function of free calcium.

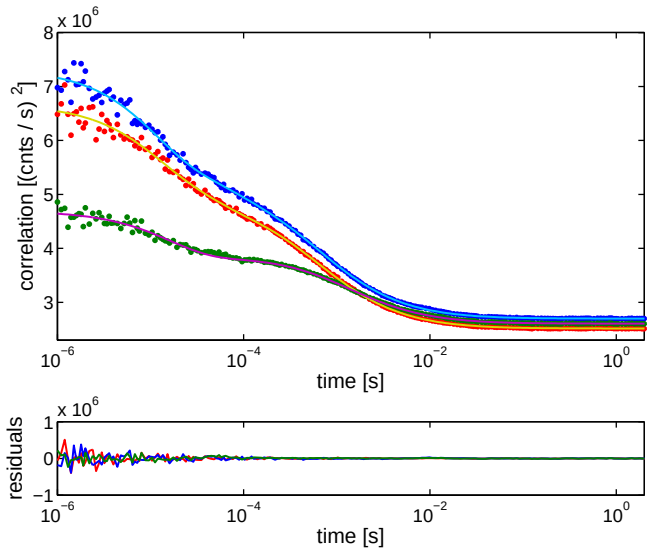

Fig. 29: 2fFCS measurement of recoverin in an aqueous buffer containing 16 nM free calcium. Measurement time was 6 min. Circles are experimental values, solid lines are the global fit for all three curves together. Autocorrelation curves of both lasers are virtually identical. Two additional exponential terms per correlation curve were used to describe the impact of blinking dynamics at short lag-times.

The red fluorescent dye Alexa647-maleimide was covalently bound to the single cystein at position 38 within the amino acid sequence of recoverin. It has been shown in previous publications that attaching Alexa647-maleimide to this

cystein does neither influence the switching properties of recoverin nor its basic biological properties (Gensch *et al.*, 2006).

A typical measurement result for recoverin in a calcium buffer is shown in Fig. 29 together with a global fit of all three curves using Eq. (5.7). In these fits two additional exponential terms for each correlation curve were used to account for the microsecond blinking dynamics of the dye (resulting blinking times are ranging from 0.1 µs to 5 µs). Each measurement lasted for 6 min and was repeated several times ($n \geq 10$) to obtain a standard deviation. As can be seen, the obtained fit quality is excellent.

The determined values of hydrodynamic radii are shown in Fig. 30 as a function of free calcium concentration. Values of the hydrodynamic radius which were more than 10 % off the mean value were rejected. Such large deviations from the mean value are considered to be due to protein aggregation and the presence of fluorescent impurities in the used buffers. At very low calcium concentrations (16 nM) recoverin is in its calcium-free conformation, whereas at high calcium concentrations (>100 µM) recoverin adopts its calcium conformation.

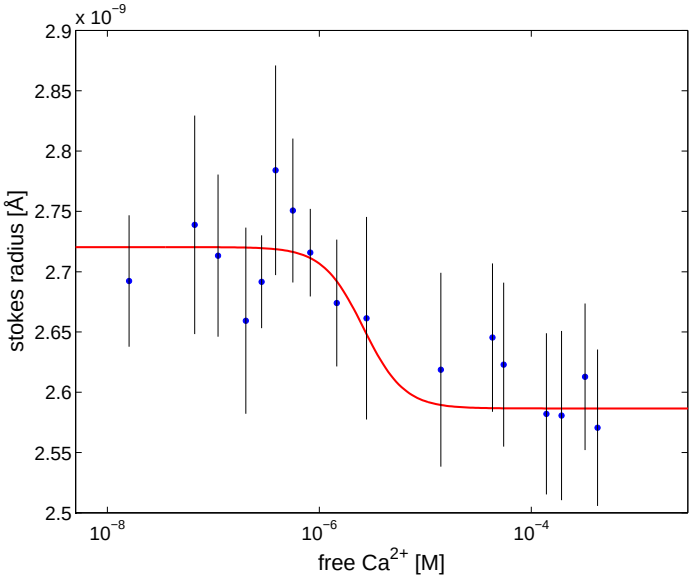

Fig. 30: Stokes radii of recoverin, in buffers containing different concentrations of free calcium. Measurements lasted for 6 min and were repeated ten times at 25 °C. Additionally, measurements were repeated on different days. Values for the hydrodynamic radius which were more than 10 % off the mean value were not taken into account. Vertical black lines represent the standard deviation. The red line is a Hill-fit with a hill coefficient of 2.3 and a binding constant of 2.6 µM.

Fitting of the hydrodynamic radius vs. calcium concentration curve was done by using a standard Hill model. A Hill coefficient of 2.3 and a binding constant of 2.6 µM were obtained. However, depending on the initial guess values of the fit parameters, a Hill coefficient of 0.9 with a binding constant of 8 µM was also found frequently. We discarded

the latter result, since calcium binding is taking place sequentially and cooperatively, which should lead to a Hill coefficient larger than one.

The obtained calcium binding constant of $k_D = 2.6$ µM (Hill coefficient 2.3) is quite low compared to previous findings. Previous publications reported values of 11 µM (Hill coefficient: 1.13) (Gensch *et al.*, 2006), 17 µM (Hill coefficient: 1.75) (Ames *et al.*, 1995) or 17.6 µM (Hill coefficient: 1.9) (Senin *et al.*, 2002b). However, these relatively high binding constants are difficult to understand when considering the rather low calcium concentrations around 1 µM in living cells. On the other hand, studies have shown that recoverin binds to retinal outer segment (ROS) membranes with a binding constant of 4.0 - 7.7 µM (Lange & Koch, 1997) respectively 2.1 µM (Zozulya & Stryer, 1992) free calcium. Until now it is not fully understood why binding of calcium and binding to ROS membranes should take place at different calcium concentrations because recoverin is thought to bind to membranes only in the calcium-saturated conformation.

7.3. Unfolding the Tryptophan-Cage

Since the diffusion coefficient as measured with 2fFCS is not sensitive to refractive index changes (see section 5.1), it is an ideal tool for monitoring chemically and thermally induced unfolding of proteins, where the refractive index of the buffer solution may change dramatically (either due to the addition of a chemical in high concentrations, or due to higher or lower sample temperatures). Chemical unfolding is often done by adding large concentrations of urea or guanidine hydrochloride (GdHCl) to the sample solution. Both chemicals change the refractive index of the solution significantly, leading to considerable optical aberrations and corresponding changes of the MDF. Due to this reason, it is rather impossible to use single-focus FCS for quantitatively monitoring the change in hydrodynamic radius of a protein during unfolding. A similar argument applies for thermal unfolding, where the refractive index of the solution decreases significantly with increasing temperature due to thermal expansion of the solvent (aqueous buffers solution). Different attempts have been made to apply single-focus FCS for monitoring chemically induced protein unfolding (Chattopadhyay *et al.*, 2005). In these attempts, aberrations caused by refractive index mismatch where compensated by appropriately re-adjusting the correction collar of a water inmersion objective. This procedure is time consuming and difficult, and the used optimization procedures (Hess & Webb, 2002) may not converge towards the best adjustment (Enderlein *et al.*, 2005). Another difficulty is that the fit quality of measured autocorrelation curves is not indicative of an optimal adjustment, contrary to what was stated by Chattopadhyay *et al.*, see (Enderlein *et al.*, 2005). 2fFCS overcomes all of these problems. In the present section we show first results of measured hydrodynamic radius of a protein upon thermal unfolding.

As a model system for studying protein unfolding, a protein called Tryptophan-Cage (TC) was chosen. TC is the smallest known protein (consisting of only 20 amino-acids) that still folds into a completely folded structure. Its amino-acid sequence has been derived from the poorly folded 39-residue peptide exendin-4 from Gila monster saliva (Neidigh *et al.*, 2002). The solution structure of TC features a hydrophobic core, built by tight packing of a short proline-rich carboxyl-terminal domain to an amino-terminal-helical segment (Neidigh *et al.*, 2002). A single Trp residue is buried in the core, well shielded from solvent exposure. Folding of TC has been characterized by NMR as well as circular dichroism spectroscopy (CD) and has been proposed to follow a highly cooperative two-

state transition (Neidigh *et al.*, 2002). Also, Neuweiler *et al.* investigated unfolding of this protein with contact quenching of the red fluorescent dye MR121 (Neuweiler *et al.*, 2005). It is known that MR121 is quenched by Trp when they come to very close proximity (contact) (Vaiana *et al.*, 2003; Doose *et al.*, 2005). This quenching has its origin in photoinduced electron transfer (PET). Neuweiler *et al.* attached MR121 to TC and observed that in the folded state the Trp residue is not accessible for MR121. However if the hydrophobic core is broken Trp gets exposed to solvent and is able to quench MR121 via PET.

For our measurements the MR121 labeled TC was kindly donated from Prof. Sauer, University of Bielefeld, Germany (for details concerning labeling and synthesis of TC look at (Neuweiler *et al.*, 2005)). We dissolved the protein in a standard phosphate buffered saline solution with 0.05 % Tween, pH 7.4. At different temperatures the sample was let to thermally equilibrate before starting the 2fFCS measurements. At each temperature, the diffusion coefficient was measured 10 times for 6 min in order to calculate standard deviation and mean value of the diffusion coefficient.

The diffusion coefficient of a particle depends not only on hydrodynamic radius, but also on temperature T and solvent viscosity η, which itself is a function of temperature. Thus, a precise knowledge of sample temperature is of crucial importance for precise determination of the hydrodynamic radius from diffusion measurements:

$$D(T) = \frac{k_B T}{6\pi\,\eta(T)\,r_S} \tag{7.6}$$

As can be seen from Eq. (7.6), the hydrodynamic radius r_S is *per definitionem* neither temperature- nor viscosity-dependent. Thus, any temperature dependent change in hydrodynamic radius is due to some change in conformation or hydration. In Fig. 31, the hydrodynamic radius as calculated from the measured diffusion coefficients following Eq. (7.6) is presented as a function of temperature. The measured data are fitted with an empirical two state transition model given by:

$$r_s = \frac{p_2}{\left(1+\frac{T_{melt}}{T}\right)^{p_1}} - p_3 \tag{7.7}$$

Principal fit parameters are T_{melt} and p_1, where T_{melt} is the melting temperature and p_1 describes the steepness of the curve. p_2 and p_3 are auxiliary parameters related to the amplitude and offset of the curve.

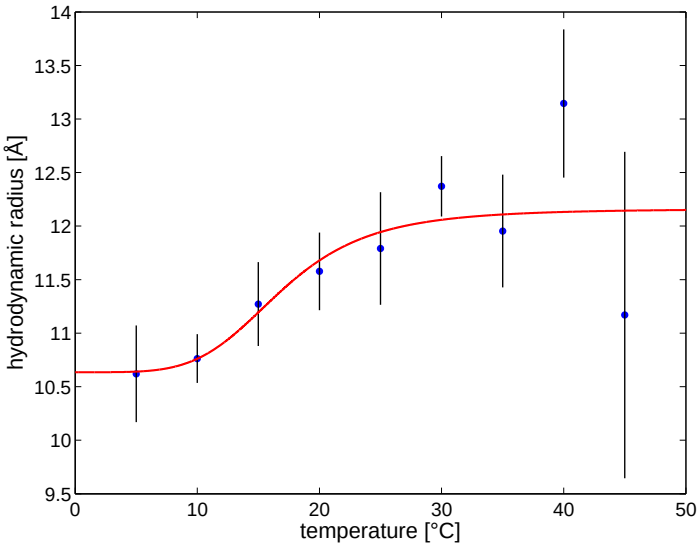

Fig. 31: Hydrodynamic radius of TC in a PBS buffer containing 0.05 % Tween as a function of temperature. Measurements lasted for 6 - 12 min and were repeated ten times. Vertical black lines represent the standard deviation. The red line is the fit result according to Eq. (7.7).

As can be seen, there is a change of hydrodynamic radius with temperature. The estimated melting temperature of TC lies at 17 °C, which is significantly lower than previously reported values (35 °C) (Neuweiler *et al.*, 2005).

The origins of this discrepancy may be manifold: The change in hydrodynamic radius that was observed with 2fFCS is about 14 %. This corresponds to a change of diffusion coefficient of also 14 %, whereas the change in diffusion coefficient due to temperature and viscosity is 290 %. Thus, the change in diffusion coefficient due to conformational change is monitored on top of the temperature and viscosity induced change that is ca. 20 times bigger. In Fig. 32, the change of diffusion coefficient due to temperature is compared to the change of diffusion coefficient caused by conformational change. It is evident that without perfect temperature control the calculated hydrodynamic radii are heavily prone to error.

Another potential artifact may be thermally induced hydrodynamic convection within the sample solution. These convections can be the result of temperature gradients within the sample chamber. We suppose that the big errors at higher temperatures reflect the contributions from convection. Because the measurement system uses a water immersion objective which is in direct thermal contact with the sample chamber, preventing thermal gradients without heating the complete microscope is rather impossible. Finally, vapor pressure increases with increasing temperature, which makes keeping the sample in thermal equilibrium even more difficult.

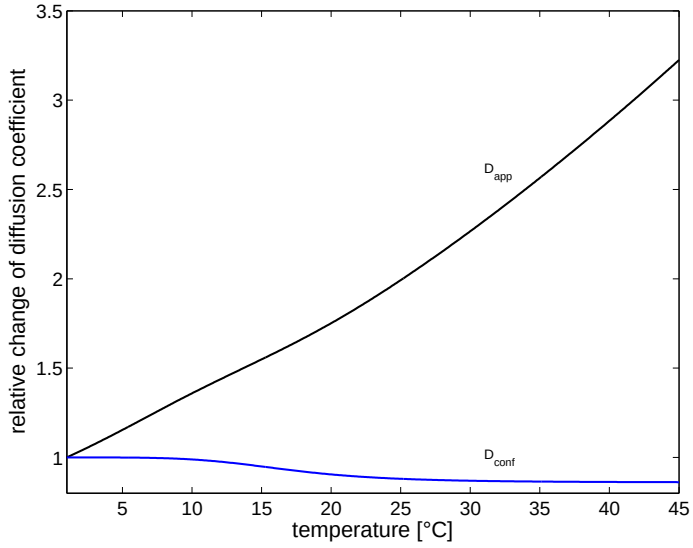

Fig. 32: Apparent diffusion coefficient upon thermal unfolding. Black line: Measured diffusion coefficient. Blue line: Diffusion coefficient corrected for temperature and temperature-dependent viscosity changes. Remaining is the contribution caused by a conformational change with melting temperature 17 °C with impact of 14 % on the diffusion coefficient.

Besides these potential artifacts, there remains the fundamental question whether measurements of hydrodynamic radius and measurements of photoelectron-transfer (PET) mediated fluorescence quenching as used by Neuweiler *et al.* are equivalently monitoring the unfolding of TC. PET mediated fluorescence quenching is sensitive to the accessibility of the Trp to the aqueous environment, whereas the hydrodynamic radius is a global structural parameter including contributions from hydration as well as overall protein conformation. Assuming that Trp becomes water-accessible only during the very last step of unfolding, PET monitors mainly the disintegration of the last residual structure around Trp while the major part of TC can be already in an unfolded state. However, Neidigh *et al.* have shown, by using CD and NMR, that the melting temperatures for TC are most likely identical for α–helical and β–sheet structures (42 °C). On the other hand, Neuweiler *et al.* argue that the breaking of the hydrophobic core of TC does not necessarily indicate that the helical structure is also disintegrating. The authors further state that the CD signal at 222 nm is ”convoluted with a strong contribution from the Trp side chain (Neidigh & Andersen, 2002). Recently, indications for residual helical structure in the denatured state of TC have been reported by using UV-resonance Raman spectroscopy (Ahmed *et al.*, 2005), suggesting the early formation of helical structure.” (Neuweiler *et al.*, 2005). Since it is not clear what contribution of TC has the strongest influence on the hydrodynamic radius, it is difficult to directly compare different measurement results. In other words, the term “melting temperature” may not refer to the same feature in different experiments. For example, Ahmed *et al.* performed UV-resonance Raman spectroscopy (UVRS) experiments on TC

and found evidence that TC adopts its most compact state at 20 °C (i.e. Trp is best shielded from water) – above and below this temperature TC is melting (Ahmed *et al.*, 2005). The authors assign this behavior to protein-water interactions. Although comparison of 2fFCS with UVRS observables may not be appropriate either, it may be possible that we monitor the same behavior of the protein as UVRS.

8. Summary

The goal of this work was to advance conventional (single-focus) fluorescence correlation spectroscopy (FCS) towards a high precision tool for the absolute estimation of diffusion coefficients. With conventional FCS, absolute determination of diffusion coefficients is hardly possible, due to the uncertainty concerning the exact size and shape of the molecule detection function (MDF) that determines the measured correlation curves. The molecule detection function is influenced by optical aberrations and photophysical effects, in particular refractive index mismatch between sample solution and objective's immersion medium, coverslide thickness deviation, laser beam astigmatism, optical saturation and even 'dead time' effects from the signal processing electronics. These effects lead to a distorted and inflated molecule detection function, making conventional FCS sensitive to optical / electronic artifacts.

To overcome these problems, the developed two-focus-FCS (2fFCS) measurement scheme takes advantage of two distinct features: The first feature is the generation of two laterally shifted, but overlapping laser foci of the same wavelength. Thus, instead of using the size and shape of the MDF as a ruler, 2fFCS utilizes the well-defined distance between both foci. Since the shifted foci are generated by a commercially available Nomarski-prism made for differential interference contrast (DIC-) microscopy, this ruler depends only on easy-to-control parameters such as the objective's magnification and presumably excitation wavelength (color-dispersion) and temperature. Although aberrations may deform the MDF of each focus (in an identical way), the distance *between* both detection regions remains unchanged.

- Checking the MDF-model

The appropriate description of the underlying MDF is of crucial importance for the quantitative evaluation of recorded correlation curves. Thus, as the second feature of 2fFCS we developed a new, semi-empirical description of the MDF. Like the commonly used three-dimensional Gaussian-shaped MDF model, the new MDF model needs only two principal parameters, but describes the MDF much better than the 3D-Gaussian. We checked the validity of the adopted description by means of 3D-scans of fluorescent beads. Subsequent fitting with the new MDF-model yielded perfect agreement, whereas the 3D-Gaussian model is known to be a rather inappropriate approximation of the actual MDF.

This experimental finding is also consistent with recent wave-optical calculations (Enderlein & Dertinger, 2007).

Thus, having introduced an external nanometric ruler into the measurement and having developed an appropriate description of the MDF, data evaluation of correlation curves has been put on a firm fundament.

- Precision of 2fFCS and its insensitivity to optical artifacts

We have proven that the apparent diffusion coefficient measured with 2fFCS is no longer dependent on refractive index mismatch, which also implies its insensitivity to coverslide thickness deviations, since these deviations introduce quite similar spherical aberrations. The comparison of our results with results achieved with pulsed-field gradient NMR (PFG-NMR) showed excellent agreement. This reassures us that beneath the insensitivity concerning the refractive index mismatch also the achieved *absolute* value of diffusion coefficient is correct; the determined diffusion coefficient for the red fluorescent dye Atto655-(COOH) in water at 25 °C is $(4.26 \pm 0.08) \cdot 10^{-6}\, cm^2/s$.

In a follow-up experiment, we verified the insensitivity of 2fFCS with respect to optical saturation. This was checked both for the saturation caused by pure singlet excited state saturation (Atto655) as well as for photoinduced cis-trans isomerization of the red fluorescent dye Cy5, where saturation starts to play a role already at low excitation powers.

Both the insensitivity to optical saturation and to refractive index mismatch is in stark contrast to results achieved with conventional single-focus FCS. Using single-focus FCS in combination with a three-dimensional Gaussian MDF-model, a prominent decrease (up to ~ 46 % for refractive index mismatch and ~ 20 % for optical saturation) of the apparent diffusion coefficient was observed. This decrease has its origin in the inflation and distortion of the actual MDF under increasingly aberrational measurement conditions. Although the new MDF model will no longer be exact under strong aberrational measurement conditions, it is flexible enough to lead to exact values (with an error of ca. 2 %) of the diffusion coefficient when evaluating 2fFCS measurements.

For the sake of completeness it is worth mentioning that 2fFCS is *per se* insensitive to laser beam astigmatism (Enderlein & Dertinger, 2007), which can be shown theoretically.

Thus, the new 2fFCS measurement scheme is insensitive to common FCS-inherent artifacts; namely refractive index mismatch, coverslide thickness deviations, laser beam astigmatism, and optical saturation. Especially its insensitivity with respect to refractive index mismatch makes 2fFCS an ideal tool for protein unfolding experiments, since high

concentrations of unfolding chemicals or high temperatures lead to a significant refractive index mismatch.

- Two-dimensional, planar diffusion

An important feature of 2fFCS is that it can be easily applied to diffusion in planar systems, for example when measuring diffusion within cell membranes. We specifically addressed the problem of surface adsorption/desorption of molecules diffusing in a supported phospholipid bilayer. A theoretical model describing this issue was developed and successfully applied to 2fFCS and also to the *z*-scan FCS technique developed in Martin Hof's group in Prague (Benda *et al.*, 2003). For both methods, we obtained equal diffusion coefficients and equal *on*- and *off* rates for the adsorption/desorption of molecules to/from the support.

Furthermore, we measured the influence of different buffers on the diffusion coefficient of labeled lipids diffusing in giant unilamellar vesicles. It was found that glucose as well as sucrose leads to slower diffusion coefficients, whereas salt-containing buffers compensate this effect. Compared to supported lipid bilayers, a larger diffusion coefficient by a factor of two was observed. These findings are in fair agreement with recently published data from Przybylo *et al.* (Przybylo *et al.*, 2006).

- Conformational changes of Proteins

The hydrodynamic radii of two calcium-binding proteins (calmodulin and recoverin) were measured as a function of free calcium. We observed minute changes of the hydrodynamic radius due to calcium-dependent conformational changes of these proteins. This has never achieved before with conventional FCS.

In comparison to other published hydrodynamic radii of calmodulin, we found slightly smaller values. Furthermore, we could not observe that the calcium saturated conformation of calmodulin has a smaller hydrodynamic radius then its apo-conformation as has been observed with gel permeation chromatography (Sorensen & Shea, 1996). We found equal values for both conformations. However, at intermediate calcium concentrations we monitored a conformational state of calmodulin which has a slightly larger hydrodynamic radius than the apo-/holo conformation. This intermediate conformation has also been observed by other groups while e.g. monitoring the accessibility of certain peptide bonds to proteolytic cleavage, using quantitative thrombin footprinting (Shea *et al.*, 1996).

The measurements concerning hydrodynamic radius of recoverin resulted in a calcium binding curve which was fitted with a standard Hill model. The fit yielded a binding constant of 2.7 µM and a Hill coefficient of 2.3. To our knowledge, we are the first group who publishes the hydrodynamic radius for recoverin.

In a last preliminary experiment we monitored the thermal unfolding of a small protein (tryptophane cage) as a change in its hydrodynamic radius. The acquired data yielded a melting temperature of 17° C, which does not agree well with findings by Neuweiler *et al.* using photoelectron-transfer (T_{melt} = 35° C) (Neuweiler *et al.*, 2005), but is comparable to the results achieved with UV Raman resonance spectroscopy from Ahmed *et al.* (20° C) (Ahmed *et al.*, 2005). Since the term "melting temperature" may not refer to the same feature in different experiments, it is difficult to directly compare different measurement results.

- Perspective

In addition to the multitude of advantages of 2fFCS over conventional FCS, upgrading a conventional (single-focus) confocal microscope to a 2fFCS system is surprisingly easy, and several research groups around the globe have already started to reproduce our system in their lab.

Compared to other methods such as PFG-NMR, gel permeation chromatography, or dynamic light scattering, the most striking advantage of 2fFCS is that it needs only nanomolar sample concentrations. Especially when working with proteins, all other methods sometimes fail due to proteins aggregation at concentrations needed by these methods for obtaining sufficient measurement signal. Thus, 2fFCS combines the advantages of conventional FCS while reaching the accuracy of the most up to date measurement schemes.

The two-focus measurement scheme is not necessarily restricted to precise diffusion measurements. A possible application is the extension into the field of fluorescence intensity (multiple-) distribution analysis FI(M)DA etc. (Kask *et al.*, 1999; Palo *et al.*, 2000) concerning the estimation of molecular brightness and concentration. Since also in FIDA and related techniques (Chen *et al.*, 1999; Kask *et al.*, 2000; Palo *et al.*, 2002; Palo *et al.*, 2005) the data-analysis and estimated results are highly dependent on the MDF, here too, the two-focus measurement scheme can help to bring these techniques to a level of higher precision.

9. Acknowledgements

This work would not have been possible if not for the assistance, support and guidance of numerous people who have somehow been involved (knowingly or not knowingly) in the present thesis.

I remember at the end of one of my first talks, I mentioned Jörg Enderlein as my inspiring supervisor and continued saying, that he has one brilliant idea nearly every day…….The audience was laughing. They had unintentionally read between the lines and considered me as the guy whose job it is to try out all these daily “brilliant” ideas. Unfortunately I did not have had the time to try out even a small fraction of these ideas, although I really would have liked it, because these ideas are not “brilliant” but brilliant (one of these ideas made its way straight to the field of astronomy and told the astronomers how to find the metric of a rotating black hole (Enderlein, 1997)). Thus, working together with him means that one is let partake of this amazing mind, which I was so lucky to be. Jörg is far off dogmatic thinking, which I consider the most important thing I could learn from him. He spent so much time to discuss things with me, that I doubt there are many supervisors around, caring so much about their students at the same time not hemming them in and being too much demanding. When working together with Jörg I realized that he really considers you as a partner on an equal footing. Thus, discussions where at any time productive, motivating, very much inspiring and never ended without having learned something new. On the other hand Jörg is also just a nice guy. During three years not everything is going straight, and Jörg always cares for problems and fears apart from physics. He’s been encouraging whenever necessary and I found always an open door to his office. I really do appreciate this and I am sincerely grateful for the great time I had during my PhD thesis. Thank you Jörg!

Even though our group is not only consisting of Jörg, he can be considered to be the head, or brain of our group. But let us now talk about the body.

There is Iris von der Hocht, and we both know that there are hard times during a PhD-thesis. We shared car and had time to talk about many things during this time. I’m deeply impressed of her natural and straight sense to dismantle (not only scientific) problems and cook them down to the appropriate level. And yes, we had quite good laughter in the lab. We even produced special interest movies for eastern, and I’m still fascinated by one very special skill of her: Iris can combine chemicals in such a way that odors arising from these

solutions have never been smelled by a human creature before and probably should never be after – especially when there is no air-con in the lab. And of course I really want to say that this thesis had never, ever come to this stage if not she would have supported me so much: For helping me performing experiments and also discussing experiments with never ending enthusiasm I'm deeply grateful.

Of course our lab would not be complete without Ingo Gregor. He's experienced, he sees how the cat jumps and he can repair everything what has been misadjusted or just damaged. His knowledge seems to be all-embracing. And overall - he is so patient. You can ask him thousands of questions, bore him with stories of your progress or not-progress, he'll never run away or show any sign of disinterest. If Ingo tells you, things will work out well, you know things will work out well. Thank you Ingo!

A good mood is necessary for good scientific work. Top persons in charge for this were my office mates at the research centre, "Pan Tau"-Honsa Sykora and Luru Dai (who by the way was blaming all of self-proclaimed experts for soccer (like me) by guessing best the results for the games during the world championship….). We had a good time, and we laughed quite a lot. And I can still assure Honsa, that our 'secretary' and our 'electrician' are as fascinating as we found out one night in the lab.

I'm also grateful to Abhishek Cukkemane for introducing me into the latest and best of Asian martial arts movies and of course for all invaluable discussions about soccer.

From the INB-2 I'd like to thank Jörg Fitter and Jana Kriegmann for support as well as many fruitful discussions.

Also I'm grateful to Wolfgang Bönigk, who prepared and purified different calmodulin mutants for me.

I want to thank also all the other people at the institute who somehow supported my work. Some of them just because they have been there always ready to have a short intermissive chat, some of them just because they cared about my work; like Arndt Baumann whose critical input was at any time enriching. And speaking of the institute I'd like to thank also Prof. U.B. Kaupp the institute's director, never doubting my abilities and giving me the opportunity to finish this work in his institute.

I really enjoyed the time being at the research centre in such a fantastic group.

For preparing and donating recoverin I'm grateful to Prof. Karl-Wilhelm Koch and Konstantin Komolov at the AG Biochemistry, University of Oldenburg and Belozersky

Institute of Physico-Chemical Biology at Moscow State University respectively. Also I'd like to thank Prof. Markus Sauer at University of Bielefeld for the donation of the tryptophan cage.

Since this thesis is also the result of cooperation with PicoQuant GmbH and the research center of Jülich, I spent quite a time at PicoQuant. Beneath giving me deep insight into company affairs, the support I experienced was overwhelming. Not only that setting up such a measurement scheme would have been hardly possible within the time of my thesis without the aid of PicoQuant, but also sending me to conferences all over the world is one of the extraordinary gifts they made to me. I was involved in workshops and courses and had the exciting opportunity to be part of a company working at the cutting edge in the field of science.

A company consists of people working there. So I'd like to express my gratitude to Rainer Erdmann, the head of the company making this cooperation possible, keeping things easy especially considering that I was caught between two stools - employed by the research centre but using infrastructure of PicoQuant. Felix Koberling, the head of the microscope system group, Benedikt Kraemer and Henrik Bauer for technical advice and never ending willingness to support this work, even though their own schedule is tightly packed. My gratitude goes also to the guys dealing with pico-second electronics, Michael Wahl, Hans Rahn and Tino Röhlicke, explaining me the secrets of FIFO's, FPGA's, Bits'n'Bytes, Quantum Crytpography and developing special electronics for me – these guys are burning! The mechanic workshop of Volker Völlkopf was the first proof that working at light speed and looking relaxed at the same time is possible. Thank you, for immediately preparing so many components I urgently needed during the setup of my system. Also Angelika Zoufahl I'd like to mention and not to forget to thank her for patient understanding and always having some words of confidence for me.

Not only people at work have been involved in my thesis. In particular I want to thank my parents who are always there for me and brought me quite a good way till here. I'd like to thank all my friends liking me even though I had to bore them sometimes with my stories about diffusion, proteins, measurement schemes, unsolved problems, solved problems, nearly solved problems, and other technical details they really did not want to know about and still pretending to be interested. They understood the situation of a young father who's been partially separated from his beloved family not having much opportunity to share time with them. Encouraging me and never letting me down even thought sometimes I worked on my thesis at the expense of my neglect of them. I'm especially

grateful to ‘das Haus’, Omanette, Katharina and Steve. Without you, I wonder whether this thesis would have been finished at all. You were helping out any time there was need for a babysitter in Berlin during my stay in Cologne – and there was often a need. Thank you, Momo for taking my intermittent absence easy and kisses to you, my beloved Caroline supporting me everywhere at anytime. There are no words describing the merits you have on the success of this work.

10. Appendix

In this section, the theoretical foundations of FCS will be explained and all equations needed for data analysis will be derived. At first, the fluorescence correlation function of freely diffusing molecules as measured with a confocal microscopy will be discussed. The analysis will then be extended to the case of 2fFCS. This includes a general description of the 2fFCS correlation function as well as a new model for describing the molecule detection function (MDF). Two-dimensional planar diffusion will be treated separately, discussing alternative measurement methods such as the *z*-scan technique proposed by Benda *et al.* (Benda *et al.*, 2003). Finally, a model for describing surface adsorption/desorption effects of molecules diffusing within a supported lipid bilayer will be derived.

The most important equation to mention is the Stokes-Einstein relation formulated by Einstein in 1905 in his dissertation and also in his papers (Einstein, 1905a; Einstein, 1905b), which describes the dependence of the diffusion coefficient *D* of a small particle (a sugar molecule in Einstein's work) on solvent viscosity, temperature and its hydrodynamic radius, which is also called Stokes radius:

$$D = \frac{k_B T}{6\pi\eta r_s} \tag{10.1}$$

where *T* denotes the absolute temperature, k_B the Boltzmann constant, η the viscosity, and r_S the hydrodynamic radius. This equation interconnects the fundamental parameters determining the diffusion coefficient and is therefore essential for all following considerations.

A good starting point for further investigations is the derivation of the autocorrelation function as measured with a confocal microscope.

10.1. General aspects of the autocorrelation function

Any motion or photophysical process of fluorescent particles in the confocal observation volume leads to fluctuations of the detected signal. These fluctuations are evaluated in fluorescence correlation spectroscopy (FCS). For this purpose, the so called second-order two-point autocorrelation function (ACF) g of the fluorescence signal I is calculated:

$$g(t_1,t_2)=\langle I(t_1)\,I(t_2)\rangle \tag{10.2}$$

where $\langle\cdot\rangle$ denotes ensemble averaging. The ensemble averaging can be replaced by time averaging if the system of interest is an ergodic system and if it is in equilibrium. If so, the correlation function depends only on the time-difference:

$$g(t_1,t_2)=g(|t_1-t_2|) \tag{10.3}$$

Thus, Eq. (10.2) can be written as:

$$g(\tau)=\langle I(t+\tau)\,I(t)\rangle \tag{10.4}$$

wherein $I(t)$ is the fluorescence intensity at time t and $I(t+\tau)$ is the intensity at time $t+\tau$. In this context, the value of the ACF can be understood as a measure of the probability of detecting a photon at time τ if there was a photon detected at time zero.

In the following we try to find a more detailed description of the intensity as a function of time. $I(t)$ is composed of the overall detection efficiency, the concentration of fluorophores and of course the shape of the detection function:

$$I(t)=\varepsilon\int_V U(\boldsymbol{r})\,c(\boldsymbol{r},t)\,d\boldsymbol{r} \tag{10.5}$$

wherein $c(\boldsymbol{r},t)$ is the concentration of the fluorescent molecules. ε represents the overall excitation power and detection efficiency (including the fluorophores properties, such as quantum yield and extinction coefficient). *U(**r**)* denotes the probability density to detect a photon from a molecule located at ***r***, that is the MDF. Since the system of interest is in equilibrium, fluctuations of the concentration can be written as zero-mean fluctuations around a constant mean value:

$$c(\boldsymbol{r},t) = \langle c \rangle + \delta c(\boldsymbol{r},t); \qquad \langle \delta c(\boldsymbol{r},t) \rangle = 0 \tag{10.6}$$

Inserting Eqs. (10.5) (10.6) into Eq. (10.4) yields:

$$g(\tau) = \varepsilon^2 \int_V \int_V U(\boldsymbol{r}_1) \langle \delta c(\boldsymbol{r}_1,\tau)\, \delta c(\boldsymbol{r}_2,0) \rangle U(\boldsymbol{r}_2)\, d\boldsymbol{r}_1\, d\boldsymbol{r}_2 + \left[\varepsilon \langle c \rangle \int_V U(\boldsymbol{r})\, d\boldsymbol{r} \right]^2 \tag{10.7}$$

This equation splits the detected signal in two parts: A time-dependent part and a time-independent part. The latter can also contain contributions from uncorrelated background noise I_{bg}.

In order to further evaluate the correlation function, an expression for $\langle \delta c(\boldsymbol{r}_1,\tau)\, \delta c(\boldsymbol{r}_2,0) \rangle$ has to be found. If fluctuations of the local concentration are solely caused by Brownian motion (diffusion), then the fluctuations satisfy the diffusion equation

$$\frac{\partial \delta c(\boldsymbol{r},t)}{\partial t} = D \cdot \Delta_r \delta c(\boldsymbol{r},t) \tag{10.8}$$

wherein *D* is the diffusion coefficient of the fluorescent molecule and Δ_r denotes the three-dimensional Laplace operator. The solution of this equation can be expressed with the help of the Green function $G(\boldsymbol{r},t \mid \boldsymbol{\rho},0)$ as:

$$\delta c(\boldsymbol{r},t) = \int_V \delta c(\boldsymbol{\rho},0)\, G(\boldsymbol{r},t \mid \boldsymbol{\rho},0)\, d\boldsymbol{\rho} \tag{10.9}$$

The Green-function describes the probability density that a molecule moves from $\boldsymbol{r}$ to $\boldsymbol{\rho}$ within time *t*. It is itself is a solution of the diffusion equation, satisfies the boundary conditions of the given sample and obeys the initial condition:

$$G(\boldsymbol{r}_1, 0 \mid \boldsymbol{r}_2, 0) = \delta(\boldsymbol{r}_1 - \boldsymbol{r}_2) \tag{10.10}$$

Thus, we can write:

$$\langle \delta c(\boldsymbol{r}_1, \tau)\, \delta c(\boldsymbol{r}_2, 0) \rangle = \int_V \langle \delta c(\boldsymbol{\rho}, 0)\, \delta c(\boldsymbol{r}_2, 0) \rangle G(\boldsymbol{r}_1, \tau \mid \boldsymbol{\rho}, 0)\, d\boldsymbol{\rho} \tag{10.11}$$

As long as the concentration fluctuations are not spatially correlated the following expression holds:

$$\langle \delta c(\boldsymbol{\rho}, 0)\, \delta c(\boldsymbol{r}_2, 0) \rangle = \langle \delta c^2 \rangle \delta(\boldsymbol{\rho} - \boldsymbol{r}_2) \tag{10.12}$$

If we further take into account that the number of (non-interacting) particles in a finite volume follows the Poisson statistics, we can write:

$$\langle \delta c^2 \rangle = \langle c \rangle \tag{10.13}$$

This leads to:

$$\langle \delta c(\boldsymbol{r}_1, \tau)\, \delta c(\boldsymbol{r}_2, 0) \rangle = \langle c \rangle G(\boldsymbol{r}_1, \tau \mid \boldsymbol{r}_2, 0) \tag{10.14}$$

Inserting Eq. (10.14) into Eq.(10.7) yields the final form of the correlation function:

$$g(t) = \varepsilon^2 c \int_V \int_V U(\boldsymbol{r}_1)\, G(\boldsymbol{r}_1, t \mid \boldsymbol{r}_2, 0)\, U(\boldsymbol{r}_2)\, d\boldsymbol{r}_1 d\boldsymbol{r}_2 + \left[\varepsilon c \int_V U(\boldsymbol{r})\, d\boldsymbol{r} + I_{bg} \right]^2, \tag{10.15}$$

wherein *c* is the concentration of fluorescent molecules in *molecules / sample volume V*. I_{bg} is the background intensity which accounts for uncorrelated detection events, such as dark counts from the detectors etc.

Often, Eq. (10.15) is written in the so called normalized form:

$$\tilde{g}(t) = \frac{g(t)}{g(\infty)} \tag{10.16}$$

For free d-dimensionally diffusing molecules $G(\boldsymbol{r}_1, \tau \mid \boldsymbol{r}_2, 0)$ is given by:

$$G(\boldsymbol{r}_1, t \mid \boldsymbol{r}_2, 0) = G(\boldsymbol{r}_1 - \boldsymbol{r}_2, t) = \frac{1}{(4\pi D t)^{d/2}} exp\left[-\frac{(\boldsymbol{r}_1 - \boldsymbol{r}_2)^2}{4Dt} \right] \tag{10.17}$$

Note that Eq. (10.15) and (10.16) are only valid as long as the following requirements are satisfied:

The system of interest has to be in the equilibrium and has to fulfill the ergodic theorem (Birkhoff, 1931). Furthermore, we assumed that the fluorescent molecules do not interact and that any correlation between the detected fluorescence photons is due to diffusion, i.e. the molecules do not blink or exhibit other photophysical properties. As soon as other processes occur which correlate the fluorescent properties of the molecules (i.e. anti-bunching, triplet state dynamics) Eq. (10.15) and (10.16) have to be extended.

An interesting feature of the ACF is that from Eq. (10.15) the concentration of molecules in the sample can be derived:

$$\begin{aligned} g(0) - g(\infty) &= \varepsilon^2 c \int_V \int_V U(\boldsymbol{r}_1) G(\boldsymbol{r}_1 - \boldsymbol{r}_2, 0) U(\boldsymbol{r}_2)\, d\boldsymbol{r}_1 d\boldsymbol{r}_2 \\ &= \varepsilon^2 c \int_V \int_V U(\boldsymbol{r}_1) \delta(\boldsymbol{r}_1 - \boldsymbol{r}_2) U(\boldsymbol{r}_2)\, d\boldsymbol{r}_1 d\boldsymbol{r}_2 \\ &= \varepsilon^2 c \int_V U^2(\boldsymbol{r})\, d\boldsymbol{r} \end{aligned} \tag{10.18}$$

Dividing Eq. (10.18) by $g(\infty)$ and taking the reciprocal, Eq. (10.18) can be written as:

$$\frac{g(\infty)}{g(0) - g(\infty)} = c \cdot \frac{\left[\int_V U(\boldsymbol{r})\, d\boldsymbol{r} + I_{bg} \right]^2}{\int_V U^2(\boldsymbol{r})\, d\boldsymbol{r}} \tag{10.19}$$

If I_{bg} is negligible, one can define the effective volume V_{eff}

$$V_{eff} = \frac{\left[\int_V U(\boldsymbol{r})\, d\boldsymbol{r}\right]^2}{\int_V U^2(\boldsymbol{r})\, d\boldsymbol{r}} \tag{10.20}$$

so that

$$\frac{g(\infty)}{g(0) - g(\infty)} = c \cdot V_{eff} = N \tag{10.21}$$

where N is the average number of particles within the detection volume. A typical autocorrelation function of a free diffusing dye (Atto655) is shown in Fig. 33.

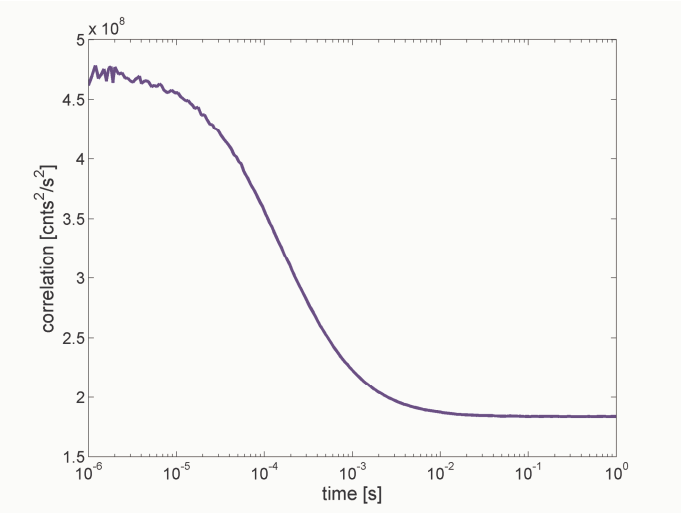

Fig. 33: Typical autocorrelation curve representing free three-dimensional diffusion of the fluorescent dye Atto655 in water. Atto655 has the property that it exhibits no triplet state in its unbound form, and is thus perfectly applicable for diffusion measurements.

The leveling-off of the ACF at long lag time represents the time-independent part of Eq. (10.15), which in turn is equal to the square of the mean number of photons detected within measurement time T.

10.2. Extending the theory to two-focus FCS

Let us now consider two identical MDF's which are laterally shifted by a fixed distance $\delta \boldsymbol{x}$. This can be expressed simply by shifting the origin of one MDF by $\delta \boldsymbol{x}$:

$$U(\boldsymbol{r}) \rightarrow U(\boldsymbol{r} + \delta \boldsymbol{x}) \tag{10.22}$$

With a simple coordinate transformation

$$\boldsymbol{r}_1 \rightarrow \boldsymbol{r}_1 + \delta\boldsymbol{x} \tag{10.23}$$

one can express this shift also through the Green function from Eq. (10.17) and leave the MDF unchanged:

$$G\left(\boldsymbol{r}_1 - \boldsymbol{r}_2 - \delta\boldsymbol{x}, t\right) = \frac{1}{\left(4\pi D t\right)^{d/2}} exp\left[-\frac{\left(\boldsymbol{r}_1 - \boldsymbol{r}_2 - \delta\boldsymbol{x}\right)^2}{4Dt}\right] \tag{10.24}$$

When using two MDFs, it may be useful to modify Eq. (10.15) slightly since during an experiment the overall excitation power and detection efficiency ε may be different for both MDF's and should be better referred to as ε_1 and ε_2, respectively:

$$g\left(t, \delta\boldsymbol{x}\right) = \varepsilon_1 \varepsilon_2 c \int_V \int_V U\left(\boldsymbol{r}_1\right) G\left(\boldsymbol{r}_1 - \boldsymbol{r}_2 - \delta\boldsymbol{x}, t\right) U\left(\boldsymbol{r}_2\right) d\boldsymbol{r}_1 d\boldsymbol{r}_2 + g_\infty \tag{10.25}$$

where g_∞ now is given by

$$g_\infty = \left[\varepsilon_1 c \int_V U\left(\boldsymbol{r}_1\right) d\boldsymbol{r}_1 + I_{bg}\right]\left[\varepsilon_2 c \int_V U\left(\boldsymbol{r}_2\right) d\boldsymbol{r}_2 + I_{bg}\right] \tag{10.26}$$

When setting $\delta = 0$ in Eq. (10.25) and replacing $\varepsilon_1\varepsilon_2$ by either ε_1^2 or ε_2^2, one yields the ACF for separate detection volumes, respectively. All subsequent derivations will be done on the basis of Eqs. (10.24)-(10.26).

10.3. Finding a good description for the MDF

A crucial point for evaluating the integrals in Eqs.(10.25) and (10.26) is to find an appropriate description of the MDF $U\left(\boldsymbol{r}\right)$. In conventional FCS, the MDF is often assumed to have a 3D-Gaussian shape, i.e.

$$U\left(\boldsymbol{r}\right) = U_0\, exp\left[-\frac{2\left(x^2 + y^2\right)}{r_0^2} - \frac{2z^2}{z_0^2}\right] \tag{10.27}$$

where $\{x, y, z\}$ are Cartesian coordinates with *z* along the optical axis, and the parameters r_0 and z_0 define the transverse and axial extension of the MDF (i.e. detection volume). An advantage of this description is that the resulting correlation function can be given in a closed analytical expression. Unfortunately, this model does not describe the MDF sufficiently well as is shown in section 4.2. A more realistic expression is given by

$$U(\boldsymbol{r}) = \frac{\kappa(z)}{w^2(z)} exp\left[-\frac{2}{w^2(z)}\left(x^2 + y^2\right)\right] \tag{10.28}$$

where $w(z)$ and $\kappa(z)$ are given by

$$w(z) = w_0\left[1+\left(\frac{\lambda_{ex} z}{\pi w_0^2 n}\right)^2\right]^{1/2} \tag{10.29}$$

and

$$\kappa(z) = 2\int_0^a \frac{\rho}{R^2(z)} exp\left(-\frac{2\rho^2}{R^2(z)}\right) d\rho = 1 - exp\left(-\frac{2a^2}{R^2(z)}\right) \tag{10.30}$$

and the function $R(z)$ is defined by an expression similar to Eq. (4.2):

$$R(z) = R_0\left[1+\left(\frac{\lambda_{em} z}{\pi R_0^2 n}\right)^2\right]^{1/2} \tag{10.31}$$

In the above equations, λ_{ex} is the excitation wavelength, and λ_{em} the center-emission wavelength, *n* is the refractive index of the immersion medium (water), *a* is the radius of the confocal aperture divided by magnification, and w_0 and R_0 are two (generally unknown) model parameters. Eq. (4.2) is nothing else than the scalar approximation for the radius of a diverging laser beam with beam waist radius w_0 (see e.g. (Enderlein & Pampaloni, 2004)), and Eq. (4.3) is inspired by earlier work of Qian and Elson (Qian & Elson, 1991) and Rigler *et al.* (Rigler *et al.*, 1993) concerning the point spread function of confocal imaging. It should be noted that, although Eq. (4.1) looks like the sometimes used

Gauss-Lorentz profile, it is *not* such a profile due to the presence of the non-trivial amplitude function $\kappa(z)$ given in Eq. (4.3). Thus, in each plane perpendicular to the optical axis, the MDF is approximated by a 2D-Gaussian distribution having width $w(z)$ and amplitude $\kappa(z)/w^2(z)$.

10.4. Evaluation of the resulting correlation function

As mentioned above, the description of the MDF as given by Eq. (4.1) is characterized by just two parameters; w_0 and R_0, similarly to the standard Gaussian model. In this regard, the proposed new model and the Gaussian model are equally well applicable; although gives a much more realistic description of the actual MDF. The proposed new MDF model does not lead to a closed analytical form of the resulting ACF, but hat to be evaluated numerically via the double-integral:

$$g(t) = g_\infty + \frac{\varepsilon_1 \varepsilon_2 c}{4}\sqrt{\frac{\pi}{Dt}}\int_{-\infty}^{\infty}\int_{-\infty}^{\infty}\frac{\kappa(z_1)\kappa(z_2)}{8Dt + w^2(z_1) + w^2(z_2)} \exp\left[-\frac{(z_2 - z_1)^2}{4Dt}\frac{2\delta^2}{8Dt + w^2(z_1) + w^2(z_2)}\right] dz_2 dz_1 \tag{10.32}$$

Nonetheless, using state-of-the art PCs, numerical evaluation of this expression is fast and no hindrance to practical applications of the above expression in experimental data fitting. For doing that it is convenient to change variables to

$$a = \frac{z_2 - z_1}{2\sqrt{Dt}}, \quad b = \frac{z_2 + z_1}{2} \tag{10.33}$$

leading to the expression

$$g(t,\delta) = g_\infty + 2\varepsilon_1\varepsilon_2 c\sqrt{\pi}\int_0^\infty da \int_0^\infty db \frac{\kappa\left(b-\sqrt{Dt}a\right)\kappa\left(b+\sqrt{Dt}a\right)}{8Dt + w^2\left(b-\sqrt{Dt}a\right)+w^2\left(b+\sqrt{Dt}a\right)} \exp\left[-a^2 - \frac{2\delta^2}{8Dt + w^2\left(b-\sqrt{Dt}a\right)+w^2\left(b+\sqrt{Dt}a\right)}\right]. \quad (10.34)$$

It should be mentioned again that setting $\delta = 0$ in Eq. (10.34) and replacing $\varepsilon_1\varepsilon_2$ by either ε_1^2 or ε_2^2 one yields the ACF for the individual detection volumes, respectively.

Because *w* and κ are rapidly decaying functions for large argument, the infinite integrations over *a* and *b* can be approximated by numerically evaluating the integrals within a finite two-dimensional strip defined by $\left|b \pm \sqrt{Dt}a\right| < M$, where *M* is a truncation value chosen in such a way that the numerical integration result does not change when increasing *M* further. Numerical integration is done by using a simple finite element scheme. Convergence is checked by testing whether the numerical result remains the same upon refining the finite element size and when increasing the threshold value *M*.

The above equations are becoming slightly more complex when the laser focus is not described by a circular but an elliptic Gaussian distribution (which is always the case when focusing a linearly polarized beam). Assuming that the principal axes of the laser beams are parallel to the *x*- and *y*-axes, and denoting now the smallest beam waist radii along the principal axes with $w_{0,1}$ and $w_{0,2}$, one has now two functions $w_1(z)$ and $w_2(z)$ describing the laser profile, and $w^2(z)$ in Eq. (10.32) has to be replaced by $\left[w_1^2(z)+w_2^2(z)\right]/2$. Two keep things simple and not to increase the number of independent parameters, we will assume that the *effective* radius $w_{eff}(z) = \sqrt{\left[w_1^2(z)+w_2^2(z)\right]/2}$ is still sufficiently well described by the right hand side of Eq. (4.2) with a single parameter w_0.

Data fitting is performed with least square fitting of a model curve, Eq. (10.34), against the measured ACF ($\delta = 0$, $\varepsilon_1\varepsilon_2$ replaced by either ε_1^2 or ε_2^2) and cross-correlation *simultaneously* in a global fit. As fit parameters one has $\varepsilon_1\sqrt{c}$, $\varepsilon_2\sqrt{c}$, *D*, w_0 and R_0, as well as three offset values g_∞. The distance δ between the detection regions is determined by the properties of the Nomarski prism (see section 4.3) and has to be exactly known *a priori*, thus introducing an external length scale into data evaluation. It is important to

notice that a crucial criterion of fit quality is not only to simultaneously reproduce the temporal shape of both ACFs and the cross-correlation function, but also to reproduce their three amplitudes $g_{t\to 0}-g_\infty$ using only the two parameters $\varepsilon_1\sqrt{c}$ and $\varepsilon_2\sqrt{c}$. The relation between the amplitudes of the cross-correlation function and the amplitudes of the ACFs is determined by the overlap between the two MDFs, and thus by the shape parameters w_0 and R_0. Thus, achieving good fit quality for the relative amplitudes of ACF and cross-correlation strongly helps to find the correct values of these parameters. Typical fitting time on a state of the art PC takes ca. 1 min using a custom written *Matlab* routine.

10.5. Free, two-dimensional, planar diffusion

For evaluating the correlation function of two-dimensional planar diffusion, we need to find expressions for a two dimensional MDF, whereas The Green function describing two-dimensional free diffusion is already given by Eq. (10.24) setting $d=2$.

Since two-dimensional, planar diffusion proceeds orthogonally to the optical axis (z-direction) of the microscope, the two-dimensional MDF is derived by taking a slice of the three-dimensional MDF in Eq. (4.1) at the appropriate *z*-position. Thus, the two-dimensional MDF is given by

$$U(\boldsymbol{r})=U(x,y\,|\,z_0)=\frac{\kappa(z_0)}{w^2(z_0)}exp\left[-\frac{2}{w^2(z_0)}\left(x^2+y^2\right)\right] \tag{10.35}$$

Note that in the above equation z_0 is fixed. To get an expression for the resulting correlation function, the MDF from Eq. (4.5) is put into the two-focus correlation function, Eq.(10.25),

$$\begin{aligned} g(t\,|\,z_0,\delta) &= \frac{c\varepsilon_1\varepsilon_2\kappa(z_0)^2}{4\pi Dtw^4(z_0)}\int_{\mathbb{R}^2}\int_{\mathbb{R}^2} d\boldsymbol{r}_2 d\boldsymbol{r}_1 \exp\left(-\frac{2\boldsymbol{r}_2^2}{w^2(z_0)}-\frac{2\boldsymbol{r}_1^2}{w^2(z_0)}-\frac{(\boldsymbol{r}_2-\boldsymbol{r}_1+\delta\boldsymbol{x})^2}{4Dt}\right)+g_\infty \\ &= \frac{\pi c\varepsilon_1\varepsilon_2}{4}\frac{\kappa(z_0)^2}{4Dt+w^2(z_0)}\exp\left[-\frac{\delta^2}{4Dt+w^2(z_0)}\right]+g_\infty \end{aligned} \tag{10.36}$$

with

$$g_\infty = \frac{\pi^2 c^2 \varepsilon_1 \varepsilon_2}{4} \kappa \left(z_0 \right)^2 \tag{10.37}$$

In its normalized form, the ACF now reads

$$g_{norm}\left(t \mid z_0, \delta\right) = \frac{g\left(t \mid z_0, \delta\right)}{g_\infty} - 1 = \frac{1}{\pi c} \frac{1}{4Dt + w\left(z_0\right)^2} \exp\left[- \frac{\delta^2}{4Dt + w\left(z_0\right)^2} \right] \tag{10.38}$$

When setting δ equal to zero one yields the ACF for one detection volume:

$$ACF_{norm}\left(t \mid z_0\right) = \frac{1}{\pi c} \frac{1}{4Dt + w\left(z_0\right)^2} \tag{10.39}$$

If $w\left(z_0\right)$ is known, D can be calculated from the above equation. Unfortunately, estimating $w\left(z_0\right)$ is difficult, since one would have precise knowledge of the position of the laser focus relative to the plane where diffusion takes place. Benda *et al.* (Benda *et al.*, 2003; Humpolickova *et al.*, 2006) developed a smart technique to measure absolute diffusion coefficients in planar systems by performing measurements at various positions z_0. This technique is called z-scan FCS. When introducing the diffusion time τ_D .

$$\tau_D\left(z_0\right) = \frac{w\left(z_0\right)^2}{4D} \tag{10.40}$$

Eq. (10.39) can be expressed as

$$ACF_{norm}\left(t \mid z_0\right) = \frac{1}{N\left(\frac{t}{\tau_D\left(z_0\right)} + 1 \right)}; \qquad N = V_{eff} c = \pi w\left(z_0\right)^2 c \tag{10.41}$$

When applying the z-scan FCS, one measures ACFs of diffusing molecules within a planar lipid membrane for different vertical positions of the membrane with respect to the focal plane and estimates $\tau_D\left(z\right)$. Because there is a stringent correlation between divergence and waist of the MDF (see Eq. (4.2)), Eq. (10.40) can be rewritten as

$$\tau_D(z) = \frac{w^2(z)}{4D} = \frac{w_0^2}{4D}\left[1 + \left(\frac{\lambda_{ex} z}{\pi w_0^2 n}\right)^2\right] \tag{10.42}$$

We verify the accuracy of this assumption by scanning the PSF as shown in section 4.2. Thus, plotting the measured diffusion time as a function of the vertical position of the laser focus (i.e. the objectives position) will lead to a parabolic graph. This graph is fitted with the diffusion coefficient and the focus beam waist as fit parameters and yields absolute values for them.

Alternatively, using 2fFCS and knowing the exact distance δ between the laser foci, one can obtain the values of $w(z_0)$ and D already from a single measurement. Dividing the measured cross-correlation curve (XCF) through the ACF leads to (see Eq. (10.38)):

$$\frac{XCF_{norm}}{ACF_{norm}} = \exp\left[-\frac{\delta^2}{4Dt + w(z_0)^2}\right] = \exp\left[-\frac{\overbrace{\delta^2/4D}^{p_1}}{\underbrace{w(z_0)^2/4D}_{p_2} + t}\right] \tag{10.43}$$

Here we assumed that $\varepsilon_1 = \varepsilon_2$. It is evident that from the fitting parameters p_1 the diffusion coefficient can be extracted easily and from p_2 $w(z_0)$ can be derived.

Thus, both methods will give the same values for diffusion coefficients. On the other hand, the distance δ between both foci in the two-focus setup can be found demanding that *z*-scan FCS and 2fFCS yield identical results. In section 4.3 we apply this method to achieve the exact distance between the two foci of our system and in section (6) we apply 2fFCS and *z*-scan FCS to the special case of two-dimensionally diffusing molecules who tend to adsorb to the supporting surface.

It should be also noted that, due to the slight off-centre position of the two laser foci with respect to the confocal aperture, the apparent distance between the Gaussian intensity distributions becomes slightly smaller when moving farther away (> 2 µm) from the focal plane. However, in the subsequent 2fFCS data analysis, this slight bending of the MDF is ignored and we used the model MDF as described in Eqs. (4.1)-(4.4), assuming axial symmetric MDFs with a lateral distance that is independent on *z*-position.

10.6. Surface adsorption/desorption in planar systems

In the following we will consider two-dimensional diffusion of molecules within a supported lipid bilayer which can undergo adsorption and desorption to/from the supporting surface. The situation and mathematical approach is similar to (Lieto *et al.*, 2003; Starr & Thompson, 2001), where the authors considered three-dimensional diffusion in solution above a surface and adsorption/desorption kinetics to the surface. However, the final result will be quite different, and no closed analytical solution can be derived in our case.

The starting point for the calculations is again the correlation function as given by Eq. (10.25). The two-dimensional MDF $U(\boldsymbol{r})$ is again described by Eq. (4.5). Then, the two focus-correlation function $g(t \mid z_0, \delta)$ is given by:

$$g(t \mid z_0, \delta) = \varepsilon_1 \varepsilon_2 c \kappa^2(z_0) w^{-4}(z_0) \int_A \int_A \exp\left[-\frac{2(\boldsymbol{r}_1 + \delta \boldsymbol{x})^2}{w^2(z_0)}\right] G(\boldsymbol{r}_1 - \boldsymbol{r}_2, t) \exp\left[-\frac{2\boldsymbol{r}_2^{\,2}}{w^2(z_0)}\right] d\boldsymbol{r}_1 d\boldsymbol{r}_2 + g_\infty \tag{10.44}$$

where g_∞ is given by Eq. (10.37). As before, the Green function $G(\boldsymbol{r}_1 - \boldsymbol{r}_2, t)$ denotes the probability density that a molecule moves from position $\boldsymbol{r}_1$ to position $\boldsymbol{r}_2$ within time *t*, taking now into account possible adsorption and desorption to and from the supporting surface. All integrations are performed over the whole two-dimensional surface A. It should be noticed that the final result $g(t \mid z_0, \delta)$ depends only on the absolute value δ but not on its direction. The result for the autocorrelation of one focus is again obtained by setting $\delta = 0$ in the above expression.

The problem now is to find an expression for $G(\boldsymbol{r}_1 - \boldsymbol{r}_2, t)$. Let us denote the probability density to find a freely diffusing molecule at position $\boldsymbol{r}$ and time *t* by $a(\boldsymbol{r}, t)$ and the corresponding probability density to find an adsorbed (bound) molecule at position $\boldsymbol{r}$ and time *t* by $b(\boldsymbol{r}, t)$. The equations governing the temporal evolution of these functions are

$$\begin{aligned}\frac{\partial a}{\partial t} &= D\Delta a - k_+ a + k_- b \\ \frac{\partial b}{\partial t} &= k_+ a - k_- b\end{aligned} \tag{10.45}$$

where D is the diffusion coefficient, Δ denotes the two-dimensional Laplace operator, and k_+ and k_- are the adsorption and desorption rate constants of molecule to and from the supporting surface, respectively. Under equilibrium conditions, the probabilities to find a molecule in a freely diffusing or an adsorbed state are $k_-/(k_+ + k_-)$ and $k_+/(k_+ + k_-)$, respectively. Since the partial differential equation system from Eq. (10.45) is linear, $G(\boldsymbol{r}_1 - \boldsymbol{r}_2, t)$ can be found as the sum of solutions of $a(\boldsymbol{r}_1 - \boldsymbol{r}_2, t)$ and $b(\boldsymbol{r}_1 - \boldsymbol{r}_2, t)$, with initial conditions:

$$\begin{aligned}a(\boldsymbol{r}_1 - \boldsymbol{r}_2, 0) &= \frac{k_-}{k_+ + k_-}\delta(\boldsymbol{r}_1 - \boldsymbol{r}_2) \\ b(\boldsymbol{r}_1 - \boldsymbol{r}_2, 0) &= \frac{k_+}{k_+ + k_-}\delta(\boldsymbol{r}_1 - \boldsymbol{r}_2)\end{aligned} \tag{10.46}$$

Applying a Fourier transform to Eq. (10.45), the solution for the Fourier transform of $G(\boldsymbol{r}_1 - \boldsymbol{r}_2, t)$ can be found in a straightforward way as:

$$\begin{aligned}G(\boldsymbol{q}, t) = &\frac{(k_+ + k_-)(k_+ + k_- + \Delta) + (k_+ - k_-)D\boldsymbol{q}^2}{2(k_+ + k_-)}\exp(\omega_1 t - i\boldsymbol{q}\cdot\boldsymbol{r}_2) \\ &- \frac{(k_+ + k_-)(k_+ + k_- - \Delta) + (k_+ - k_-)D\boldsymbol{q}^2}{2(k_+ + k_-)}\exp(\omega_2 t - i\boldsymbol{q}\cdot\boldsymbol{r}_2)\end{aligned} \tag{10.47}$$

where $\boldsymbol{q}$ is the Fourier transformed coordinate, and the abbreviations

$$\begin{aligned}\omega_{1,2} &= -\frac{D\boldsymbol{q}^2 + k_+ + k_- \mp \Delta}{2}, \\ \Delta^2 &= \left(D\boldsymbol{q}^2 + k_+ - k_-\right)^2 + 4k_+ k_-\end{aligned} \tag{10.48}$$

were used. Converting Eq. (10.47) back to real space, and inserting the result into Eq.(10.44), yields the final result for the auto-/cross-correlation function

$$g(t \mid z_0, \delta) = A_0 \int_0^\infty q\left[A_+ \exp(\omega_1 t) - A_- \exp(\omega_2 t)\right] J_0(q\delta) \exp\left(-\frac{q^2 w^2}{4}\right) dq + g_\infty \qquad (10.49)$$

with

$$\begin{aligned} A_0 &= \varepsilon_1 \varepsilon_2 c\, \kappa^2(z_0)\, w^{-4}(z_0) \\ A_+ &= \frac{(k_+ + k_-)(k_+ + k_- + \Delta) + (k_+ - k_-) Dq^2}{2(k_+ + k_-)\Delta} \\ A_- &= \frac{(k_+ + k_-)(k_+ + k_- - \Delta) + (k_+ - k_-) Dq^2}{2(k_+ + k_-)\Delta} \end{aligned} \qquad (10.50)$$

wherein J_0 is Bessel's function of the first kind (Abramowitz & Stegun, 1984), and g_∞ denotes the constant offset of the autocorrelation function reached at $t \to \infty$ In the limit of vanishing adsorption rate constant, i.e. uninhibited free diffusion in a plane, this results reduces to the standard expression of Eq. (10.36):

$$\begin{aligned} g(t \mid z_0, \delta) &= A_0 \int_0^\infty dq q J_0(q\delta) \exp\left[-\frac{4Dq^2 t + q^2 w^2}{4}\right] + g_\infty \\ &= \frac{\pi c \varepsilon_1 \varepsilon_2}{4} \frac{\kappa(z_0)^2}{4Dt + w(z_0)^2} \exp\left[-\frac{\delta^2}{4Dt + w(z_0)^2}\right] + g_\infty \end{aligned} \qquad (10.51)$$

When using Eq.(10.49) for fitting our experimental data, the occurring integral was evaluated numerically by using a standard Romberg integration scheme (Teukolsky *et al.*, 1992).

10.7. General considerations: Microsecond blinking

Most fluorescent dyes used in FCS experiments exhibit fast photophysical transitions between fluorescent and non-fluorescent states. These transitions can be e.g. light induced transitions into the non-fluorescent triplet state (intersystem crossing) with subsequent

return to the ground state, or conformational fluctuations between a fluorescent and a non-fluorescent state such as the trans-cis-conformational transitions in many cyanine dyes. This so-called blinking of molecules may appear on timescales ranging from nanoseconds up to hours (e.g. in photoswitchable proteins (Habuchi *et al.*, 2005)). A typical ACF with µs-blinking is shown in Fig. 34.

The red dotted part of the ACF is clearly different from that in Fig. 34. This µs-decay reflects the probability that the diffusing molecule which was fluorescent at time zero has switched into a non-fluorescent state. A standard assumption in modeling these fast blinking processes in an ACF is that blinking occurs on a much faster time scale than the diffusion out of the detection volume. In that case, the ACF decay due to blinking can be simply described by multiplying the diffusion-generated ACF with an additional exponential term of the form (Widengren *et al.*, 1995)

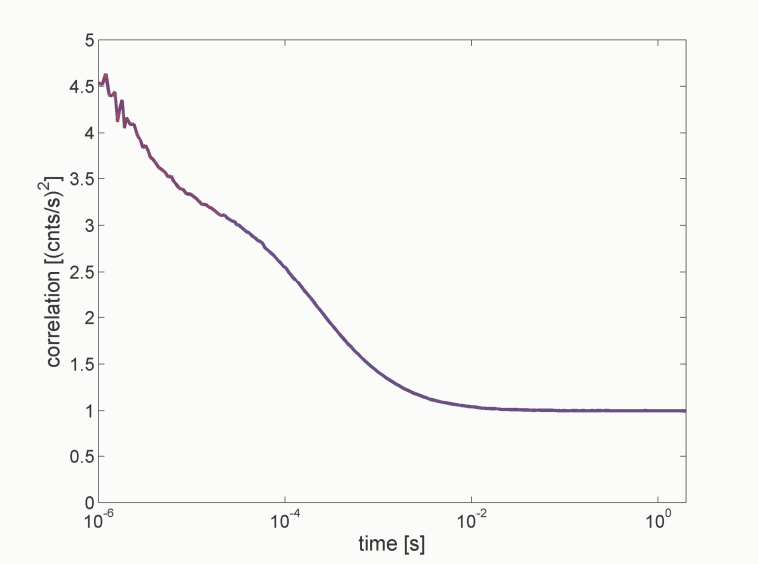

Fig. 34: A typical autocorrelation curve with µs-blinking dynamics (indicated with red dots). The sample was Cy5 in water. This dye exhibits µs-blinking because of a light driven cis-trans-isomerization, where only one state is fluorescent. Excitation power was 40 µW @ 40/3 MHz repetition frequency.

$$g_{blink}(t) = 1 - T + T\,exp\left(-\frac{t}{\tau_{blink}}\right) \qquad (10.52)$$

where T is the fraction of molecules which are in the in the non-fluorescent state, and τ_{blink}^{-1} is the total transition rate into and out of the non-fluorescent state.

11. Materials and Methods

- Chemicals

Red fluorescent beads (PS-Speck Microscope Point Source Kit P7220) were purchased by Invitrogen GmbH (Karlsruhe, Germany). Guanidine hydrochloride (> 99 %, GdHCl) was purchased from Sigma-Aldrich Chemikalien GmbH (Munich, Germany). Atto655 in the form of carboxylic acid and as NHS-ester were purchased from Atto-Tec GmbH (Siegen, Germany). Deuterized methanol-d_4 (99.8 atom %) was purchased from Sigma-Aldrich Chemikalien GmbH (Munich, Germany). DOPC and DOPE-Biotin was purchased from Avanti Polar Lipids (Alabaster, AL, USA). DOPE was purchased from Sigma (St. Louis, MO, USA). Other chemicals (methanol, chloroform, glucose, $CaCl_2$, KCl, MgCl, HEPES, etc) were purchased from Sigma, Fluka (St. Gallen, Switzerland) or kmf Laborchemie Handels GmbH (Lohmar, Germany). Neutravidin was purchased from Pierce Biotechnology Inc. (Rockford, IL, USA). ITO-coated cover slides were purchased from SPI Supplies (West Chester, PA, USA).

- Preparation of guanidine hydrochloride solutions

A 6.63 M stock solution of GdHCl in water was prepared. By diluting this stock, solutions with lower GdHCl concentrations were made. Concentration of the dilutions was checked by measuring the refractive indices. Solvent viscosities were estimated out of the concentrations following Kawahara and Tanford (Kawahara & Tanford, 1966). For measurements a small fraction of Atto655 carboxylic acid dissolved in bi-distilled water was added (5 µl / ml).

- Preparation of calcium buffers

The calcium buffers are prepared according to a method described by Tsien and Pozzan (Tsien & Pozzan, 1989). This method is based on the principle that when the concentrations of calcium and EGTA are very close to each other, the only free calcium available is that which is in equilibrium with EGTA. Thus, the free calcium concentration is a function of the dissociation constant (K_d) of Ca-EGTA. The K_d of a chelator, varies with ionic strength, pH and temperature. To attain calcium and EGTA concentrations sufficiently close to each other, one must carefully generate a solution of the CaEGTA complex. This is accomplished by a “pH-metric” method, which makes use of the fact that the ion binding of EGTA causes an acidification of the solution. With this method, the

concentrations of calcium and EGTA can be verified to be within 0.5 % of each other. Thus one prepares a buffer containing 10 mM CaEGTA and a buffer containing 10 mM K_2EGTA. By cross-diluting both buffer at different ratios different free calcium concentrations are set up. The free calcium concentration in each dilution can be calculated from the K_d of CaEGTA.

Our buffers have the same composition as the buffers, which can be purchased from Invitrogen GmbH (Karlsruhe, Germany). Calcium concentrations of the self made buffers could therefore directly be cross checked with the Calcium Calibration Kit with Magnesium #2 from Invitrogen GmbH using the calcium sensitive dye fura-2 and bis-fura-2 (both from Invitrogen GmbH) as well as calcium electrodes. For this reason we recorded a response curve of fura-2 / bis-fura-2 and the calcium electrodes depending on free calcium concentration with the calcium calibration kit with and afterwards we measured the self-made buffers under the same conditions and estimated the free calcium concentration by using the reference curves.

At higher free calcium concentrations buffering with EGTA is not anymore appropriate due to its low K_d. Thus, we used a different calcium chelator, namely nitrilotriacetic acid (NTA), which has a lower K_d for calcium. These buffers where only checked with the calcium electrode. It was checked that the different calcium concentrations have no effect on viscosity, i.e. all calcium buffers have the same viscosity. Also, the viscosity of the different buffers where not affected by the use of different calcium chelators (difference in viscosity < 1 %). Compared to water the calcium buffers were 1.8 % more viscous at 20 °C.

Measurement chambers were stored with 2 % BSA and 0.2 % NaH_3. Before use they were washed gently with bi-distilled water.

- Preparation of wild-type calmodulin

Cloning of the calmodulin WT (wild-type) gene was done by Dr. Wolfgang Boenigk, INB-1, Forschungszentrum Juelich, Germany. The calmodulin gene has been amplified via PCR from single stranded cDNA from bovine retina with primers, which have been synthesised based on human, rat, and mousesequence. The PCR product has been cloned and sequenced with an pBluescript SK(-) vector. Expression of calmodulin was facilitated in E. coli BL211ys E. For this purpose 500 ml LB medium with 100 mg Ampicillin and 18 mg Chloramphencol have been inoculated in cells overnight that way that at the beginning an OD_{600} (optical density at 600 nm) of 0.025 was achieved. The cells have incubated

under permanent movement at 37 °C until OD_{600} was at 0.6. Then induction was has been done by adding IPTG to a final concentration of 1mM. The cells have then been incubated for 2-3 more hours. After that, cells have been cooled with ice and filled into pellets via centrifugation. Pellets are put in 20 ml ice cold water 20 mM TrisHCl, pH 8.0. They are then sonified 6 times for 10 s. Subsequently the solution is centrifuged for 30 min at 4 °C with 17600 g. The excess is incubated for 10 min at 94 °C. After cooling down to 4 °C the solution is again centrifuged under the same conditions as before. 120 µl $CaCl_2$ is added to the excess. Purification is done with a phenylsepharose CL4B-column.

- Labeling calmodulin with Atto655-NHS-ester

CaM was labelled with Atto655-NHS-esther an amine reactive dye and followed a standard labeling procedure like proposed from Invitrogen. To 1 ml protein [~10 µM] solution in PBS buffer 100µl 1M $NaHCO_3$ (pH 8.3) was added and also equimolar amounts of Atto655 in DMSO (only few µl) were added. Labeling was done overnight. Unbound dye was removed with a PD 10 desalting column from GE Healtcare, Germany (former Amersham Biosciences). To remove unspecific bound dye from the CaM the sample was twice dialyzed against 2l HEPES buffer containing 100 mM $MgCl_2$, 150 mM KCl overnight at 4 °C.

- Purification and labeling of recoverin

Recombinant wild-type (WT) recoverin was heterologously expressed in *E. coli* and purified by column chromatography exactly as described in (Permyakov *et al.*, 2000a; Senin *et al.*, 2003). Myristoylated forms were obtained by co-expression of the plasmid pBB-131 containing the *N*-myristoyltransferase 1 (NMT1) from *Saccharomyces cerevisiae* (kindly provided by Dr. J.I. Gordon, Washington University School of Medicine, St. Louis, USA) as described previously (Permyakov *et al.*, 2000b; Senin *et al.*, 2003). The degree of myristoylation was determined by reversed-phase high performance liquid chromatography (HPLC) analysis as described (Hwang & Koch, 2002) using either Vydac 238TP C18 reverse-phase column (4.6 × 250 mm^2) or a Phenomenex Luna reverse phase column (5 µm; 18; 4.6 × 250 mm^2). The Alexa647-maleimide dye (Invitrogen GmbH, Karlsruhe, Germany) was attached to a cystein at position 39. Labeling was done with an Alexa647: recoverin ratio of 3 (6 µM : 2 µM) in 2 ml 100 mM KCl, 30 mM HEPES pH 7.2, 1mM EGTA overnight at room temperature. Separation of unbound dye via a PD 10 desalting gel filtration column from GE Healthcare, Germany (former: Amersham).

- Labeling of DOPE with Atto655-NHS-ester

1.14 µmol DOPE, 1.14 µmol triethylamine and 1.6 µmd Atto655-NHS-ester were dissolved in 60 µl anhydrous methanol and incubated for 90 min at room temperature. Reaction progress was followed by thin layer chromatography using silica gel 60-F_{254} plates (Merck, Darmstadt, Germany). The plates were developed with a 60:25:4 (v/v) mixture of chloroform: methanol: water. Atto655-DOPE was purified by chromatography on a silica gel column (eluent: chloroform: methanol: water 60: 25: 4 (v/v)). The presence of Atto655-DOPE in each fraction was monitored by thin layer chromatography. The solvent was removed and Atto655-DOPE was solved in anhydrous methanol and stored at -20 °C under a nitrogen atmosphere until use.

- Preparation of giant unilamellar vesicles

Giant unilamellar vesicles (GUVs) were prepared using the electro-formation method introduced by Angelova and Dimitrov (Angelova & Dimitrov, 1986). Solutions of lipids in chloroform were handled in glassware only and stored at -20 °C under nitrogen atmosphere. A mixture of labelled and unlabelled lipids (labeling ratio 1:400,000) containing 0.1mol % biotinylated lipids in chloroform was distributed evenly on one ITO-coated glass slide. The solvent was evaporated under reduced pressure. 4-5 µg / cm² remains on the glass slide. A second ITO-coated glass slide was incubated with a neutravidin (0.1 mg/ml) solution for 15 minutes to build a self-assembled protein layer (Bolinger *et al.*, 2004).

The electro-formation cell was assembled by placing a tailored 1 mm thick soft silicone seal in-between these two cover slides and filled with glucose solution. An electric field (15 V/cm, 15 Hz) was applied for 2 hours. After formation giant vesicles were immobilised at the neutravidin-coated glass by binding of the biotinylated lipids to neutravidin.

- Preparation of supported phopholipid bilayers

DOPC (1, 2 – Dioleoyl-sn-Glycero-Phophocholine) was purchased from Avanti Polar Lipids (Alabaster, AL). DOPE (1, 2 – Dioleoyl-sn-Glycero-3-Phosphoethanolamine) was purchased from Sigma (St. Louis, MO). Atto655-NHS-ester was purchased from Atto-Tec GmbH (Siegen, Germany). All other chemicals were purchased from Sigma, Fluka (St. Gallen, Switzerland) and kmf Laborchemie Handels GmbH (Lohmar, Germany).

To label the headgroups of the phospholipids with the fluorescent dye, 1.14 µmol DOPE, 1.14 µmol triethylamine and 1.6 µmol Atto655-NHS-ester were dissolved in 60 µl anhydrous methanol and incubated for 90 min at room temperature. Reaction progress was followed by thin layer chromatography using silica gel 60-F_{254} plates (Merck, Darmstadt, Germany). The plates were developed with a 60:25:4 (v/v) mixture of chloroform: methanol: water. Atto655-DOPE was purified by chromatography on a silica gel column (eluent: chloroform: methanol: water 60: 25: 4 (v/v)). The presence of Atto655-DOPE in each fraction was monitored by thin layer chromatography. The solvent was removed and Atto655-DOPE was dissolved in anhydrous methanol and stored at -20 °C under a nitrogen atmosphere until use.

DOPC was dissolved in chloroform. The solutions were handled in glassware only and stored at -20 °C under a nitrogen atmosphere. A mixture of labelled and unlabelled lipids was made by mixing appropriate amounts of lipid solutions (labeling ratio 1:400,000). The solvent was evaporated under reduced pressure. The sample was kept in vacuum for additional 45 min to remove remaining solvent. The lipid-film was hydrated with double distilled water. Vesicles were produced by sonification to clarity, during which the solution was kept in an ice-bath. For sonification the tip-sonicator Sonifier Cell Disrupter B12 (Branson, Danbury, CT) was used, yielding a solution of vesicles with a diameter of 80–100 nm (verified by dynamic light scattering). The lipid concentration in the vesicular suspension was 500µM. Metal particles originating from the sonicator tip were removed by centrifugation.

Borosilicate glass cover slides (Menzel GmbH + Co KG, Braunschweig, Germany) were cleaned with freshly prepared piranha solution (30 % H_20_2 and conc. H_2SO_4 ratio 2:3), washed extensively with water and dried in a stream of nitrogen. To build a supported bilayer on the glass slide by vesicle fusion, the vesicle suspension was deposited on the glass slide and incubated for 3 min at room temperature. Redundant vesicles were washed away. The resulting membrane was never exposed to air. The formation of a continuous supported bilayer under these conditions was verified by fluorescence microscopy imaging and fluorescence recovery after photobleaching (FRAP).

- Pulsed-field gradient NMR

We performed NMR measurements in deuterated methanol-d_4 solutions of Atto655 at three different concentrations: 3.4 mM, 1.1 mM and 0.4 mM. NMR measurements were made with Variant INOVA 600 MHz spectrometer operating at the ^1H frequency of

599.644 MHz. Self-diffusion coefficient measurements were performed applying the BPP-LED sequence (Karlicek & Lowe, 1980; Chen *et al.*, 1998; Corns *et al.*, 1989; Fordham *et al.*, 1994; Wu *et al.*, 1995; Gibbs & Johnson, 1991; Morris & Johnson, 1992). The DOSY spectra were acquired at 25 °C. We used a thermostat L900 from Variant with temperature accuracy better than ± 0.05 %. The data were collected with no spinning. The self-diffusion coefficients were obtained in the following way. We calibrated our gradient using the *D*-values previously obtained by NMR at 25 °C with a methanol d_4 sample (Weingartner *et al.*, 1989), namely for CD_3OH (D = 2.22 x 10^{-9} m^2/s) and for CHD_2OD (D = 2.18 x 10^{-9} m^2/s). The gradient strength was logarithmically incremented in 15 steps from 14.52 G / cm up to 56.22 G / cm The following experimental settings were used: diffusion time, Δ was 40 ms, gradient duration, δ was 800 µs, the longitudinal eddy current delay was 20ms, acquisition time was 3 s. Details of the apparatus and procedure are given elsewhere (Holz & Weingartner, 1991; Price, 1998; Antalek, 2002; JohnsonJr., 1999) The reported self-diffusion coefficient is averages over at least 10 measurements which agreed to within ± 0.5 % and the overall accuracy of the data is estimated to be better than ± 4 % .

- Temperature control and Pifoc of the 2fFCS setup

Sample temperature was controlled by using a custom-build brass sample holder that was kept at a constant temperature by circulating water through channels in the brass holder. Water temperature was kept at the desired value with a thermostat (F12 + MB, JULABO Labortechnik GmbH, Seelbach, Germany). If not stated opposite sample temperature was kept at 25 °C throughout all 2fFCS experiments. For PSF scanning, fluorescent beads (PS-Speck Microscope Point Source Kit (P7220), (Invitrogen GmbH, Karlsruhe, Germany) were immobilized on a coverslide and scanned through the detection region of the 2fFCS system using a piezo scan table (PI P-527.2CL, Physik Instrumente, Göttingen, Germany) for moving the sample horizontally (with step size of 50 nm), and a piezo actuator (PIFOC P-721-20, Physik Instrumente, Göttingen, Germany) for moving the objective vertically.

12. Acronyms

2fFCS	two-focus Fluorescence Correlation Spectroscop*y*
3DG	Three-dimensional Gaussian
ACF	Auto-Correlation Function
ALEX	Alternating Laser Excitation
BSA	Bovine Serum Albumin
CaM	Calmodulin
Ca_4^{2+} **-CaM**	Calmodulin which has bound four calcium ions
Ca_2^{2+} **-CaM**	Calmodulin which has bound only two calcium ions
DIC	Differential Interference Contrast
DLS	Dynamic Light Scattering
DOPC	1, 2 – Dioleoyl-sn-Glycero-Phophocholine
DOPE	1, 2 – Dioleoyl-sn-Glycero-3-Phosphoethanolamine
EGTA	Ethylene Glycol-bis(beta-aminoethyl ether)-N,N,N',N' - Tetra acetic acid
FCS	Fluorescence Correlation Spectroscopy
FRAP	Fluorescence Recovery After Photobleaching
GdHCl	Guanidine Hydro Chloride
GPC	Gel Permeation Chromatography
GUV	Giant Unilamelar Vesicle
HPLC	High Performance Liquid Chromatography
MDF	Molecule Detection Function
N.A.	Numerical Aperture
NHS	N-hydroxysuccinimide
NMR	Nuclear Magnetic Resonance
NMT1	*N*-myristoyltransferase 1
NTA	NitriloTriacetic Acid
PCR	Polymerase Chain Reaction
PFG-NMR	Pulsed-Field Gradient Nuclear Magnetic Resonance
PIE	Pulsed Interleaved Excitation

PSF	Point Spread Function
ROS	Rod Outer Segement
SPAD	Single-photon Avalanche Diode
SPB	Supported Phospholipid Bilayer
TC	Tryptophane cage
TCSPC	Time-Correlated Single-Photon Counting
Trp	Tryptophan
TTTR	Time-Tagged Time-Resolved
UVRS	Ultraviolet resonance Raman spectroscopy
WT	Wild Type
XCF	Cross-Correlation Function

13. References

Abramowitz,M. & Stegun,I.A. (1984) *Handbook of Mathematical Functions.* Verlag Harri Deutsch, Thun.

Ahmed,Z., Beta,I.A., Mikhonin,A.V. & Asher,S.A. (2005) UV-resonance raman thermal unfolding study of Trp-cage shows that it is not a simple two-state miniprotein. *J Am.Chem.Soc.*, **127,** 10943-10950.

Ames,J.B., Porumb,T., Tanaka,T., Ikura,M. & Stryer,L. (1995) Amino-terminal Myristoylation Induces Cooperative Calcium Binding to Recoverin. *Journal of Biological Chemistry*, **270,** 4526-4533.

Angelova,M.I. & Dimitrov,D.S. (1986) Liposome electroformation. *Faraday Discuss.Chem.Soc.*, **81,** 303-311.

Antalek,B. (2002) Using pulsed gradient spin echo NMR for chemical mixture analysis: How to obtain optimum results. *Concepts in Magnetic Resonance*, **14,** 225-258.

Babu,Y.S., Bugg,C.E. & Cook,W.J. (1988) Structure of calmodulin refined at 2.2 A resolution. *J.Mol.Biol.*, **204,** 191-204.

Barbato,G., Ikura,M., Kay,L.E., Pastor,R.W. & Bax,A. (1992) Backbone dynamics of calmodulin studied by 15N relaxation using inverse detected two-dimensional NMR spectroscopy: the central helix is flexible. *Biochemistry*, **31,** 5269-5278.

Benda,A., Benes,M., Marecek,V., Lhotsky,A., Hermens,W.T. & Hof,M. (2003) How To Determine Diffusion Coefficients in Planar Phospholipid Systems by Confocal Fluorescence Correlation Spectroscopy. *Langmuir*, **19,** 4120-4126.

Benes,M., Billy,D., Hermens,W.T. & Hof,M. (2002) Muscovite (mica) allows the characterisation of supported bilayers by ellipsometry and confocal fluorescence correlation spectroscopy. *Biol.Chem.*, **383,** 337-341.

Berland,K. & Shen,G. (2003) Excitation saturation in two-photon fluorescence correlation spectroscopy. *Appl.Opt.*, **42,** 5566-5576.

Berne,B.J. & Pecora,R. (2000) *Investigations on the Theory of the Brownian Movement*.New York.

Birkhoff,G.D. (1931) Proof of the Ergodic Theorem. *Proceedings of the National Academy of Sciences*, **17,** 656-660.

Bloomfield,V.A. (2000) Survey of Biomolecular Hydrodynamics. *On-Line Biophysics Textbook* (ed. by T.M.Schuster), pp. 1-16.

Böhmer,M., Pampaloni,F., Wahl,M., Rahn,H.J., Erdmann,R. & Enderlein,J. (2001) Time-resolved confocal scanning device for ultrasensitive fluorescence detection. *Review of Scientific Instruments*, **72,** 4145-4152.

Bolinger,P.Y., Stamou,D. & Vogel,H. (2004) Integrated nanoreactor systems: triggering the release and mixing of compounds inside single vesicles. *J Am.Chem.Soc.*, **126,** 8594-8595.

Callaghan,P.T. (1991) *Principles of Nuclear Magnetic Resonance Microscopy*. Clarendon Press, Oxford.

Chattopadhyay,K., Saffarian,S., Elson,E.L. & Frieden,C. (2005) Measuring unfolding of proteins in the presence of denaturant using fluorescence correlation spectroscopy. *Biophys.J*, **88,** 1413-1422.

Chattopadhyaya,R., Meador,W.E., Means,A.R. & Quiocho,F.A. (1992) Calmodulin structure refined at 1.7 A resolution. *J.Mol.Biol.*, **228,** 1177-1192.

Chen,A., Johnson,C.S., Lin,M. & Shapiro,M.J. (1998) Chemical Exchange in Diffusion NMR Experiments. *JOURNAL OF THE AMERICAN CHEMICAL SOCIETY*, **120,** 9094-9095.

Chen,Y., Muller,J.D., So,P.T. & Gratton,E. (1999) The photon counting histogram in fluorescence fluctuation spectroscopy. *Biophys.J*, **77,** 553-567.

Corns,R.M., Hoch,M.J.R., Sun,T. & Markert,J.T. (1989) Pulsed field gradient stimulated echo methods for improved NMR diffusion measurements in heterogeneous systems. *Journal of Magnetic Resonance (1969)*, **83,** 252-266.

Crivici,A. & Ikura,M. (1995) Molecular and structural basis of target recognition by calmodulin. *Annu.Rev.Biophys.Biomol.Struct.*, **24,** 85-116.

Davis S.K. & Bardeen C.J (2002) Using two-photon standing waves and patterned photobleaching to measure diffusion from nanometers to microns in biological systems. *Review of Scientific Instruments*, **73,** 2128-2135.

Dertinger,T., v.d.Hocht,I., Benda,A., Hof,M. & Enderlein,J. (2006) Surface sticking and lateral diffusion of lipids in supported bilayers. *Langmuir*, **22,** 9339-9344.

Dizhoor,A.M., Chen,C.K., Olshevskaya,E., Sinelnikova,V.V., Phillipov,P. & Hurley,J.B. (1993) Role of the acylated amino terminus of recoverin in Ca(2+)-dependent membrane interaction. *Science*, **259,** 829-832.

Doose,S., Neuweiler,H. & Sauer,M. (2005) A Close Look at Fluorescence Quenching of Organic Dyes by Tryptophan. *Chemphyschem.*, **6,** 2277-2285.

Einstein,A. (1905b) Über die von der molekularkinetischen Theorie der Wärme geforderte Bewegung von in ruhenden Flüssigkeiten suspendierten Teilchen. *Analen der Physik*, **322,** 549-560.

Einstein,A. (1905a) Eine neue Bestimmung der Molekül Dimensionen. *Analen der Physik*, **324,** 289-306.

Enderlein,J. (1997) A heuristic way of obtaining the Kerr metric. *Am.J.Phys.*, **65,** 897-902.

Enderlein,J. & Böhmer,M. (2003) Influence of interface-dipole interactions on the efficiency of fluorescence light collection near surfaces. *Opt.Lett.*, **28,** 941-943.

Enderlein,J. & Dertinger,T. (2007) The optics of 2-focus fluorescence correlation spectroscopy. *submitted to Optics Express.*

Enderlein,J., Gregor,I., Patra,D., Dertinger,T. & Kaupp,U.B. (2005) Performance of fluorescence correlation spectroscopy for measuring diffusion and concentration. *Chemphyschem.*, **6,** 2324-2336.

Enderlein,J., Gregor,I., Patra,D. & Fitter,J. (2004) Art and artefacts of fluorescence correlation spectroscopy. *Curr.Pharm.Biotechnol.*, **5,** 155-161.

Enderlein,J. & Pampaloni,F. (2004) Unified operator approach for deriving Hermite-Gaussian and Laguerre-Gaussian laser modes. *J.Opt.Soc.Am.A Opt.Image Sci.Vis.*, **21,** 1553-1558.

Enderlein,J. (2005) Dependence of the optical saturation of fluorescence on rotational diffusion. *Chemical Physics Letters*, **410,** 452-456.

Enderlein,J. & Gregor,I. (2005) Using fluorescence lifetime for discriminating detector afterpulsing in fluorescence-correlation spectroscopy. *Review of Scientific Instruments*, **76,** 033102-033105.

Fain,G.L., Matthews,H.R., Cornwall,M.C. & Koutalos,Y. (2001) Adaptation in Vertebrate Photoreceptors. *Physiological Reviews*, **81,** 117-151.

Fallon,J.L. & Quiocho,F.A. (2003) A closed compact structure of native Ca(2+)-calmodulin. *Structure.*, **11,** 1303-1307.

Fordham,E.J., Gibbs,S.J. & Hall,L.D. (1994) Partially restricted diffusion in a permeable sandstone: Observations by stimulated echo PFG NMR. *Magnetic Resonance Imaging*, **12,** 279-284.

Gensch,T., Komolov,K.E., Senin,I.I., Philippov,P.P. & Koch,K.W. (2006) Ca(2+)-dependent conformational changes in the neuronal Ca(2+)-sensor recoverin probed by the fluorescent dye Alexa647. *Proteins.*

Gibbs,S.J. & Johnson,J. (1991) A PFG NMR experiment for accurate diffusion and flow studies in the presence of eddy currents. *Journal of Magnetic Resonance (1969)*, **93,** 395-402.

Grabarek,Z. (2005) Structure of a trapped intermediate of calmodulin: calcium regulation of EF-hand proteins from a new perspective. *J.Mol.Biol.*, **346,** 1351-1366.

Gregor,I. & Enderlein,J. (2005) Focusing astigmatic Gaussian beams through optical systems with a high numerical aperture. *Opt.Lett.*, **30,** 2527-2529.

Gregor,I., Patra,D. & Enderlein,J. (2005) Optical saturation in fluorescence correlation spectroscopy under continuous-wave and pulsed excitation. *Chemphyschem.*, **6,** 164-170.

Habuchi,S., Ando,R., Dedecker,P., Verheijen,W., Mizuno,H., Miyawaki,A. & Hofkens,J. (2005) From The Cover: Reversible single-molecule photoswitching in the GFP-like fluorescent protein Dronpa. *Proceedings of the National Academy of Sciences*, **102,** 9511-9516.

Haeberlé,O., mmar,M., urukawa,H., enjimbayashi,K. & örök,P. (2003) The point spread function of optical microscopes imaging through stratified media. *Optics Express*, **11,** 2964-2969.

Harvey,D. (2000) *Modern Analytical Chemistry*. McGraw Hill, Boston.

Hess,S.T., Huang,S., Heikal,A.A. & Webb,W.W. (2002) Biological and chemical applications of fluorescence correlation spectroscopy: a review. *Biochemistry*, **41,** 697-705.

Hess,S.T. & Webb,W.W. (2002) Focal volume optics and experimental artifacts in confocal fluorescence correlation spectroscopy. *Biophys.J.*, **83,** 2300-2317.

Holz,M. & Weingartner,H. (1991) Calibration in accurate spin-echo self-diffusion measurements using 1H and less-common nuclei. *Journal of Magnetic Resonance (1969)*, **92,** 115-125.

Humpolickova,J., Gielen,E., Benda,A., Fagulova,V., Vercammen,J., Vandeven,M., Hof,M., Ameloot,M. & Engelborghs,Y. (2006) Probing diffusion laws within cellular membranes by Z-scan fluorescence correlation spectroscopy. *Biophys.J.*, **91,** L23-L25.

Hwang,J.Y. & Koch,K.W. (2002) Calcium- and Myristoyl-Dependent Properties of Guanylate Cyclase-Activating Protein-1 and Protein-2. *Biochemistry*, **41,** 13021-13028.

Ikura,M., Spera,S., Barbato,G., Kay,L.E., Krinks,M. & Bax,A. (1991) Secondary structure and side-chain 1H and 13C resonance assignments of calmodulin in solution by heteronuclear multidimensional NMR spectroscopy. *Biochemistry*, **30,** 9216-9228.

Jaffiol,R., Blancquaert,Y., Delon,A. & Derouard,J. (2006) Spatial fluorescence cross-correlation spectroscopy. *Appl.Opt.*, **45,** 1225-1235.

JohnsonJr.,C.S. (1999) Diffusion ordered nuclear magnetic resonance spectroscopy: principles and applications. *Progress in Nuclear Magnetic Resonance Spectroscopy*, **34,** 203-256.

Kahya,N., Pecheur,E.I., de Boeij,W.P., Wiersma,D.A. & Hoekstra,D. (2001) Reconstitution of Membrane Proteins into Giant Unilamellar Vesicles via Peptide-Induced Fusion. *Biophysical Journal*, **81,** 1464-1474.

Karlicek,J. & Lowe,I.J. (1980) A modified pulsed gradient technique for measuring diffusion in the presence of large background gradients. *Journal of Magnetic Resonance (1969)*, **37,** 75-91.

Kask,P., Palo,K., Fay,N., Brand,L., Mets,U., Ullmann,D., Jungmann,J., Pschorr,J. & Gall,K. (2000) Two-dimensional fluorescence intensity distribution analysis: theory and applications. *Biophys.J*, **78,** 1703-1713.

Kask,P., Palo,K., Ullmann,D. & Gall,K. (1999) Fluorescence-intensity distribution analysis and its application in biomolecular detection technology. *Proc.Natl.Acad.Sci U.S.A*, **96,** 13756-13761.

Kawahara,K. & Tanford,C. (1966) Viscosity and density of aqueous solutions of urea and guanidine hydrochloride. *J Biol.Chem.*, **241,** 3228-3232.

Kettling,U., Koltermann,A., Schwille,P. & Eigen,M. (1998) Real-time enzyme kinetics monitored by dual-color fluorescence cross-correlation spectroscopy. *Proc.Natl.Acad.Sci.U.S.A*, **95,** 1416-1420.

Kiefhaber,T., Rudolph,R., Kohler,H.H. & Buchner,J. (1991) Protein aggregation in vitro and in vivo: a quantitative model of the kinetic competition between folding and aggregation. *Biotechnology (N.Y.)*, **9,** 825-829.

Korlach,J., Schwille,P., Webb,W.W. & Feigenson,G.W. (1999) Characterization of lipid bilayer phases by confocal microscopy and fluorescence correlation spectroscopy. *Proc.Natl.Acad.Sci.U.S.A*, **96,** 8461-8466.

Kuboniwa,H., Tjandra,N., Grzesiek,S., Ren,H., Klee,C.B. & Bax,A. (1995) Solution structure of calcium-free calmodulin. *Nat.Struct.Biol.*, **2,** 768-776.

Lange,C. & Koch,K.W. (1997) Calcium-Dependent Binding of Recoverin to Membranes Monitored by Surface Plasmon Resonance Spectroscopy in Real Time. *Biochemistry*, **36,** 12019-12026.

Lieto,A.M., Cush,R.C. & Thompson,N.L. (2003) Ligand-receptor kinetics measured by total internal reflection with fluorescence correlation spectroscopy. *Biophys.J*, **85,** 3294-3302.

Linse,S., Helmersson,A. & Forsen,S. (1991) Calcium binding to calmodulin and its globular domains. *Journal of Biological Chemistry*, **266,** 8050-8054.

Liu,W., Cellmer,T., Keerl,D., Prausnitz,J.M. & Blanch,H.W. (2005) Interactions of lysozyme in guanidinium chloride solutions from static and dynamic light-scattering measurements. *Biotechnol.Bioeng.*, **90,** 482-490.

Lucas,L.H. & Larive,C.K. (2004) Measuring Ligand-Protein Binding Using NMR Diffusion Experiments. *Concepts in Magnetic Resonance Part*, **20A,** 24-41.

Magde,D., Elson,E. & Webb,W.W. (1972) Thermodynamic Fluctuations in a Reacting System - Measurement by Fluorescence Correlation Spectroscopy. *Physical Review Letters*, **29,** 705-708.

Makino,C.L., Dodd,R.L., Chen,J., Burns,M.E., Roca,A., Simon,M.I. & Baylor,D.A. (2004) Recoverin regulates light-dependent phosphodiesterase activity in retinal rods. *J Gen.Physiol*, **123,** 729-741.

Merkel,R., Sackmann,E. & Evans,E. (1989) Molecular friction and epitactic coupling between monolayers in supported bilayers. *Journal de Physique*, **50,** 1535-1555.

Morris,K.F. & Johnson,C.S. (1992) Diffusion-ordered two-dimensional nuclear magnetic resonance spectroscopy. *J Am.Chem.Soc.*, **114,** 3139-3141.

Müller,B.K., Zaychikov,E., Bräuchle,C. & Lamb,D.C. (2005) Pulsed interleaved excitation. *Biophys.J*, **89,** 3508-3522.

Munro,P. & Török,P. (2005) Vectorial, high numerical aperture study of Nomarski's differential interference contrast microscope. *Optics Express*, **13,** 6833-6847.

Nagy,A., Wu,J. & Berland,K.M. (2005a) Observation volumes and {gamma}-factors in two-photon fluorescence fluctuation spectroscopy. *Biophys.J.*, **89,** 2077-2090.

Nagy,A., Wu,J. & Berland,K.M. (2005b) Characterizing observation volumes and the role of excitation saturation in one-photon fluorescence fluctuation spectroscopy. *J.Biomed.Opt.*, **10,** 44015.

Neidigh,J.W. & Andersen,N.H. (2002) Peptide conformational changes induced by tryptophan-phosphocholine interactions in a micelle. *Biopolymers*, **65,** 354-361.

Neidigh,J.W., Fesinmeyer,R.M. & Andersen,N.H. (2002) Designing a 20-residue protein. *Nat.Struct.Biol.*, **9,** 425-430.

Neuweiler,H., Doose,S. & Sauer,M. (2005) A microscopic view of miniprotein folding: Enhanced folding efficiency through formation of an intermediate. *Proceedings of the National Academy of Sciences*, **102,** 16650-16655.

Nishimura,G. & Kinjo,M. (2004) Systematic error in fluorescence correlation measurements identified by a simple saturation model of fluorescence. *Anal.Chem.*, **76,** 1963-1970.

Nishimura,G. & Kinjo,M. (2005) Dead-time distortion in fluorescence correlation measurements. *Appl.Opt.*, **44,** 3458-3467.

O'Connor,D.V. & Phillips,D. (1984) *Time-Correlated Single-Photon Counting*. Academic Press, London.

O'Neil,K.T. & DeGrado,W.F. (1990) How calmodulin binds its targets: sequence independent recognition of amphiphilic [alpha]-helices. *Trends in Biochemical Sciences*, **15,** 59-64.

Palo,K., Brand,L., Eggeling,C., Jager,S., Kask,P. & Gall,K. (2002) Fluorescence intensity and lifetime distribution analysis: toward higher accuracy in fluorescence fluctuation spectroscopy. *Biophys.J*, **83,** 605-618.

Palo,K., Mets,U., Jager,S., Kask,P. & Gall,K. (2000) Fluorescence intensity multiple distributions analysis: concurrent determination of diffusion times and molecular brightness. *Biophys.J*, **79,** 2858-2866.

Palo,K., Mets,U., Loorits,V. & Kask,P. (2005) Calculation of photon count number distributions via Master equations. *Biophysical Journal*, biophysj.

Papish,A.L., Tari,L.W. & Vogel,H.J. (2002) Dynamic Light Scattering Study of Calmodulin-Target Peptide Complexes. *Biophysical Journal*, **83,** 1455-1464.

Permyakov,S.E., Cherskaya,A.M., Senin,I.I., Zargarov,A.A., Shulga-Morskoy,S.V., Alekseev,A.M., Zinchenko,D.V., Lipkin,V.M., Philippov,P.P., Uversky,V.N. & Permyakov,E.A. (2000a) Effects of mutations in the calcium-binding sites of recoverin on its calcium affinity: evidence for successive filling of the calcium binding sites. *Protein Eng.*, **13,** 783-790.

Permyakov,S.E., Cherskaya,A.M., Senin,I.I., Zargarov,A.A., Shulga-Morskoy,S.V., Alekseev,A.M., Zinchenko,D.V., Lipkin,V.M., Philippov,P.P., Uversky,V.N. & Permyakov,E.A. (2000b) Effects of mutations in the calcium-binding sites of recoverin on its calcium affinity: evidence for successive filling of the calcium binding sites. *Protein Eng.*, **13,** 783-790.

Perroud,T.D., Huang,B. & Zare,R.N. (2005) Effect of bin time on the photon counting histogram for one-photon excitation. *Chemphyschem.*, **6,** 905-912.

Petersen,N.O. (1986) Scanning fluorescence correlation spectroscopy. I. Theory and simulation of aggregation measurements. *Biophys.J*, **49,** 809-815.

Petersen,N.O., Johnson,D.C. & Schlesinger,M.J. (1986) Scanning fluorescence correlation spectroscopy. II. Application to virus glycoprotein aggregation. *Biophys.J*, **49,** 817-820.

Price,W.S. (1998) Pulsed-field gradient nuclear magnetic resonance as a tool for studying translational diffusion: Part II. Experimental aspects. *Concepts in Magnetic Resonance*, **10,** 197-237.

Przybylo,M., Sykora,J., Humpolickova,J., Benda,A., Zan,A. & Hof,M. (2006) Lipid Diffusion in Giant Unilamellar Vesicles Is More than 2 Times Faster than in Supported Phospholipid Bilayers under Identical Conditions. *Langmuir*, **22,** 9096-9099.

Pugh,J., Nikonov,S. & Lamb,T.D. (1999) Molecular mechanisms of vertebrate photoreceptor light adaptation. *Current Opinion in Neurobiology*, **9,** 410-418.

Purcell,E.M. (1977) Life at low Reynolds number. *American Journal of Physics*, **45,** 3-11.

Qian,H. & Elson,E.L. (1991) Analysis of confocal laser-microscope optics for 3-D fluorescence correlation spectroscopy. *Applied Optics*, **30,** 1185-1195.

Richter,R.P., Berat,R. & Brisson,A.R. (2006) Formation of Solid-Supported Lipid Bilayers: An Integrated View. *Langmuir*, **22,** 3497-3505.

Rigler,R. & Elson,E.L. (2001) *Fluorescence Correlation Spectroscopy*. Springer, Berlin.

Rigler,R., Mets,U., Widengren,J. & Kask,P. (1993) Fluorescence correlation spectroscopy with high count rate and low background: analysis of translational diffusion. *European Biophysics Journal*, **22,** 169-175.

Rigneault,H. & Lenne,P.-F. (2003) Fluorescence correlation spectroscopy on a mirror. *J.Opt.Soc.Am.B*, **20,** 2203-2214.

Sackmann,E. (1996) Supported Membranes: Scientific and Practical Applications. *Science*, **271,** 43-48.

Schwertner,M., Booth,M.J. & Wilson,T. (2005) Simple optimization procedure for objective lens correction collar setting. *J Microsc.*, **217,** 184-187.

Schwille,P. (2001) Fluorescence correlation spectroscopy and its potential for intracellular applications. *Cell Biochem.Biophys.*, **34,** 383-408.

Schwille,P., Kummer,S., Heikal,A.A., Moerner,W.E. & Webb,W.W. (2000) Fluorescence correlation spectroscopy reveals fast optical excitation-driven intramolecular dynamics of yellow fluorescent proteins. *Proc.Natl.Acad.Sci.U.S.A*, **97,** 151-156.

Seamon,K.B. (1980) Calcium- and magnesium-dependent conformational states of calmodulin as determined by nuclear magnetic resonance. *Biochemistry*, **19,** 207-215.

Senin,I.I., ., Koch,K.W., Akhtar,M. & Philippov,P.P. (2002a) Ca2+-dependent control of rhodopsin phosphorylation: recoverin and rhodopsin kinase. *Adv.Exp.Med.Biol.*, **514,** 69-99.

Senin,I.I., Fischer,T., Komolov,K.E., Zinchenko,D.V., Philippov,P.P. & Koch,K.W. (2002b) Ca2+-Myristoyl Switch in the Neuronal Calcium Sensor Recoverin Requires Different Functions of Ca2+-binding Sites. *Journal of Biological Chemistry*, **277,** 50365-50372.

Senin,I.I., Vaganova,S.A., Weiergraber,O.H., Ergorov,N.S., Philippov,P.P. & Koch,K.W. (2003) Functional Restoration of the Ca2+-myristoyl Switch in a Recoverin Mutant. *Journal of Molecular Biology*, **330,** 409-418.

Shea,M.A., Verhoeven,A.S. & Pedigo,S. (1996) Calcium-induced interactions of calmodulin domains revealed by quantitative thrombin footprinting of Arg37 and Arg106. *Biochemistry*, **35,** 2943-2957.

Sorensen,B.R. & Shea,M.A. (1996) Calcium binding decreases the stokes radius of calmodulin and mutants R74A, R90A, and R90G. *Biophys.J.*, **71,** 3407-3420.

Squire,P.G. & Himmel,M.E. (1979) Hydrodynamics and protein hydration. *Arch.Biochem.Biophys.*, **196,** 165-177.

Starr,T.E. & Thompson,N.L. (2001) Total internal reflection with fluorescence correlation spectroscopy: combined surface reaction and solution diffusion. *Biophys.J*, **80,** 1575-1584.

Taylor,D.A., Sack,J.S., Maune,J.F., Beckingham,K. & Quiocho,F.A. (1991) Structure of a recombinant calmodulin from Drosophila melanogaster refined at 2.2-A resolution. *Journal of Biological Chemistry*, **266,** 21375-21380.

Teukolsky,S.A., Vetterling,W.T. & Flannery,B.P. (1992) *Numerical Recipes in C*. Cambridge University Press, Cambridge.

Török,K., Lane,A.N., Martin,S.R., Janot,J.M. & Bayley,P.M. (1992) Effects of calcium binding on the internal dynamic properties of bovine brain calmodulin, studied by NMR and optical spectroscopy. *Biochemistry*, **31,** 3452-3462.

Török,P., Varga,P., Laczik,Z. & Booker,G.R. (1995) Electromagnetic diffraction of light focused through a planar interface between materials of mismatched refractive indices: an integral representation. *JOSA A*, **12,** 325-332.

Török,P. & Varga,P. (1997) Electromagnetic diffraction of light focused through a stratified medium. *Applied Optics*, **36,** 2305-2312.

Tsien,R. & Pozzan,T. (1989) [14] Measurement of cytosolic free Ca2+ with quin2. *Methods in Enzymology Biomembranes Part S* (ed. by Sidney Fleischer and Becca Fleischer), pp. 230-262. Academic Press.

Vaiana,A.C., Neuweiler,H., Schulz,A., Wolfrum,J., Sauer,M. & Smith,J.C. (2003) Fluorescence Quenching of Dyes by Tryptophan: Interactions at Atomic Detail from Combination of Experiment and Computer Simulation. *JOURNAL OF THE AMERICAN CHEMICAL SOCIETY*, **125,** 14564-14572.

Wahl,M., Gregor,I., Patting,M. & Enderlein,J. (2003) Fast calculation of fluorescence correlation data with asynchronous time-correlated single-photon counting. *Optics Express*, **11,** 3583-3591.

Wang,H.J. (1954) Theory of the Self-diffusion of Water in Protein Solutions. A New Method for Studying the Hydration and Shape of Protein Molecules. *JOURNAL OF THE AMERICAN CHEMICAL SOCIETY*, **76,** 4755-4763.

Weingartner,H., Holz,M., Sacco,A. & Trotta,M. (1989) The effect of site-specific isotopic substitutions on transport coefficients of liquid methanol. *The Journal of Chemical Physics*, **91,** 2568-2574.

Weljie,A.M., Yamniuk,A.P., Yoshino,H., Izumi,Y. & Vogel,H.J. (2003) Protein conformational changes studied by diffusion NMR spectroscopy: Application to helix-loop-helix calcium binding proteins. *Protein Science*, **12,** 228-236.

Widengren,J. & Mets,Ü. (2002) *Conceptual Basis of Fluorescence Correlation Spectroscopy and Related Techniques As Tools in Biosciences*. Wiley-VCH, Berlin.

Widengren,J., Mets,U. & Rigler,R. (1995) Fluorescence correlation spectroscopy of triplet states in solution: a theoretical and experimental study. *J.Phys.Chem.*, **99,** 13368-13379.

Widengren,J. & Schwille,P. (2000) Characterization of Photoinduced Isomerization and Back-Isomerization of the Cyanine Dye Cy5 by Fluorescence Correlation Spectroscopy. *Journal of Physical Chemistry A*, **104,** 6416-6428.

Wu,D.H., Chen,A.D. & Johnson,C.S. (1995) An Improved Diffusion-Ordered Spectroscopy Experiment Incorporating Bipolar-Gradient Pulses. *Journal of Magnetic Resonance, Series A,* **115,** 260-264.

Zhang,L. & Granick,S. (2005) Lipid diffusion compared in outer and inner leaflets of planar supported bilayers. *J Chem.Phys.,* **123,** 211104.

Zhang,M., Tanaka,T. & Ikura,M. (1995) Calcium-induced conformational transition revealed by the solution structure of apo calmodulin. *Nat.Struct.Biol.*, **2,** 758-767.

Zozulya,S. & Stryer,L. (1992) Calcium-myristoyl protein switch. *Proceedings of the National Academy of Sciences*, **89,** 11569-11573.

Erklärung gem. §3 Abs. 1, Punkt 10 der Promotionsordnung von 1994 der Universität zu Köln:

Ich versichere, daß ich die von mir vorgelegte Dissertation selbständig angefertigt, die benutzten Quellen und Hilfsmittel vollständig angegeben und die Stellen der Arbeit - einschließlich Tabellen, Karten und Abbildungen -, die anderen Werken im Wortlaut oder dem Sinn nach entnommen sind, in jedem Einzelfall als Entlehnung kenntlich gemacht habe; daß diese Dissertation noch keiner anderen Fakultät oder Universität zur Prüfung vorgelegen hat; daß sie - abgesehen von unten angegebenen Teilpublikationen - noch nicht veröffentlicht worden ist sowie, daß ich eine solche Veröffentlichung vor Abschluß des Promotionsverfahrens nicht vornehmen werde. Die Bestimmungen dieser Promotionsordnung sind mir bekannt. Die von mir vorgelegte Dissertation ist von priv. Doz. Dr. Jörg Enderlein betreut worden.